The role of layer-induced anisotropy
in seismic exploration

Johannes Henricus Hake

The role of layer-induced anisotropy in seismic exploration

Johannes Henricus Hake

THE ROLE OF LAYER-INDUCED ANISOTROPY IN SEISMIC EXPLORATION

De rol van door gelaagdheid veroorzaakte anisotropie in de seismische exploratie

(met een samenvatting in het Nederlands)

PROEFSCHRIFT

TER VERKRIJGING VAN DE GRAAD VAN DOCTOR AAN DE RIJKSUNIVERSITEIT TE UTRECHT, OP GEZAG VAN DE RECTOR MAGNIFICUS PROF. DR. J.A. VAN GINKEL, VOLGENS BESLUIT VAN HET COLLEGE VAN DECANEN IN HET OPENBAAR TE VERDEDIGEN OP MAANDAG 11 JANUARI 1993 DES NAMIDDAGS TE 2.30 UUR

DOOR

JOHANNES HENRICUS HAKE

GEBOREN OP 2 OKTOBER 1956 TE EMMEN

PROMOTOR: PROF. DR. K. HELBIG

Aan Ellen en Louise

Figure on cover page: A reflected shear wave in the intercept time versus ray parameter (τ-p) domain. In this domain the arrival time curves are scaled slowness surfaces. The example here is for a transversely isotropic medium above a horizontal reflector.

Content

List of symbols

ρ density

μ shear modulus

$\underline{C}$ elastic stiffness or elasticity tensor, with elements
   c_{jkmn} (4 suffices notation, j,k,m,n = 1,2,3) or
   c_{mn} (2 suffices notation, m,n = 1,2,...,6).

$\underline{\varepsilon}$ strain tensor, with elements
   ε_{jk} (2 suffices notation, j,k = 1,2,3) or
   ε_{m} (1 suffix notation, m = 1,2,...,6).

$\underline{\sigma}$ stress tensor, with elements
   σ_{jk} (2 suffices notation, j,k = 1,2,3) or
   σ_{m} (1 suffix notation, m = 1,2,...,6).

$\underline{S}$ slowness vector with elements s_i (i=1,2,3 or i=x,y,z)

$\underline{V}$ phase or normal velocity vector with elements v_i (i=1,2,3 or i=x,y,z)

$\underline{G}$ group or ray velocity vector with elements g_i (i=1,2,3 or i=x,y,z)

$\underline{Q}$ ray slowness with elements q_i (i=1,2,3 or i=x,y,z)

$\underline{U}$ displacement vector with elements u_i (i=1,2,3 or i=x,y,z)

$\underline{\alpha}$ polarization vector

$\underline{\beta}$ unit vector parallel to the slowness vector

$\underline{\gamma}$ unit vector parallel to the ray velocity vector

P   P-wave

S1   S1-wave

S2   S2-wave

$\underline{X}$ space vector: $\underline{X} = (x_1, x_2, x_3)$ or $\underline{X} = (x, y, z)$

δ_{ij} Kronecker delta

δ_i partial derivative with respect to x_i

δ_t partial derivative with respect to time

t   time

λ wavelength, also normalized elastic parameter

f   frequency

ω angular frequency

$\underline{W}$ displacement-stress vector

$\underline{P}$ propagator matrix

d   thickness of period, consisting of layers a and b

h   thickness fraction of layer a, also normalized elastic parameter

τ intercept time, also normalized elastic parameter

θ squared ratio of isotropic shear and compressional velocity

< >   average, weighted by layer thickness

R   reflectivity

r   plane wave reflection coefficient, also wave mode index

Chapter 1

Introduction

1.1 Introduction to anisotropy

Inhomogeneity and anisotropy

Imagine a physical parameter of a material, that is calculated from or measured by some sort of physical experiment. This parameter may be a scalar, vectorial or tensorial quantity. The material is homogeneous for this parameter if the parameter is the same for all locations, spatial dependence makes the material inhomogeneous for this parameter. The material is anisotropic if the parameter depends on the direction of the measurement. The material can be both inhomogeneous and anisotropic. The parameter is then direction dependent and in addition varies with location.

Anisotropy and inhomogeneity are both a matter of scale. Every material is inhomogeneous on the scale of a crystal size. But the physical experiment is carried out with a certain spatial resolution, that may be much larger than the crystal size. Imagine an elementary volume of material, which is inhomogeneous on the scale of the dimensions of this volume. When changing the resolution of the experiment to scales large compared to the dimensions of the volume, the elementary volume becomes homogeneous with respect to the physical parameter. However, the intrinsic inhomogeneity of the elementary volume is still there. When this intrinsic inhomogeneity has some sort of ordering, i.e. the elementary parts inside the volume are not randomly distributed, the volume is

for the large scale resolutions not only homogeneous but also anisotropic. Hence material anisotropy can be defined as ordered intrinsic inhomogeneity. In a physical experiment a range of wavelengths may be involved. For small wavelengths the material may be inhomogeneous and isotropic, for long wavelengths it may be homogeneous and anisotropic. In a middle range the material is then dispersive.

Causes of anisotropy

Anisotropy occurs in velocities of elastic waves, originating from earthquakes or from seismic sources used in exploration geophysics. Anisotropy is not restricted to geophysics. It is, for example, observed for electromagnetic waves in the ionosphere (Budden 1961, Felsen and Marcuvitz 1973, p.740). It is also a well known phenomenon in optics (Born and Wolf 1980, for example). Anisotropy occurs for elastic waves in crystals (Nye 1957, Musgrave 1970). For an aggregate of crystals the physical properties may depend on two factors: the anisotropy of the unit crystal and the orientation distribution function of the aggregate. The symmetry of the crystal may be overshadowed by the symmetry of the distribution function. The earth possesses anisotropy for various physical parameters. Magnetic permeability and electrical conductivity show anisotropy (Combee 1991), but perhaps best known is the anisotropy for seismic waves. Anisotropy has been observed in the inner core (Morelli et al. 1986), upper mantle (e.g. Raitt 1969) and crust (e.g. Koshubin et al. 1984, Mair and Lyons 1981, Stephan 1981 and Crampin et al. 1986). Specific observations in crystalline rock have been made by, for example, Babuska and Prosz (1984) and Leary and Henyey (1985).

Anisotropy has been measured in a wide variety of sedimentary rocks, such as shales (Jones and Wang 1981, White et al. 1983, Banik 1984), deep-sea carbonates (Carlson et al. 1979, 1984, Milholland 1980), coals (Levine and Davis 1984), limestone (Bamford 1979), turbidites (Davies 1986) and fan deposits (Wetzel 1986). A complete list of anisotropy observations in sedimentary rock is too long to mention. Especially in recent years numerous observations were reported. The cause of anisotropy can be fine layering (as in, for example, turbidites), preferred crystal orientation (as in, for example, shales), or the cause can be of tectonic origin; preferentially oriented fractures and/or micro-cracks resulting from stresses, either as remnants of ancient stresses or as the

consequence of present-day stresses. A common situation in the earth is that stress is not uniform in all directions. The vertical weight of the overburden is in general different from horizontal forces of tectonic origin. The reaction of rock to stress, brittle versus ductile, depends on lithology, porosity, layer thickness etc. In general, non-uniform stress will cause velocity anisotropy. Together with the overall occurrence of fine layering in sedimentary rocks it makes the occurrence of anisotropy a normal property of these rocks.

1.2 Anisotropy and exploration geophysics

Anisotropy has been recognized for a long time. The early works of Bruggeman (1937), Riznichenko (1949), Postma (1955), Uhrig and van Melle (1955), Krey and Helbig (1956), Rytov (1956), Helbig (1956, 1958) and Backus (1962) all dealt with layer-induced anisotropy. Seismic exploration has for a long time been restricted to P-waves, and layer-induced anisotropy was thought to have little effects on P-waves (Krey and Helbig 1956).

The general opinion about anisotropy started to change in the beginning of the 1980's. The use of shear waves received an important stimulus from the Conoco Shear Wave Group Shoot, which recorded several miles of S-wave reflection seismic data. Its results, together with the pioneering work of Crampin on micro-crack induced anisotropy, made the geophysical world aware of the general occurrence of stress-related anisotropy in sedimentary rock. Since fractures and cracks are important in the characterization and development of hydrocarbon reservoirs, many experiments have been carried out since, confirming the existence of this type of anisotropy. Whereas in the past anisotropy was considered as a worry (how to correct for it), it is nowadays more and more often the objective of (still experimental) surveys. Possibly we are at the start of a new period in geophysical exploration. Just as the step from 2D seismic to 3D seismic was a major step forward (Nestvold 1992), the step from isotropy or simple layer-induced anisotropy towards complex anisotropy may be another major step forward. It requires not only 3D seismic (since the anisotropy is 3D) but also multi-component seismic sources and multi-component receivers to obtain the full data matrix of P-waves, S-waves and their conversions.

1.3 <u>About this thesis</u>

Motivation

Why is layer-induced anisotropy still important if apparently stress-related anisotropy is more significant for hydrocarbon reservoirs? The motivation to study layer-induced anisotropy is three-fold. Firstly, fine layering is a major characteristic of many sediments (Fig. 1.1, for example) and has its effects on seismic wave propagation in various ways. Secondly, although studied for a long time, still some problems have not been solved. This is for example the question on how large the seismic wavelength should be, to make a stack of layers effectively anisotropic. Is it three times the thickness of a pair of layers as suggested by Helbig (1984) or does this also depend on the character of the data itself, as questioned by Hsu et al. (1988). Thirdly, the subsurface anisotropy will in general be complex due to a superposition of causes. In order to use anisotropy for resolving reservoir properties, one needs to separate the effects of the different anisotropies. Hence the anisotropy-component due to layering must be well understood.

Objectives

The objectives of this monograph are to investigate how layering results in anisotropy, with special attention for the scaling of wavelength to layer thickness, to show how this affects seismic exploration, both in P-wave seismic as in future multi-component seismic, and to indicate ways to retrieve anisotropy information from seismic data.

Outline

The fundamental properties of waves in an elastic medium are considered in chapter two. The characteristic equation is derived that describes the direction dependence of the three body waves and their polarizations. The concepts of phase and ray velocity and the polar reciprocity between wave surface and
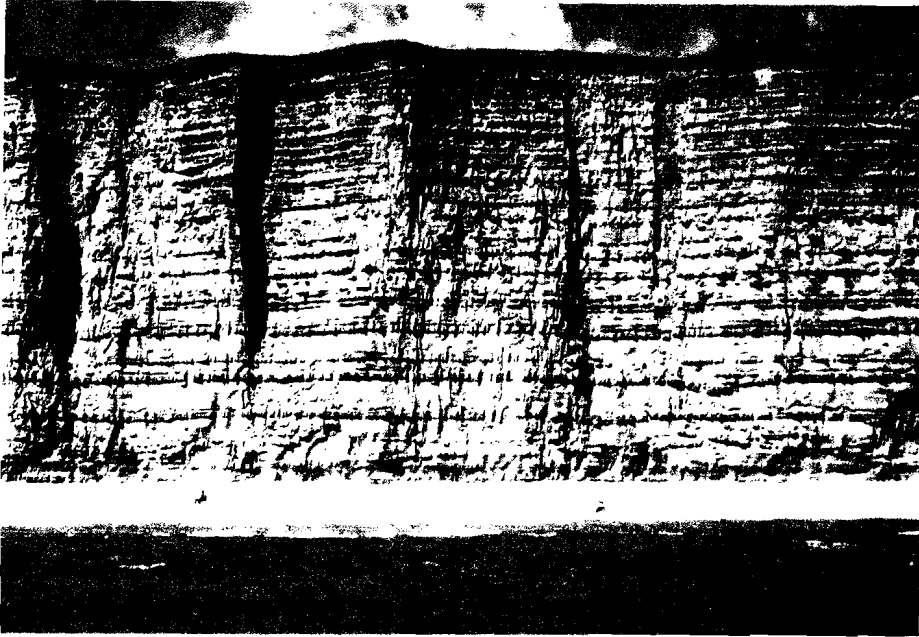
Fig. 1.1 *Outcrop of the Upper Lias (Bridport) Sands on the coast.*
Alternation of clay-rich sandstone and carbonate-cemented sandstone
(stand out as resistant bands). Courtesy KSEPL

slowness surface are discussed. Next the behaviour of seismic waves at interfaces
(reflection and transmission) is investigated. Some examples are given for
propagation of wave fronts with cusps. Anisotropy with hexagonal symmetry is
discussed in more detail since this type of anisotropy results from layering.
In chapter three the problem of how fine layering results in anisotropy is studied.
The reflectivity method is used to compare the response of a stack of layers to
that of its equivalent anisotropic medium. The condition for the seismic
wavelength with respect to layer thickness is addressed, with attention paid to
the angle dependence of this condition and its dependence on the intrinsic layer

parameters. Fine layers can be effectively homogeneous and anisotropic with a fair amount of attenuation.

Chapter four deals with the relationship between stacking velocities and anisotropy due to layering.

Some practical aspects of the use of the theory are discussed in chapter five and illustrated with real data examples.

An anisotropic slowness surface is easier to interpret than a wave surface. The equivalence of the polar reciprocity between slowness surface and wave surface is found in the forward and inverse tau-p transform, as discussed in chapter six. The ease of interpretability and inversion of tau-p curves is demonstrated with geometrical considerations.

In chapter seven we look at the role of layer-induced anisotropy in fracture characterization from seismic anisotropy measurements. An expression for shear wave polarizations is derived for media that are anisotropic due to a superposition of layering and fracturing.

Chapter 2

Elastic waves in anisotropic media

2.1 Introduction

In this chapter I look at general phenomena of seismic wave propagation in anisotropic media. First I consider arbitrary anisotropy and later more specifically anisotropy with hexagonal symmetry.

Various methods exist to investigate seismic wave fields. For horizontally stratified models a possible approach is to use Fourier transforms with respect to time and with respect to horizontal spatial coordinates. Applying the inverse transforms then leads to the result in the time-space domain. Examples of this frequency-wavenumber integration method are given by Booth and Crampin (1983) and by Fryer and Frazer (1984). An alternative technique is the Cagniard-de Hoop method (van der Hijden 1987). For complex, laterally varying 3D layered structures finite-element and finite-difference techniques (for example Dellinger 1991) can be used. Another possibility is to use the asymptotic high-frequency approximation. For this approximation to be valid requires that the medium properties only vary over a scale large compared to the seismic wavelength. In media with large velocity gradients or sharp boundary edges the method fails. The high-frequency approximation method or ray trace method has computational advantages over the other methods, especially when the paraxial ray method (for example Cerveny 1985) is used. Another advantage of ray tracing is that the wave field is decomposed into individual arrivals. Compressional, shear and converted waves, multiples etc. can be studied separately. This makes the method attractive for developing an understanding of the appearance of the various arrivals in seismic recordings over anisotropic

subsurfaces.

In this thesis I use ray theory to introduce the fundamental kinematic and dynamic wave properties for models with homogeneous anisotropic layers and smooth interfaces. Later chapters make use of the concepts, definitions and equations presented here. It goes too far to mention all books and papers published on the subject. Here I name only those which I found very useful for reference. As classical book is by Musgrave (1970) on elastic waves in crystals. The recent book by Helbig (1992) discusses the fundamental concepts of anisotropy thoroughly. Furthermore, the work by Cerveny (1972, 1985), Crampin (1981) and Geoltrain (1989) are to be mentioned.

First I define phase velocity and polarization of the three body waves. Then I look at the propagation of energy and ray velocities. The relation between slowness and ray velocity is derived and the polar reciprocal relationship between slowness surface and wave surface is explained. Then I analyse the wave field behaviour at interfaces and define Snell's law for anisotropic layers. Expressions for reflection and transmission coefficients are derived using the boundary conditions of continuity of displacements and stresses across the interface. A characteristic phenomenon of anisotropy is the possible occurrence of a cusp in the wave front. An example illustrates how anisotropy cusps propagate and how their shape is affected by scattering at an interface. Whereas up to now the discussion was for general anisotropy, the Appendix focuses on the special case of anisotropy with hexagonal symmetry. Fine parallel layering results in this type of anisotropy and therefore has the major attention in this thesis. Furthermore, its relative simplicity makes it possible to derive analytical expressions for quantities such as velocity, polarization etc. in terms of the elastic medium parameters. This is in general not possible for anisotropy with less symmetry, for which these quantities have to be calculated numerically.

2.2   Wave propagation in a homogeneous anisotropic halfspace

The equation of motion

The equation of motion is the starting point for the description of wave motion in elastic homogeneous anisotropic media. We have Newton's law, stating

that force is the product of density and acceleration. This force equals the spatial derivative of stress. With external forces excluded, this reads

$$\delta_k \, \sigma_{jk} - \rho \, \delta_t^2 \, u_j = 0 \qquad\qquad (2.1)$$

with

ρ = density,

u_j = the j-th component of particle displacement vector $\underline{U}$,

σ_{jk} = element jk of the stress tensor,

δ_t = time derivative,

δ_k = derivative with respect to the spatial coordinate x_k.

The stress tensor $\underline{\sigma}$ is of second rank and is symmetrical:

$$\sigma_{jk} = \sigma_{kj} \qquad\qquad (2.2)$$

The medium is assumed to be linearly elastic. Stress and strain are then related according to Hooke's law, which states that each component of the stress tensor $\underline{\sigma}$ is a linear combination of all components of the infinitesimal strain tensor $\underline{\varepsilon}$:

$$\sigma_{jk} = c_{jkmn} \, \varepsilon_{mn} \qquad\qquad (2.3)$$

Note that throughout this monograph Einstein's summation convention on repeated subscripts applies. $\underline{C}$ is the elastic stiffness tensor and is of rank 4. It has $3^4 = 81$ elements. Alternatively the stress-strain relation can be written as

$$\varepsilon_{jk} = D_{jkmn} \, \sigma_{mn} \qquad\qquad (2.4)$$

where $\underline{D}$ is the elastic compliance tensor. The tensors $\underline{C}$ and $\underline{D}$ are each other inverses.

$$c_{mnij} \, D_{ijkl} = I_{mnkl} = \tfrac{1}{2}(\delta_{mk} \, \delta_{nl} + \delta_{nk} \, \delta_{ml}), \qquad\qquad (2.5)$$

in which $\underline{I}$ is the 4-th rank unity tensor and δ the Kronecker delta.

Equation (2.4) implies that in general shear stresses (σ_{ij}, i≠j) as well as normal stresses (σ_{ij}, i=j) contribute to the strain in a normal direction (ε_{mn}, m=n). This is in contrast to an isotropic medium where only the normal stresses contribute to normal strain.

The strain tensor is, just as the stress tensor, of second rank and symmetric:

$$\varepsilon_{nm} = \varepsilon_{mn} \qquad\qquad (2.6)$$

The elements of the infinitesimal strain tensor $\underline{\varepsilon}$ are defined by the spatial derivatives of the particle displacements:

$$\varepsilon_{mn} = \tfrac{1}{2}(\delta_m u_n + \delta_n u_m) \qquad\qquad (2.7)$$

The symmetry of the stress and strain tensors imply the following symmetries for $\underline{C}$:

$$c_{jkmn} = c_{kjmn} \qquad\qquad (2.8)$$

and

$$c_{jkmn} = c_{jknm} \qquad\qquad (2.9)$$

In addition $\underline{C}$ has the symmetry

$$c_{jkmn} = c_{mnjk} \qquad\qquad (2.10)$$

which follows when we insert equation (2.3) into the expression for the elastic energy, being $\tfrac{1}{2}\sigma_{jk}\,\varepsilon_{jk}$, and shuffle indices (see for example Helbig, 1992). These symmetries reduce the number of independent elements of $\underline{C}$ to 21 for the most general elastic anisotropic solid.

From equations (2.1), (2.3), (2.6) and (2.7) it follows

$$c_{jkmn}\delta_k\delta_n u_m - \rho\,\delta_t^2\,u_j = 0 \qquad\qquad (2.11)$$

This is a system of linear partial differential equations of the second order, relating displacement and the elastic stiffness tensor.

High frequency solutions

We consider the high frequency wave field solutions of the wave equation, so that the concepts of Huygen's principle and Snell's law apply. It means that we consider only the leading term of the displacement field written as a series of increasing powers of $1/i\omega$.

$$u_j = \exp[i\omega\,(\underline{S}\cdot\underline{X} - t)] \sum_{q=0}^{\infty} \frac{A\,\alpha_j^{(q)}}{(i\omega)^q}, \qquad (2.12)$$

with

$\underline{\alpha}$ = polarization vector,

A = amplitude,

ω = the angular frequency,

$\underline{S}$ = slowness vector and

$\underline{X}$ = space vector.

The asymptotic field is characterized by displacement vector $A\underline{\alpha}$ and travel time function $(\underline{S}\cdot\underline{X} - t)$. The gradient of the travel time function is the slowness. If we take only the first term of the series in (2.12), equation (2.11) becomes

$$(c_{jkmn}s_k s_n - \rho\,\delta_{jm})\,\alpha_j = 0, \qquad (2.13)$$

which is the Christoffel equation.

We write slowness vector $\underline{S}$ as a scalar S and a unit vector $\underline{\beta}$

$$\underline{S} = S\,\underline{\beta}, \qquad (2.14)$$

and equation (2.13) becomes

$$(c_{jkmn}\beta_k\beta_n - \rho\,S^{-2}\,\delta_{jm})\,\alpha_j = 0 \qquad (2.15)$$

Equation (2.15) describes how for a given direction of propagation $\underline{\beta}$, the slowness and the polarization are related to the elastic medium parameters. The non-zero solutions of (2.15) are obtained by solving the eigenvalue equation

$$\mathrm{Det}(c_{jkmn}\beta_k\beta_n - \rho\,S^{-2}\,\delta_{jm}) = 0 \qquad (2.16)$$

Equation (2.16) is known as the eikonal equation. Matrix $c_{jkmn}\beta_k\beta_n$ is positive definite. This follows from the strain energy being positive definite, $\tfrac{1}{2}\,c_{jkmn}\varepsilon_{jk}\varepsilon_{mn} > 0$, which is a consequence of the assumption of stable elastic media, i.e. a deformation of the material requires energy (see Musgrave). Therefore the three solutions of equation (2.16), the eigenvalues ρS^{-2}, are positive. The associated eigenvectors $\underline{\alpha}$ are mutually perpendicular because the

matrix $c_{jkmn}\beta_k\beta_n$ is real and symmetrical

$$(\Gamma_{jm}=c_{jkmn}\beta_k\beta_n=c_{jnmk}\beta_n\beta_k= c_{mkjn}\beta_n\beta_k=c_{mknj}\beta_n\beta_k=\Gamma_{mj})$$

Thus, for a given propagation direction three wave types exist, each with its own specific slowness and particle motion. For a common propagation direction the particle motions of the three waves are mutually orthogonal. The solutions to (2.16) are direction dependent and hence the medium is anisotropic with respect to velocity. Because of the square in ρS^{-2}, there are six solutions for S, consisting of pairs that differ only in sign (which means propagating in opposite direction). Slowness S may be real or complex, corresponding to homogeneous respectively inhomogeneous waves (see for example Appendix 2A, equation (2A.23)).

The simplicity of $\underline{C}$ in the isotropic case reduces equation (2.16) to three second-order equations for the slowness components, which can be written as (Aki and Richards, 1980)

$$(\rho - \mu S^2)\,\underline{\alpha}\times\underline{S} = 0 \qquad\qquad\qquad (2.17)$$

and

$$(\rho - (k+4\mu/3)S^2)\,\underline{\alpha}\cdot\underline{S} = 0 \qquad\qquad\qquad (2.18)$$

where μ is the shear modulus and k the bulk modulus. Either $\underline{\alpha}\times\underline{S} = 0$ (particle motion parallel to $\underline{S}$) and $S^2 = \rho/(k+4\mu/3)$, the P-wave, or $\underline{\alpha}\cdot\underline{S} = 0$ (particle motion perpendicular to $\underline{S}$) and $S^2 = \rho/\mu$, the S-waves. The P-wave displacement is rotation free and the S-wave displacements are divergence free. This is in general not true for anisotropic media (Fig. 2.1).

Nomenclature

Often the waves are referred to as quasi-P and quasi-S waves since in general (for moderate anisotropy) the polarizations are almost that of isotropic P- and S-waves. Here the term P-wave will be used for the wave with the largest velocity (and polarization nearly parallel to the propagation direction). The other two waves will be referred to as S1- and S2-wave. The discrimination between these two waves is either based on the magnitude of their slowness or is based on their polarizations. Which of the criteria is used will be mentioned where needed. Misleading are the terms quasi-SH (qSH) and quasi-SV (qSV) waves. These terms find their origin in the terminology used in isotropic media. In the isotropic
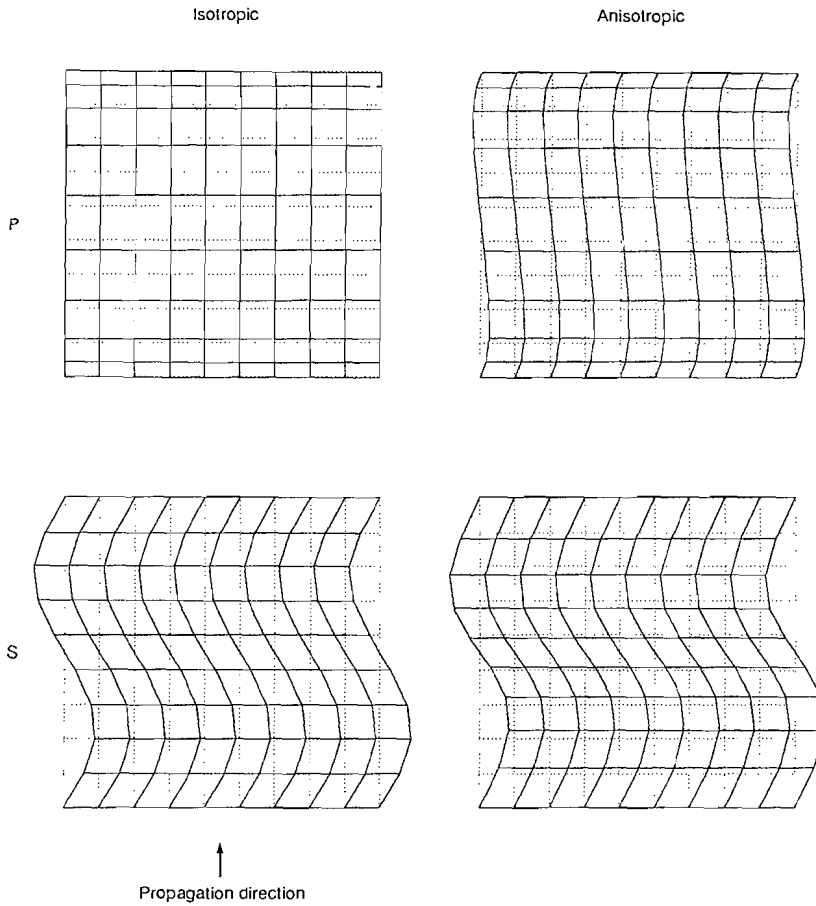
Fig. 2.1 Displacement of a grid due to propagation of monochromatic plane P- and S-waves in isotropic and anisotropic media. The undisturbed grid is dashed.

limit the two quasi-shear velocities are equal, which means that the two shear modes do not separate in time while propagating through the isotropic medium. At any observer point in space the two waves arrive at the same time and the observed polarization can be anywhere in the plane perpendicular to the propagation direction. The particle motion is not fixed by the medium parameters as in an anisotropic medium. To make a distinction between the two waves it is then common to choose an arbitrary direction, say Y, and to call the component polarised in this direction the SH wave and to call the remaining component the

SV wave. When the terms qSH and qSV are now used one might erroneously think that in a weakly anisotropic medium one of the wave modes is approximately polarised in the arbitrarily chosen Y direction. This is in general wrong; it is only true if, by coincidence, the choice for Y happens to be parallel to one of the eigenvectors that are determined by the medium. To avoid confusion it is therefore better no to use these terms.

Ray velocity

In a previous paragraph we derived the expressions for slownesses and polarizations. Now we consider the displacement amplitude and look at the propagation of energy.

First we define instantaneous energy I as the sum of elastic and kinetic energy per unit volume of solid

$$I = \tfrac{1}{2} \sigma_{jk} \varepsilon_{jk} + \tfrac{1}{2} \rho \, \delta_t u_j \, \delta_t u_j \qquad\qquad (2.19)$$

The leading order term of the displacement field, given by equation (2.12), results in

$$I = \tfrac{1}{2} \omega^2 (c_{jkmn} \, u_j u_m s_k s_n + \rho u_j u_j) \exp[2i\omega(\underline{S} \cdot \underline{X} - t)] \qquad\qquad (2.20)$$

However, with

$$c_{jkmn} u_m s_k s_n = \rho u_j \qquad\qquad (2.21)$$

(use Newton's law and the leading order term for displacement), we see that elastic energy and kinetic energy are equal.

Next the energy density E is defined as

$$E = I \exp[-2i\omega(\underline{S} \cdot \underline{X} - t)] \qquad\qquad (2.22)$$

From (2.20) and the argument of equivalence of kinetic and elastic energy it follows that we can express the energy density as

$$E = \rho \, \omega^2 \, u_j u_j \qquad\qquad (2.23)$$

or

$$E = \omega^2 \, c_{jkmn} \, u_j u_m s_k s_n \qquad\qquad (2.24)$$

To come to the expression for the propagation of energy, we use both the first order and second order term of the displacement field expansion (2.12) as a solution for the wave equation. Then, with use of the eikonal equation, it follows

$$\delta_k(\omega^2 c_{jkmn} u_j s_m s_n) = 0 \qquad (2.25)$$

This can be written as

$$\delta_k(E\, g_k) = 0 \qquad (2.26)$$

where E is again the energy density and g_k is the k-th component of vector $\underline{G}$, having the dimension of velocity. Equation (2.26) is known as the transport equation. The term $(E\, g_k)$ is the energy flux vector. The conservation of the energy along $\underline{G}$ (see (2.26)) means that the energy of the wave field propagates along $\underline{G}$. $\underline{G}$ is known as the group or ray velocity. Taking for E the expression (2.23) and using (2.25) and (2.26) we obtain

$$g_k = c_{jkmn}\, u_j u_m s_n / (\rho u_h u_h) \qquad (2.27)$$

and we see that the ray velocity is not necessarily parallel to the slowness vector.

Phase velocity and ray-slowness

In the previous paragraphs I discussed slowness and ray velocity. The inverse of slowness is called phase- or normal velocity, denoted by $\underline{V}$. $\underline{V}$ is the vector parallel to $\underline{S}$ with inverse magnitude:

$$v_i = s_i / (s_j s_j) \qquad (2.28)$$

The inverse of ray velocity is called ray-slowness ($\underline{Q}$, elements q_i):

$$q_i = g_i / (g_j g_j) \qquad (2.29)$$

The ray velocity is made up of the vector sum of phase velocity and a vector perpendicular to the phase velocity. To prove this, both sides of equation (2.27) are multiplied with s_k. The resulting term on the right side of the equation then contains the ratio of elastic to kinetic energy (see 2.20). We have seen before that this ratio is equal to unity. Therefore

$$s_i\, g_i = 1 \qquad (2.30)$$

Because

$$s_i = v_i / (v_j v_j) \qquad\qquad (2.31)$$

we can write

$$v_i g_i = v_j v_j \qquad\qquad (2.32)$$

This means that the projection of the ray velocity on the phase velocity has the magnitude of the phase velocity. Hence we can write

$$g_j = V \beta_j + \delta V/\delta \beta_j \qquad\qquad (2.33)$$

where $\delta V/\delta \beta_j$ is perpendicular to $\underline{V}$ (see Fig. 2.2)
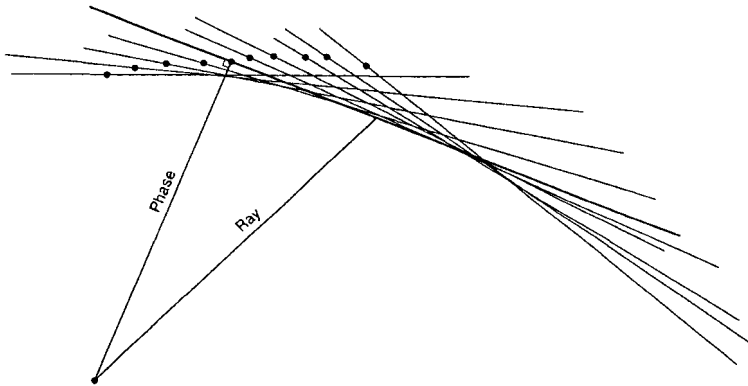
Fig. 2.2   The relation between phase vector and ray vector. The ray vector has its endpoint on the wave surface, which is formed by the envelope of the plane wave fronts.

Characteristic surfaces

When we consider waves originating from a point source then we can form a surface connecting all the end-points of $\underline{S}$ for all directions $\underline{\beta}$. This surface is the slowness surface. Similarly we have the surface formed by all the end-points of the normal velocity, the normal surface. The surface connecting the end-points of the ray-slowness in all directions is the ray-slowness surface, and the end-points of the ray velocity form the wave surface. Normal surface and slowness surface

are mutually inverse surfaces since slowness and normal velocity are each others inverse. Similarly, wave surface and ray-slowness surface are each others inverse.

The wave field emitted from a point-source can be regarded as the superposition of plane-wave fronts where at time zero all plane-wave fronts intersect at one point (the location of the point source). The front of this point-source wave field is formed by the envelope of the plane-wave fronts. Since the ray velocity is the vector sum of phase velocity $\underline{V}$ and a vector perpendicular to $\underline{V}$, this point-source wave field front is hence the wave surface, propagating with the ray velocity.

The relationship between slowness surface and wave surface is that of polar reciprocity: (i) for a given slowness direction β the tangent plane at the corresponding point of the wave surface is perpendicular to β, (ii) for a given direction of the ray velocity,γ, the tangent plane at the corresponding point at the slowness surface is perpendicular to γ. From (2.30) it follows that

$$dg_i\, s_i + ds_i\, g_i = 0 \tag{2.34}$$

$\underline{dg}$ Is a vector tangential to the wave surface and $\underline{ds}$ is a vector tangential to the slowness surface. Point (i) follows immediately from the fact that the wave surface is formed by the envelope of the plane-wave fronts. This means

$$dg_i\, s_i = 0 \tag{2.35}$$

Hence from (2.35) and (2.34)

$$ds_i\, g_i = 0, \tag{2.36}$$

which proves point (ii).

Examples

Figure 2.3 illustrates the P-, S1- and S2-wave slowness surfaces of an anisotropic medium with hexagonal symmetry. The elastic parameters (see Fig. caption) result from fine layering. The intrinsic layers (two constituents with equal thickness) have the parameters: layer a; Vp=2 (km/s), Vs=1, ρ=2 g/cm^3, layer b; Vp=4.4, Vs=2.2, ρ=3.

Figure 2.4 gives the corresponding wave surfaces. The four characteristic surfaces of the S2-wave are shown in Fig. 2.5.
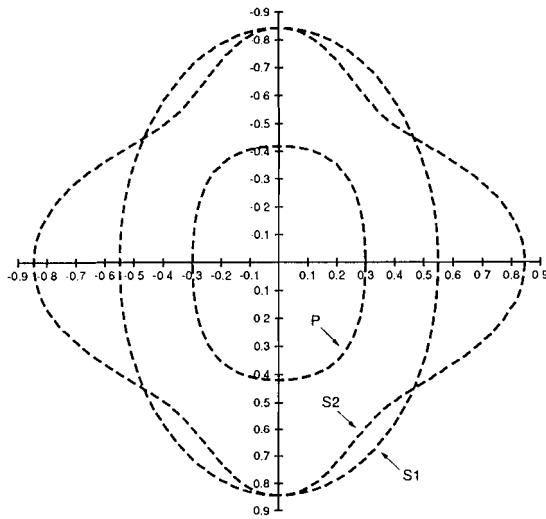
Fig. 2.3 Slowness surfaces P-, S1- and S2-wave, for anisotropy with hexagonal symmetry: c_{11}=28.3 (*10^{12} g/(s^{2}m)), c_{13}=7.03, c_{33}=14.06, c_{44}=3.52, c_{66}=8.26, ρ=2.5 g/(cm^3)
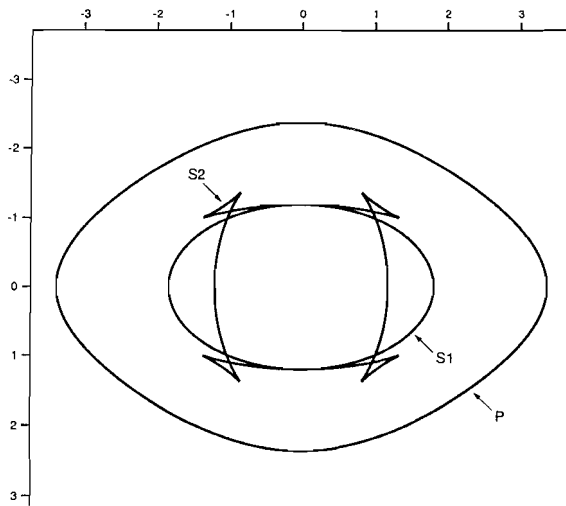
Fig. 2.4 Wave surfaces P-, S1- and S2 wave, medium parameters as in Fig. 2.3
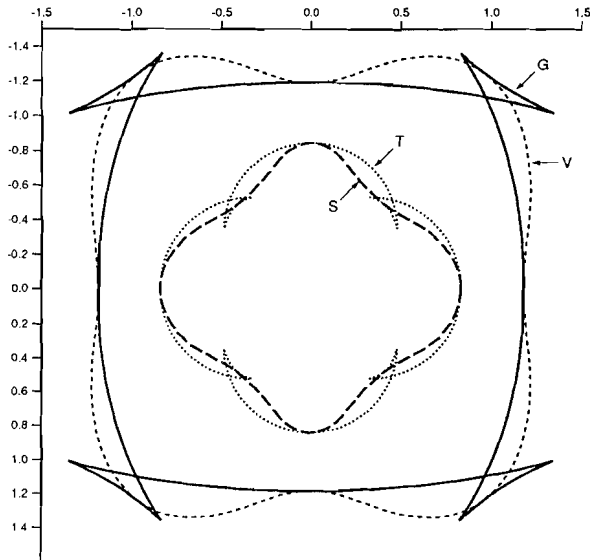
Fig. 2.5 Characteristic surfaces. S2-wave, medium parameters as in Fig. 2.3. S=slowness surface, V=normal surface, G=wave surface, T=ray slowness surface

In Fig. 2.6 a quadrant of the P-wave wave surface is shown. Indicated are the ray directions, polarizations and the slowness directions. The same is illustrated for the S2-wave in Fig. 2.7.

Ray velocity in terms of slowness components

Suppose the slowness is computed from the eigenvalue equation (2.16). The wave surface can then be computed numerically using the equations in the previous paragraph. The objective of this paragraph is to derive the expressions for the ray velocity components g_i in terms of the slowness components s_j. These will later be used to derive analytical expression for $\underline{G}$ in terms of the elasticity tensor elements for specific cases of anisotropy.
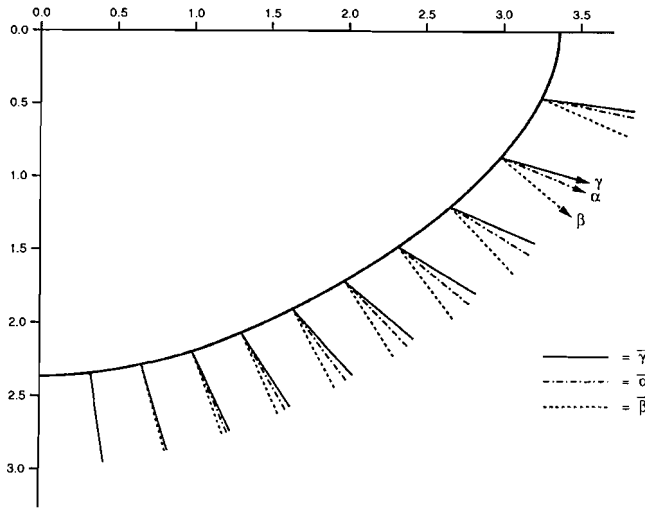
Fig. 2.6 Wave surface P-wave, with indicated ray direction γ, polarization vector $\underline{\alpha}$ and slowness direction $\underline{\beta}$.
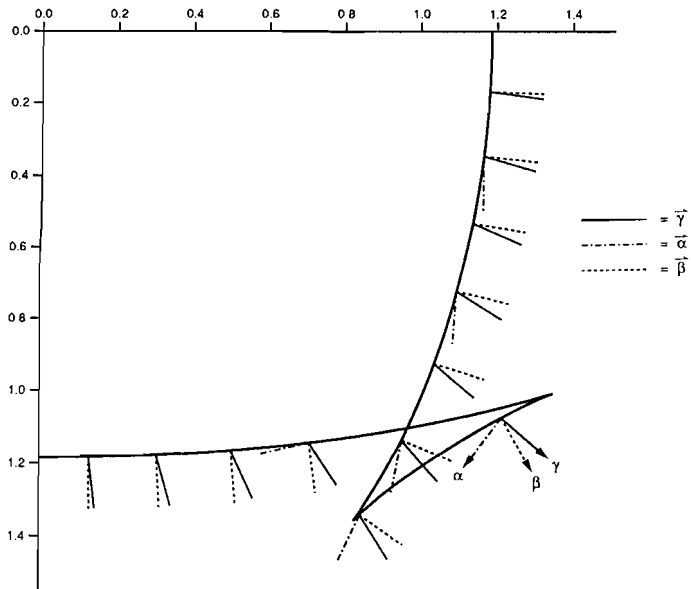
Fig. 2.7 Wave surface S2-wave, with indicated ray direction γ, polarization vector $\underline{\alpha}$ and slowness direction $\underline{\beta}$.

Two methods are used; in the first the slowness surface is parameterized, in the second method Lagrange multipliers are used. Although the final expressions look different for the two methods, they are, of course, compatible.

Method 1: parameterization of $\underline{S}$.

Since the slowness is direction dependent and direction can be parameterized by two parameters, we can in general parameterize $\underline{S}$ by two parameters, say Ω_1 and Ω_2. For anisotropy of hexagonal symmetry $\underline{S}$ depends on the angle between $\underline{\beta}$ and the symmetry axis and therefore for this type of anisotropy one parameter is sufficient. One may choose for this parameter the angle between $\underline{\beta}$ and the symmetry axis. Another choice may be the parameter $\tan(\alpha_{(P)})\tan(\beta)$ (Helbig, 1992).

In general we can write

$$\underline{S} = \underline{S}(\Omega_1, \Omega_2) \tag{2.37}$$

From equation (2.36) we then have

$$g_i \, \delta s_i / \delta \Omega_1 = g_i \, \delta s_i / \delta \Omega_2 = 0 \tag{2.38}$$

Equations (2.30) and (2.38) are satisfied when

$$g_i = M_{1;i} / (\text{Det}(\underline{M})) \tag{2.39}$$

with $M_{1;i}$ the 1,i sub-determinant of matrix $\underline{M}$ and

$$\underline{M} = \begin{bmatrix} s_1 & s_2 & s_3 \\ \delta s_1/\delta \Omega_1 & \delta s_2/\delta \Omega_1 & \delta s_3/\delta \Omega_1 \\ \delta s_1/\delta \Omega_2 & \delta s_2/\delta \Omega_2 & \delta s_3/\delta \Omega_2 \end{bmatrix} \tag{2.40}$$

Thus

$$g_1 = (\ \delta s_2/\delta \Omega_1 \, \delta s_3/\delta \Omega_2 - \delta s_2/\delta \Omega_2 \, \delta s_3/\delta \Omega_1) / \text{Det}(\underline{M})$$

$$g_2 = (-\delta s_1/\delta \Omega_1 \, \delta s_3/\delta \Omega_2 + \delta s_1/\delta \Omega_2 \, \delta s_3/\delta \Omega_1) / \text{Det}(\underline{M}) \tag{2.41}$$

$$g_3 = (\ \delta s_1/\delta \Omega_1 \, \delta s_2/\delta \Omega_2 - \delta s_1/\delta \Omega_2 \, \delta s_2/\delta \Omega_1) / \text{Det}(\underline{M})$$

For example, in the case where $\underline{S}$ can be parameterized by one parameter

$$\underline{S} = \underline{S}(\Omega) \tag{2.42}$$

and the coordinate system is chosen such that $g_2 = 0$, equation (2.38) is fulfilled

if

$$g_1 = \Phi \; \delta s_3/\delta\Omega \text{ and } g_3 = -\Phi \; \delta s_1/\delta\Omega \qquad (2.43)$$

with Φ a scaling factor. This scaling factor follows from inserting (2.43) into (2.30):

$$\Phi = (s_1 \; \delta s_3/\delta\Omega - s_3 \; \delta s_1/\delta\Omega)^{-1} = \text{Det}(\underline{M}) \qquad (2.44)$$

with

$$\underline{M} = \begin{bmatrix} s_1 & s_3 \\ \delta s_1/\delta\Omega & \delta s_3/\delta\Omega \end{bmatrix} \qquad (2.45)$$

Method 2: Lagrange multiplier.

Equation (2.16) can be written as

$$F(s_i) = 0, \qquad (2.46)$$

which means that the solutions for the slowness $\underline{S}$ is found from the condition F=0. As the function F depends on the parameters s_i, we have

$$\delta F/\delta s_i = 0 \qquad (2.47)$$

With Φ a Lagrange multiplier, this can be written as

$$(g_i + \Phi \; \delta F/\delta s_i) \; ds_i = 0 \qquad (2.48)$$

and hence

$$g_i = -\Phi \; \delta F/\delta s_i \qquad (2.49)$$

Substitute (2.49) into (2.30) to give

$$- \Phi \; \delta F/\delta s_i \; s_i = 1 \qquad (2.50)$$

from which

$$\Phi = - (s_i \; \delta F/\delta s_i) \qquad (2.51)$$

When substituted into equation (2.49) this finally gives

$$g_i = (\delta F/\delta s_i) / (s_j \; \delta F/\delta s_j) \qquad (2.52)$$

2.3 Behaviour at plane interfaces

Snell's law

So far, I have discussed the propagation of waves in homogeneous media. In this section I consider their propagation across interfaces.

In isotropic conditions the ray directions of reflected and transmitted waves are found from Snell's law. In anisotropic conditions the ray direction and the phase direction are, as we have seen before, not necessarily the same. Therefore the isotropic Snell's law has to be re-formulated for application to anisotropic conditions. This can be done using causality. The reflected and transmitted wave are caused by the incident wave. Hence, the different wave fronts must be continuous across the interface. From the leading term in the expression for the displacement field, equation (2.12), we thus have the condition $(\underline{S} . \underline{X} - t)^{(M)} = (\underline{S} . \underline{X} - t)^{(M')}$, where M and M' stand for the various wave modes in the incident and transmission media. Since this must hold at all locations along the interface, the spatial derivative of the travel time field along the interface must be the same for all wave modes. The spatial derivative of time is slowness. Thus the condition can be stated as: the slowness tangent to the interface is the same for incident, reflected and transmitted waves. This is Snell's law for anisotropic media. The slowness vectors are determined by their common projection on the interface. With the polar reciprocity relationship between slowness and ray velocity the propagation of the scattered wave fronts are then determined as well.

Figure 2.8 shows snapshots of a propagating wave front in an anisotropic medium. The wave front propagates along the ray direction, which is not parallel to the phase direction. In Fig. 2.9 the wave front is transmitted through an anisotropic-isotropic interface. Indicated is the "normal-incidence" path, i.e. the ray path with the phase velocity perpendicular to the interface. A similar example is given for a "normal-incidence" reflection in Fig. 2.10. The ray path indicated is the zero offset ray path with its reflection point not vertically below the source. Also, the ray paths of reflected waves are not necessarily symmetrical with respect to the interface normal (Fig. 2.11). In the later paragraph on cusps more examples are shown of reflected and transmitted wave fronts.
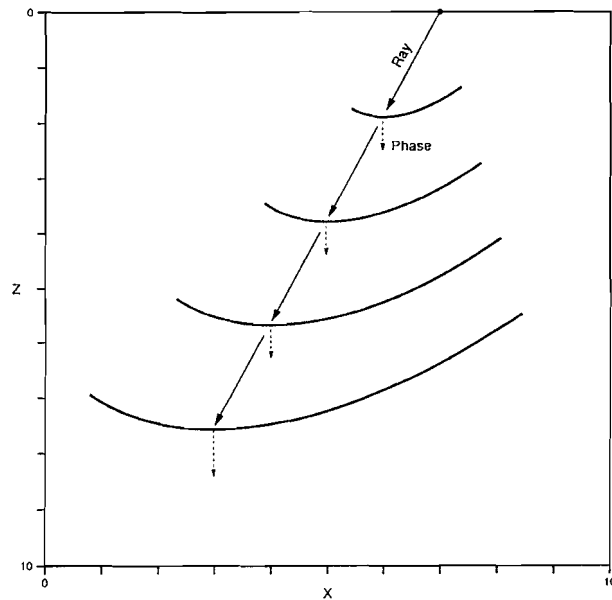
Fig. 2.8 Wave front propagation, not parallel to the wave front normal.
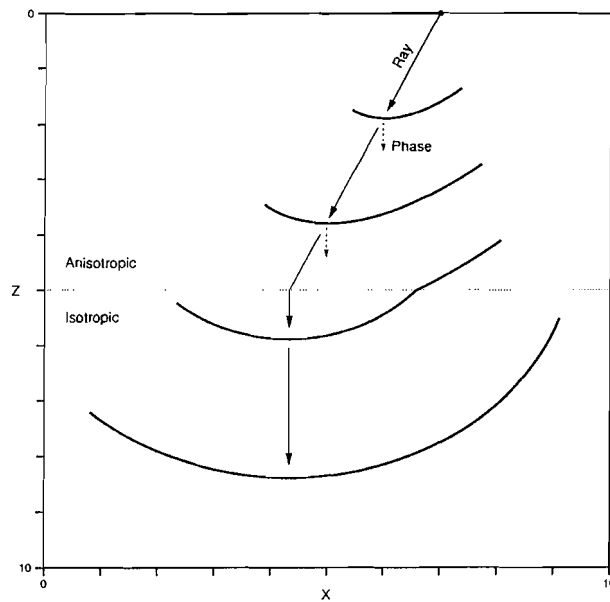
Fig. 2.9 The ray with normal incidence phase velocity, transmitted from an anisotropic layer into an isotropic layer.
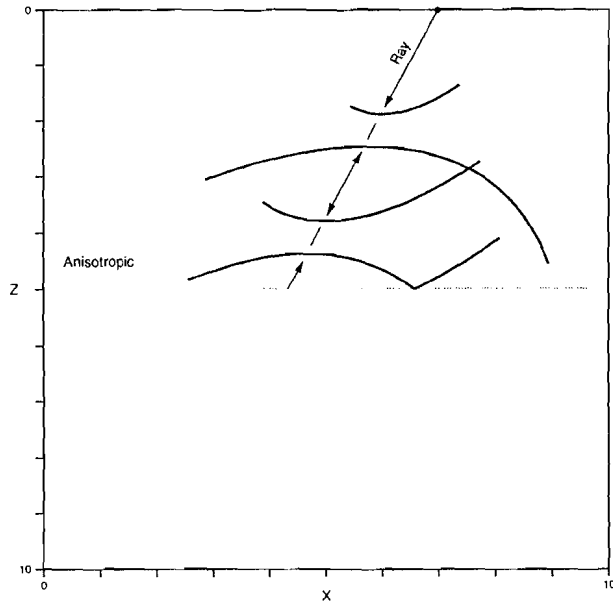
Fig. 2.10 The zero offset reflected ray (normal incidence phase velocity).
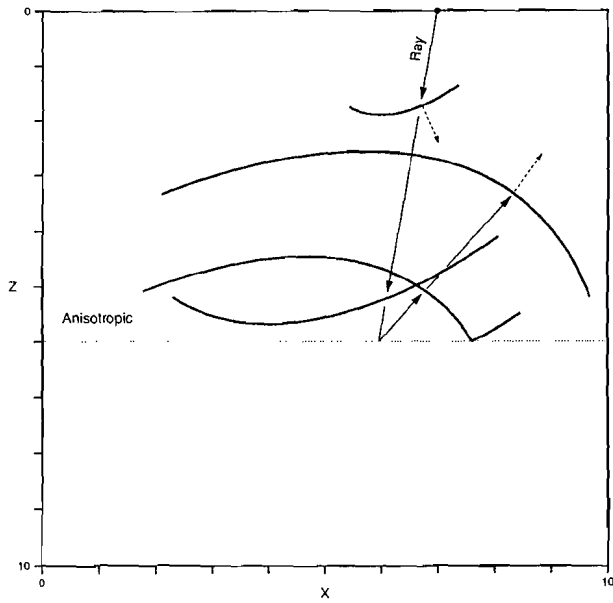
Fig. 2.11 Non-symmetrical reflection. The incident and reflected ray are non-symmetrical with respect to the interface normal.

Reflection and transmission coefficients

The expressions for the plane wave reflection and transmission coefficients in the case of an interface separating anisotropic layers are quite complicated. In the isotropic elastic case the expressions are not simple. The additional elastic parameters in case of anisotropy obviously enlarge the complexity. The same boundary conditions apply for anisotropic layers as for isotropic layers. For two solids in welded contact all three components of the displacement must be continuous through the boundary. In addition, continuity of traction across the interface is required. With these boundary conditions and the expressions for displacement and stress as discussed before, the expression for reflection and transmission coefficients are derived. Due to their complexity these expressions will in general have to be evaluated numerically. Only for specific cases such as, for instance, propagation in a plane of symmetry or for anisotropy of high symmetry, one might be able to find an analytical expression. We choose the coordinate system such that the x_3-axis is perpendicular to the interface and that $s_2=0$. This choice does not limit the applicability since, if required, the stiffness tensor can be rotated to this coordinate system via the tensor transformation

$$c'_{mnrs} = a_{mi} \, a_{nj} \, a_{rk} \, a_{sl} \, c_{ijkl} \qquad (2.53)$$

where a_{ki} is a direction cosine ($a_{ki} = \cos[x'_k, x_i]$).

Snell's law states that the component of the slowness vector parallel to the interface should be equal for all rays participating in the reflection and transmission process. Here this means that s_1 is constant for all waves. The total plane wave displacement in a layer at time t and position X is given by the sum of the displacements of the six eigenvalue solutions.

$$u_j = \sum_{r=1}^{6} A(r) \, \alpha_j(r) \, \exp[i\omega(t - s_1 x_1 - s_3(r) x_3)] \qquad (2.54)$$

Here $A(r)$ is a scalar giving the amplitude of wave mode r (r=1,...,6).

From equations (2.3), (2.7) and (2.54) we then obtain for the elements of the stress tensor

$$\sigma_{jk} = i\omega \sum_{r=1}^{6} -A(r) \, \alpha_j(r) \, \{s_1 \, c_{jkm1} + s_3(r) \, c_{jkm3}\} \exp[i\omega(t - s_1 x_1 - s_3(r) x_3)] \qquad (2.55)$$

With the definition of a displacement-stress vector $\underline{W}$,

$$\underline{W} = (u_1, u_2, u_3, \sigma_{13}, \sigma_{23}, \sigma_{33})^T, \qquad (2.56)$$

an vector $\underline{F}$ containing the amplitudes of the wave modes

$$F_r = A(r) \qquad (2.57)$$

and a matrix $\underline{J}$ with the phase factors

$$J_{ir} = \exp[i\omega(t - s_1 x_1 - s_3(r)x_3)] I_{ir} \qquad (2.58)$$

where $\underline{I}$ is the 6x6 identity matrix, we can relate $\underline{W}$, $\underline{F}$ and $\underline{J}$ trough a matrix $\underline{E}$

$$\underline{W} = \underline{E} \, \underline{J} \, \underline{F} \qquad (2.59)$$

Note that strictly speaking $\underline{W}$ and $\underline{F}$ are not vectors and $\underline{E}$ is not a matrix as they do not change in the appropriate way under rotation of the coordinate system. However, we use this terminology as we assign to these arrays the same definitions for operators as multiplication and addition as for vectors and matrices.

For the elements of $\underline{E}$ we have

$$E_{jr} = \alpha_j(r) \qquad \text{for} \qquad j=1,2,3 \text{ and } r=1,...,6$$

$$E_{jr} = - i\omega\alpha_m(r)\{s_1 c_{3km1} + s_3(r)c_{3km3}\} \quad \text{for} \quad j=4,5,6, \quad r= 1,...,6,$$

$$k=j-3 \text{ and } m=1,2,3 \qquad (2.60)$$

Next we consider a two-layer model. The upper layer is indicated by suffix a, the lower layer by suffix b. The boundary conditions imply

$$\underline{W}_a = \underline{W}_b \qquad (2.61)$$

or

$$\underline{E}_a \, \underline{F}_a = \underline{E}_b \, \underline{F}_b \qquad (2.62)$$

From this equation we can compute the reflection and transmission coefficients. To illustrate this, consider a P-wave incident from layer a on the interface. In layer a we have a downward propagating P-wave and upward travelling S1, S2 and P waves. In medium b we have the transmitted S1, S2 and P waves and no upward travelling waves (Fig. 2.12).

Suppose we order the six eigenvalue solutions such that r=1 and r=4 correspond to the largest slowness values, say the S1 waves, r=2 and r=5 the intermediate slownesses, the S2 waves, and r=3 and r=6 the smallest slownesses, the P waves.
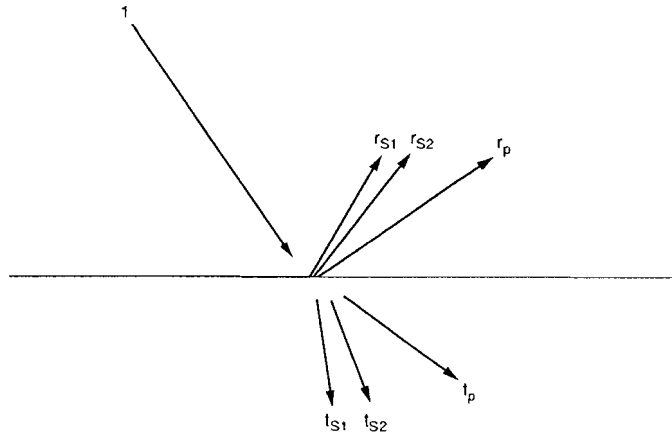
Fig. 2.12 Wave scattering at an interface due to an incident P-wave

In addition, r=1,2,3 correspond to downward travelling waves and r=4,5,6 to upward travelling waves.

Equation (2.62) then reads

$$\underline{E}_a \, (0, 0, 1, r_{S1}, r_{S2}, r_P)^T = \underline{E}_b \, (t_{S1}, t_{S2}, t_P, 0, 0, 0)^T \qquad (2.63)$$

with the amplitude of the incident P wave scaled to unity and r and t the reflection coefficient and transmission coefficient respectively.

2.4   Cusps

A characteristic phenomenon of anisotropy is the possible occurrence of cusps in the wave front.

The slowness surface is of degree 6, which follows from the eikonal equation

which is of the third order in S^2:

$$\text{Det}(c_{jkmn}\beta_k\beta_n - \rho\, S^{-2}\delta_{jm}) = 0 \qquad\qquad (2.64)$$

A surface of degree n is intersected by a straight line in at most n points. Hence it follows that any inner detached slowness sheet must be wholly convex: if it were not, a line could intersect the inner sheet in 4 or more points and yet make at least 4 further intersections with the remaining sheets. A wholly convex sheet contains no inflexion points, i.e. the curvature does not change sign. An inflexion point in the slowness surface corresponds to a cusp in the wave surface. Since the inner slowness sheet is that of the P-wave, the P-wave slowness sheet can not have inflexion points and the P-wave wave surface can not have cusps.

It is interesting to look at the propagation of cusps in multi-layered media. How does the cusp propagate across an interface into a medium with different parameters? And what happens to the cusp after reflection? As an example I take the elastic parameters of the Mesaverde laminated siltstone, as published by Thomsen (Thomsen 1986). This rock is anisotropic with hexagonal symmetry. The elastic parameters with respect to $[x_1, x_2, x_3]$, where x_3 is along the axis of rotation symmetry, are

$c_{11} = 60.13 * 10^{12}$ g/(s^2 m)

$c_{13} = 38.26 * 10^{12}$

$c_{33} = 50.87 * 10^{12}$ $\qquad\qquad$ (2.65)

$c_{44} = 17.17 * 10^{12}$

$c_{66} = 18.75 * 10^{12}$

$\rho\; = 2.57$ g/(cm^3)

Figure 2.13 displays the slowness surface of the S2-wave (polarised in the x_1-x_3 plane) and the corresponding wave surface. The wave surface has cusps near the vertical direction and near the horizontal direction. The reverse branch of the wave surface is the branch between the two cusps. The triplication area is the surface of the triangle formed by the three branches of the wave front (in Fig. 2.13 the wave surface) near the cusps.
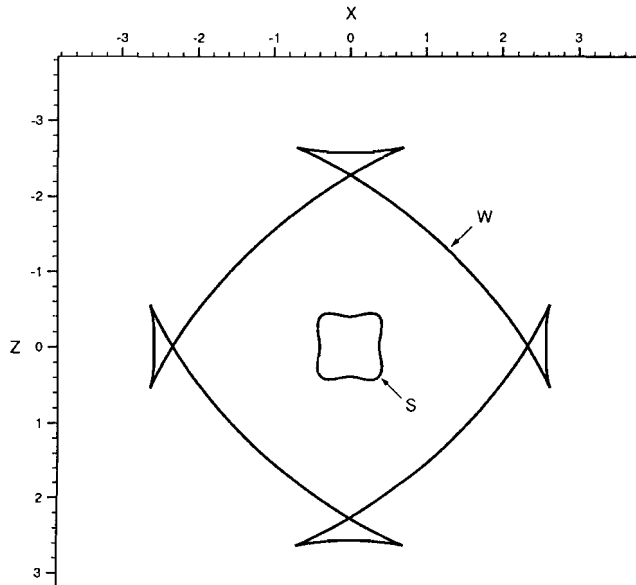
Fig. 2.13 Wave surface and slowness surface (S2-wave) of the Mesaverde laminated siltstone
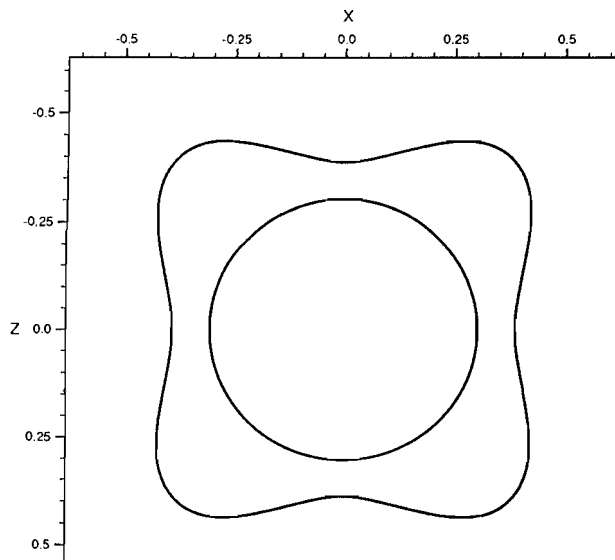
Fig. 2.14 Slowness surface of the Mesaverde laminated siltstone (S2-wave) and an isotropic slowness surface with S=1/3.3 s/km (inner circle)

We consider a two-layer model. The top layer is anisotropic, with the properties of the Mesaverde laminated siltstone, the lower layer is isotropic with Vs = 3.3 km/s (see Fig. 2.14). The point source is located at surface, which is at the top of the upper layer. Figure 2.15 shows the wave front at various times, as it propagates downwards from the source.
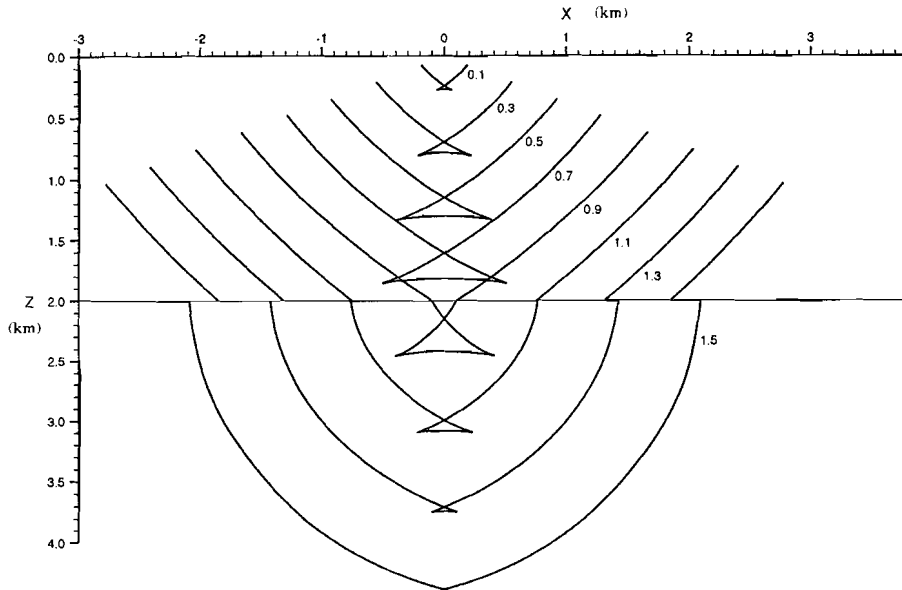
Fig. 2.15 S2 wave front propagating downwards from anisotropic upper layer into isotropic lower layer. Upper layer: Mesaverde laminated siltstone, vertical symmetry axis. Lower layer: isotropic, Vs=3.3 km/s. Interface at z=2km, snapshots at t=0.1, 0.3, ..., 1.5 s.

Note that the front of the head waves are not drawn. The triplication area increases when the wave front in the anisotropic layer propagates away from the source . We apply Snell's law to propagate the wave front across the interface. In the isotropic layer phase- and ray velocity are parallel. The wave front propagates in the direction normal to the wave front. The triplication area diminishes, the two cusps propagate towards each other. This is illustrated in Fig. 2.16. The solid line is the straight ray path, perpendicular to the wave front (at 'A'). The dashed line connects the cusp of the wave front at the various times. Note that the cusp moves along a curved path! The part of the wave front annotated by 'A', is originally close to the cusp, but upon further propagation into the isotropic layer, it moves away from the cusp. A position at the reverse branch

moves, during propagation, across the cuspidal edge, onto the normal branch.
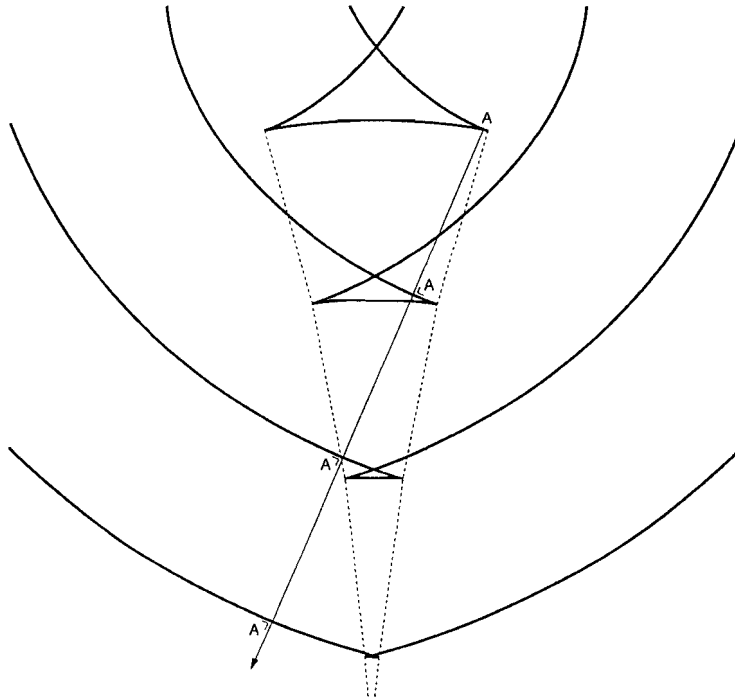
Fig. 2.16 Anisotropy cusps propagating in the isotropic layer. Solid line is the ray path for wave front patch A. The dashed line is the curved cuspidal edge path.

Perhaps more familiar are cusps in the wave front caused by reflection from a synclinal structure. These cusps are widely observed in P-wave seismic over folded subsurfaces. The reverse branch of the wave front of such 'structural' cusps is behind the normal branches (the cusp runs behind the rest of the wave front), see Fig. 2.17. This makes that the two structural cusps diverge when the wave front propagates in an isotropic medium. In contrast, anisotropy cusps are always ahead of the rest of the wave front. (If the cusps would be behind the rest of the wave surface, then its polar reciprocal surface, the slowness surface, would also have cusps. Since the slowness surface is of degree 6, it can not have cusps, for the same reasons as mentioned at the beginning of this paragraph). Because anisotropy cusps are ahead of the rest of the wave front, the two cusps approach each other when the wave front propagates in an isotropic medium.

Anisotropy cusps in the reflected wave front (dashed)
and in the transmitted wave front.

Structural cusps in the wave front reflected at a synclinal interface.
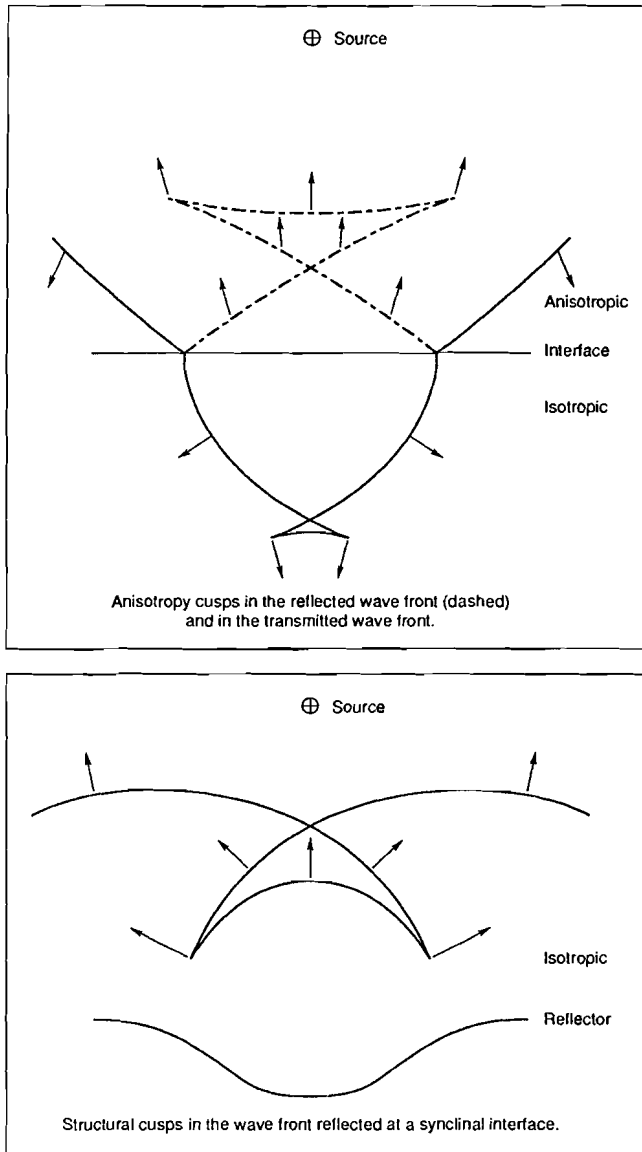
Fig. 2.17 Wave fronts with cusps in anisotropic and in isotropic media. Arrows indicate direction of propagation.

What happens to cusps and the triplication area after reflection at an interface?

The dashed lines in Fig. 2.18 represent reflected wave fronts. Because the symmetry axis of the anisotropy is perpendicular to the interface, incident and reflected ray have the same angle with the interface normal. At surface we observe a large triplication area. The situation is different when the anisotropic symmetry axis is not perpendicular to the interface. In Fig. 2.19 the symmetry axis is tilted 20 degrees. This means cusps occur for propagation directions near +20 degrees and -70 degrees. Consider an incident ray in the direction of a cusp. After reflection, the ray no longer propagates in the direction of a cusp. Hence, while the wave front propagates upwards the triplication area decreases. In this example the triplication area is very small when the reflected wave front arrives at surface. Note again the curved path for the cusps after reflection.

Note in Fig. 2.19 the asymmetrical wave front that arrives at surface. The wave front curvature at the negative offsets is different from the curvature at the positive offsets. In addition, super-critical reflections arrive at small positive offsets, together with refracted waves. For the negative offsets super-critical reflections arrive at much larger distances from the source. An other interesting phenomenon is that the cusp in the wave fronts at t=1.7 and t=1.5, towards negative offsets, is super-critically reflected while there are still no refracted waves.

From these examples we learn that in real earth situations, with multiple layers for which we can expect various types and various degrees of anisotropy, a direct recording of anisotropy cusps requires specific conditions. The triplication area shrinks when the wave field propagates into a new layer with different anisotropy (or isotropy). To record it, the receivers should be close enough to the layer that caused the cusps. Anisotropy cusps can also be masked in reflected waves because of asymmetrical reflection.
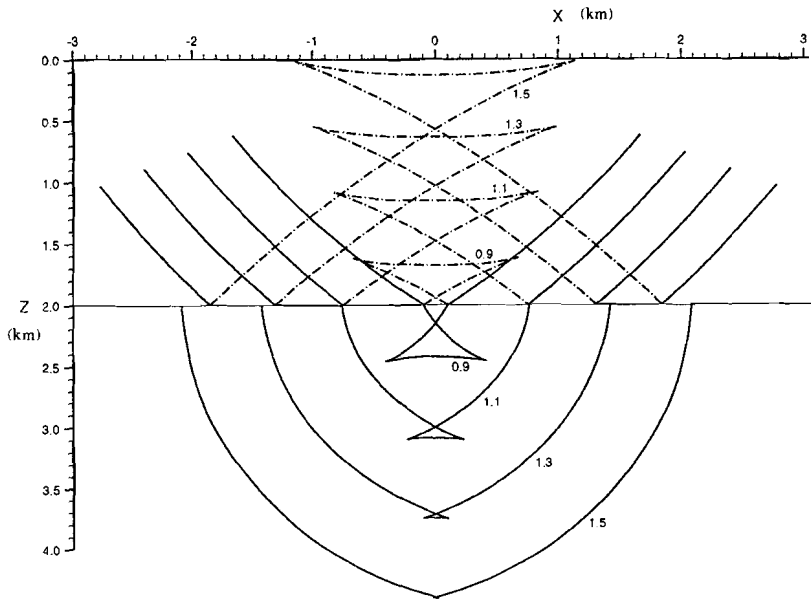
Fig. 2.18 As in Fig. 2.15, reflected wave fronts dashed, t=0.9, 1.1, 1.3 and 1.5 s.
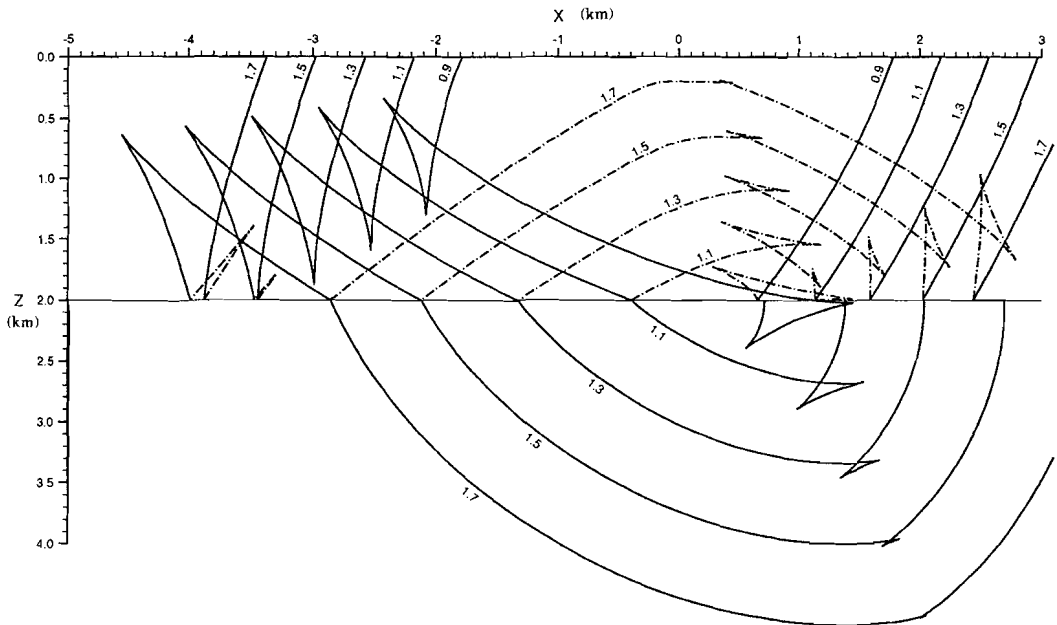
Fig. 2.19 As in Fig. 2.18, with symmetry axis at 20° against the vertical, t = 0.9, 1.1, ..., 1.7 s

Appendix 2A: Anisotropic media with hexagonal symmetry

I consider the special case of anisotropy with hexagonal symmetry. This type of anisotropy results from, for example, fine parallel layering or parallel microcracks. The symmetry implies that the characteristic surfaces are rotationally symmetrical around an axis. The direction dependence of velocity, slowness and polarization is only a dependence on the angle between propagation direction and this axis of rotation symmetry.

The elasticity tensor

An alternative way of expressing Hooke's law (see (2.3)) is to write stress and strain as 6-arrays and to relate them by a 6x6 array of stiffnesses or compliances. The suffices of the elements of this 6x6 array are related to the 4-suffix tensor elements in the following way (known as the Voigt notation):

c_{mn} <---> c_{ijkl}

m (n) <---> ij (kl)

m (n)	ij (kl)
1	11
2	22
3	33
4	23, 32
5	13, 31
6	12, 21

The same relationship holds for the suffix of stress- and strain elements in the 6-array notation and the suffices of stress- and strain tensor elements.

Hooke's law written in this alternative way is

$$\sigma_m = c_{mn}\, \varepsilon_n \qquad\qquad (2A.1)$$

with the provision that $\varepsilon = (\varepsilon_1, \varepsilon_2, \varepsilon_3, 2\varepsilon_4, 2\varepsilon_5, 2\varepsilon_6)$, see Musgrave.

In this new notation the elasticity tensor is, with respect to x_1-x_2-x_3 coordinates and the x_3-axis the axis of rotation symmetry,

$$
\underline{\underline{C}} = \begin{pmatrix}
c_{11} & c_{12} & c_{13} & 0 & 0 & 0 \\
c_{12} & c_{11} & c_{13} & 0 & 0 & 0 \\
c_{13} & c_{13} & c_{33} & 0 & 0 & 0 \\
0 & 0 & 0 & c_{44} & 0 & 0 \\
0 & 0 & 0 & 0 & c_{44} & 0 \\
0 & 0 & 0 & 0 & 0 & c_{66}
\end{pmatrix}
\tag{2A.2}
$$

with $2\,c_{66} = c_{11} - c_{12}$

Slownesses

We choose the slowness vector to be in the x_1-x_3 plane, hence $s_2 = 0$. With (2A.2), equation (2.13) becomes

$$
(c_{11}\,s_1{}^2 + c_{44}\,s_3{}^2 - \rho)\alpha_1 + (c_{13} + c_{44})s_1 s_3 \alpha_3 = 0 \tag{2A.3a}
$$

$$
(c_{66}\,s_1{}^2 + c_{44}\,s_3{}^2 - \rho)\alpha_2 = 0 \tag{2A.3b}
$$

$$
(c_{13} + c_{44})s_1 s_3 \alpha_1 + (c_{33}\,s_3{}^2 + c_{44}\,s_1{}^2 - \rho)\alpha_3 = 0 \tag{2A.3c}
$$

One solution can immediately be found by taking $\alpha_1 = \alpha_3 = 0$. The wave is polarised perpendicular to the propagation plane, the x_1-x_3 plane. The slowness surface of this wave mode, called the S1-wave, is an ellipse:

$$
c_{66}\,s_1{}^2 + c_{44}\,s_3{}^2 - \rho = 0 \tag{2A.4}
$$

Note that the criterion of polarization is used here for the nomenclature of the wave modes.

The two remaining solutions, referred to as S2- and P-wave, are polarised in the x_1-x_3 plane since they must be perpendicular to the polarization of the S1-wave. The eikonal equation (2.16) for these solutions reads:

$$
0 = (c_{11}\,s_1{}^2 + c_{44}\,s_3{}^2 - \rho)\,(c_{33}\,s_3{}^2 + c_{44}\,s_1{}^2 - \rho) - ((c_{13} + c_{44})s_1 s_3)^2 \tag{2A.5}
$$

With the new variables

$$a = c_{44}c_{33} \qquad\qquad\qquad (2A.6a)$$

$$b = (c_{13}+c_{44})^2 s_1^2 - c_{44}(c_{44}s_1^2 - \rho) - c_{33}(c_{11}s_1^2 - \rho) \qquad (2A.6b)$$

$$d = (c_{11}s_1^2 - \rho)(c_{44}s_1^2 - \rho) \qquad\qquad (2A.6c)$$

(2A.5) becomes

$$0 = a\, s_3^4 - b\, s_3^2 + d$$

$$= a \left[s_3^2 - \frac{b}{2a} + \frac{(b^2 - 4ad)^{1/2}}{2a} \right] \left[s_3^2 - \frac{b}{2a} - \frac{(b^2 - 4ad)^{1/2}}{2a} \right] \qquad (2A.7)$$

The zero solution of the term between the first pair of brackets defines the slowness of the faster wave mode, the P-wave. The term between the second pair of brackets determines the slowness of S2.

Along the symmetry axis, x_3, the slownesses are $(\rho/c_{44})^{1/2}$ for S1 and S2 and $(\rho/c_{33})^{1/2}$ for P.

Along x_1, the slownesses are $(\rho/c_{66})^{1/2}$ for S1, $(\rho/c_{44})^{1/2}$ for S2 and $(\rho/c_{11})^{1/2}$ for P.

Polarizations

The polarization vector for wave mode S1 is

$$\alpha = (0, 1, 0) \qquad\qquad\qquad (2A.8)$$

and thus this solution has a true transverse displacement. The polarizations for the S2- and the P-wave, $(\alpha_1, 0, \alpha_3)$, follow immediately from equations (2A.3a) and (2A.3c):

$$\alpha_1/\alpha_3 = \frac{-(c_{13} + c_{44})\, s_1\, s_3}{c_{11}s_1^2 + c_{44}\, s_3^2 - \rho} \qquad\qquad (2A.9)$$

with the understanding that, because of the mutual orthogonality of the displacements, $\alpha^{S2} = \alpha^{P} \pm \pi/2$.

Along the directions of symmetry, i.e. the x_1- axis and the x_3-axis, α is parallel or perpendicular to these directions. Thus in the symmetry directions the waves are truly transverse and truly longitudinal.

Ray velocities

The ray velocity is derived from the expression (see 2.52)

$$g_i = (\delta F/\delta s_i)/(s_j \, \delta F/\delta s_j) \qquad (2A.10)$$

With F= 0 given by (2A.4), we obtain for S1:

$$g_1 = (c_{66}/\rho) \, s_1 \qquad (2A.11)$$

$$g_3 = (c_{44}/\rho) \, s_3 \qquad (2A.12)$$

and

$$(\rho/c_{66}) \, g_1{}^2 + (\rho/c_{44}) \, g_3{}^2 - 1 = 0 \qquad (2A.13)$$

Thus the wave surface for the wave polarised in the x_2 direction is an ellipse.

For wave modes S2 and P, F=0 is given in (2A.7). After elaborate but straightforward computations the result is

$$g_1 = e^{-1} s_1 \{2c_{11}c_{44}s_1{}^2 + (c_{11}c_{33} + c_{44}{}^2 - (c_{13} + c_{44})^2)s_3{}^2 +$$
$$- \rho(c_{11} + c_{44})\} \qquad (2A.14)$$

$$g_3 = e^{-1} s_3 \{2c_{33}c_{44}s_3{}^2 + (c_{11}c_{33} + c_{44}{}^2 - (c_{13} + c_{44})^2)s_1{}^2 +$$
$$- \rho(c_{33} + c_{44})\} \qquad (2A.15)$$

where

$$e = \rho\{(c_{11} + c_{44})s_1{}^2 + (c_{33} + c_{44})s_3{}^2 - 2\rho\} \qquad (2A.16)$$

Along the x_3-axis the ray velocities are $(c_{44}/\rho)^{1/2}$ for S1 and S2 and $(c_{33}/\rho)^{1/2}$ for P. In case of a cusp, type a (see next section), the S2 wave has two ray velocities in the x_3 direction: the larger velocity is $(c_{44}/\rho)^{1/2}$ and belongs to the reverse branch of the wave surface.

Along the x_1-axis the ray velocities are $(c_{66}/\rho)^{1/2}$ for S1, $(c_{44}/\rho)^{1/2}$ for S2 and $(c_{11}/\rho)^{1/2}$ for P. Again is it possible for the S2 wave to have a cusp in this direction (cusp type b, see next section) resulting in two velocities for the S2 wave mode: $(c_{44}/\rho)^{1/2}$ is the larger velocity belonging to the reverse branch of the wave surface.

Cusps

From (2A.7) we see that the P-wave and the S2-wave slowness surfaces form separate sheets. The inner sheet, the P-wave, has therefore no cusps since it is necessarily convex. The S2 wave surface can have cusps. Three types of cusps exist, all three in the vicinity of points where $\gamma = \beta$: along the symmetry axis, cusp type a, perpendicular to the symmetry axis, cusp type b, or, in an intermediate direction, $\gamma = \beta$ for $\tan^2(\beta) = (c_{13} + c_{11})/(c_{13} + c_{33})$, type c-cusp.

Along the symmetry axis and in the direction perpendicular to this, we have $S^2 (=s_1{}^2 + s_3{}^2) = \rho/c_{44}$. Therefore a requirement for type a-cusps and type b-cusps to occur is $S^2 > \rho/c_{44}$. According to (2A.7) this is the case when $E < 0$ with $E = (c_{11} - c_{44})(c_{33} - c_{44}) - (c_{13} + c_{44})^2$. A requirement for cusp c-types to occur is the condition $E > 0$. Cusp type c cannot simultaneously occur with cusp type a and/or type b.

In between the 2 cuspidal edges $\delta\gamma/\delta\beta < 0$. For cusp a-type this condition reads

$$c_{11}(c_{33} - c_{44}) - (c_{13} + c_{44})^2 < 0, \qquad\qquad (2A.17)$$

for cusp type b it reads

$$c_{33}(c_{11} - c_{44}) - (c_{13} + c_{44})^2 < 0, \qquad\qquad (2A.18)$$

and for cusp type c it reads

$$G^2(G - 2E/c_{44}) - 4E^2/(Ac_{44})[G(1 + 0.75A/c_{44}) + E/c_{44}] < 0 \qquad (2A.19)$$

with $G = c_{11} + c_{33} + 2c_{13}$

and $A = c_{13} + c_{44}$

Reflection and transmission coefficients in transversely isotropic media

The term transverse isotropy is used for anisotropy of hexagonal symmetry with a vertical symmetry axis. We choose the x_3-axis to be vertical. The reflecting/transmitting interface is horizontal. Both the upper layer and the lower layer possess transverse isotropy. The x_1-x_3 plane is the sagittal plane.

At the interface the S1-wave does not interact with P and/or S2. This is because the polarization of S1 is perpendicular to the sagittal plane whereas both for P and S2 the polarizations are in this plane. This implies that matrix $\underline{E}$, see (2.60), can be split into two minor matrices: a 2x2 matrix for S1 and a 4x4 matrix for P and S2.

(i) S1-waves

For S1-waves the displacement-stress vector is

$$\underline{W} = (u_2, \sigma_{23})^T \tag{2A.20}$$

Because

$$\sigma_{23} = c_{44}\,\delta_3 u_2 \tag{2A.21}$$

if follows that

$$\underline{E} = \begin{bmatrix} 1 & 1 \\ i\omega c_{44}s_3 & -i\omega c_{44}s_3 \end{bmatrix} \tag{2A.22}$$

Note that s_3, the vertical slowness, is a function of the horizontal slowness s_1 (see (2A.4)):

$$s_3 = (\rho/c_{44} - s_1^2\, c_{66}/c_{44})^{1/2} \text{ for } s_1^2 < \rho/c_{66}$$

and $\tag{2A.23}$

$$s_3 = i(\, s_1^2\, c_{66}/c_{44} - \rho/c_{44})^{1/2} \text{ for } s_1^2 > \rho/c_{66}$$

The vertical slowness is either real (homogeneous waves) or imaginary (inhomogeneous waves).

For an incident S1-wave with unit amplitude, equation (2.62) reads

$$\underline{E}_a \begin{bmatrix} 1 \\ r_{S1} \end{bmatrix} = \underline{E}_b \begin{bmatrix} t_{S1} \\ 0 \end{bmatrix} \tag{2A.24}$$

Subscript a refers to the upper layer, containing the incident and reflected wave, subscript b refers to the lower layer. This gives for the reflection coefficient r_{S1}

$$r_{S1} = \{(c_{44}s_3)_a - (c_{44}s_3)_b\} / \{(c_{44}s_3)_a + (c_{44}s_3)_b\} \qquad (2A.25)$$

The transmission coefficient is

$$t_{S1} = (2c_{44}s_3)_a / \{(c_{44}s_3)_a + (c_{44}s_3)_b\} \qquad (2A.26)$$

I re-write (2A.25) to illustrate the differences between the reflection coefficients for isotropic layers and those for transversely isotropic layers. Let V_x be the horizontal phase velocity $(c_{66}/\rho)^{1/2}$ and V_z the vertical phase velocity $(c_{44}/\rho)^{1/2}$. Then with $B = (\rho V_z(1-V_x s_1^2))^{1/2}$ equation (2A.25) becomes:

$$r_{S1} = (B_a-B_b) / (B_a + B_b) \qquad 2A.27)$$

For normal incidence, $s_1 = 0$, the reflection coefficient depends on the products of density and vertical velocity. The reflection coefficient is constant for all angles of incidence if the horizontal velocities of upper and lower layer are equal. In Fig. 2.20 some examples are shown. Changing the difference between horizontal and vertical velocity results in a change of the horizontal slowness (or angle of incidence) at which the sign reversal occurs. Or it results in the absence of such a reversal. This latter, however, is not characteristic for anisotropy since the reversal can also be absent in case of isotropic layers, for example if $V_b<V_a$ and $\rho_b V_b > \rho_a V_a$.

(ii) P- and S2-waves

The displacement-stress vector is

$$W = (u_1, u_3, \sigma_{13}, \sigma_{33})^T \qquad (2A.28)$$

The relationship between stresses and displacements is

$$\sigma_{13} = c_{44} (\delta_1 u_3 + \delta_3 u_1) \qquad (2A.29)$$

$$\sigma_{33} = c_{13} \delta_1 u_1 + c_{33} \delta_3 u_3 \qquad (2A.30)$$
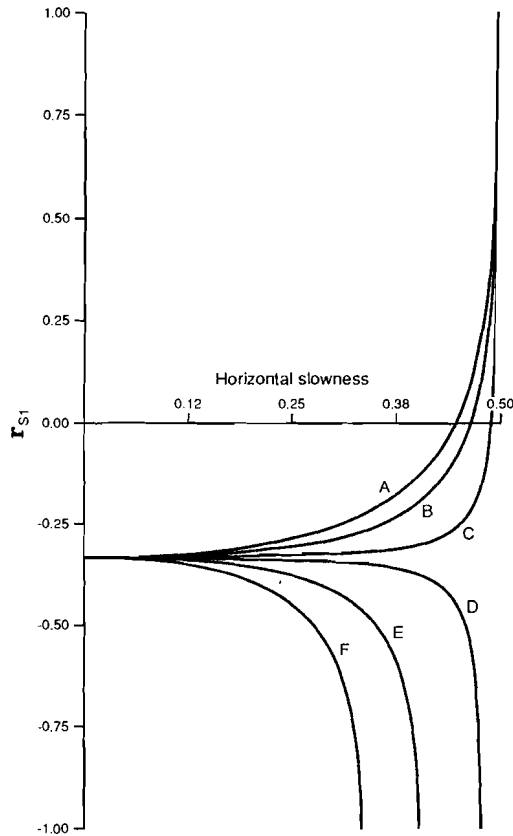
Fig. 2.20 S1 wave reflection coefficients. Upper layer transversely isotropic, vertical velocity=1, horizontal velocity is 1 (curve A), 1.5 (curve B), 1.9 (curve C), 2.1 (curve D), 2.5 (curve E) and 3.0 (curve F) respectively. Lower layer is isotropic, velocity =2. The layers have equal density.

The calculation of $\underline{E}$ is split into two parts. First the expression for the depth derivatives of displacements and stresses is written in the form

$$\delta_3 \underline{W} = \underline{A}\, \underline{W} \qquad\qquad (2A.31)$$

in which $\underline{A}$ is calculated with (2A.3), (2A.29) and (2A.30). Next the eigenvalues and eigenvectors of $\underline{A}$ are calculated, because if ψ is an eigenvalue and $\underline{v}$ the associated eigenvector, then a solution of (2A.31) is

$$\underline{W} = \underline{v}\, \exp[\psi\, x_3] \qquad\qquad (2A.32)$$

The general solution for $\underline{W}$ can be written as a linear combination of all solutions of the type in (2A.32). This is similar to writing the solution for $\underline{W}$ in the notation given in (2.59), in which the columns of $\underline{E}$ consist of the eigenvectors of $\underline{A}$.

The result is

$$E = \begin{pmatrix} \zeta p & \chi \eta & E_{11} & E_{12} \\ p^2\zeta\kappa ea & p\chi \eta^2 eb & -E_{21} & -E_{22} \\ i\omega p c_{44}\zeta\kappa[1+p^2 ea] & i\omega c_{44}\eta^2\chi[1+p^2 eb] & -E_{31} & -E_{32} \\ i\omega p^2\zeta[\kappa^2 c_{33}ea+c_{13}] & i\omega p\chi\eta[\eta^2 c_{33}eb+c_{13}] & E_{41} & E_{42} \end{pmatrix} \quad (2A.33)$$

with

$p = s_1$, the horizontal slowness or ray parameter

$a = (-p^2 c_{44} + \rho - \kappa^2 c_{33})^{-1}$

$b = (-p^2 c_{44} + \rho - \eta^2 c_{33})^{-1}$

$e = -c_{44} + c_{33}$ $\qquad\qquad\qquad\qquad\qquad\qquad (2A.34)$

and

$\kappa = s_{3;P}(p)$, the vertical P-wave slowness,

$\eta = s_{3;S2}(p)$, the vertical S2-wave slowness,

$\zeta = V_P(p)$, the P-wave phase velocity, $\qquad\qquad\qquad (2A.35)$

$\chi = V_{S2}(p)$, the S2-wave phase velocity, all as a function of ray parameter p. Again, the vertical slowness can be real or imaginary.

The method described above to calculate reflection and transmission coefficients is computationally attractive because the inverse of $\underline{E}$, needed to solve equations of the type (2.62), can be derived explicitly. In fact $\underline{E}^{-1}$ is

$$E^{-1} = \begin{pmatrix} q\,E_{42} & -y\,E_{32} & y\,E_{22} & -q\,E_{12} \\ -q\,E_{41} & y\,E_{31} & -y\,E_{21} & q\,E_{11} \\ E_{11}^{-1} & -E_{12}^{-1} & -E_{13}^{-1} & E_{14}^{-1} \\ E_{21}^{-1} & -E_{22}^{-1} & -E_{23}^{-1} & E_{24}^{-1} \end{pmatrix} \quad (2A.36)$$

with

$$q = 0.5 \, (E_{11}E_{42} - E_{12}E_{41})^{-1}$$

and   (2A.37)

$$y = 0.5 \, (E_{31}E_{22} - E_{32}E_{21})^{-1}.$$

Chapter3

Thin layers and anisotropy

Abstract

   In the quasi-static or long-wavelength approximation a set of fine layers is effectively anisotropic. We analyse this equivalence for a periodically layered sequence, where the layers have finite thicknesses. The condition that the period thickness must be small compared to the seismic wavelength is further specified. The condition for the period thickness depends on the properties of the constituent layers and on the direction of wave propagation. Any finite layer thickness results in dispersion, except for the special direction where the reflection coefficient is zero. If the layers are thin enough, which means the dispersion is less than 0.5%, the layer sequence is effectively homogeneous and anisotropic. In that case the number of periods in the sequence is not relevant. The attenuation resulting from this small dispersion can still be significant.

3.1 <u>Introduction</u>

A set of layers is homogeneous and anisotropic for seismic waves with wavelengths large compared to the thickness of this set of layers. This is known since the early work of Bruggeman (1937), Riznichenko (1949), Postma (1955), Rytov (1956), Helbig (1956, 1958) and Backus (1962). The majority of sedimentary sequences consist of by fine layers, with layer thicknesses that are much smaller than the seismic wavelength. Hence, one can expect anisotropy in sedimentary rocks to be the rule rather than the exception. An understanding of the equivalence between fine layering and anisotropy is therefore of relevance. From well log data, sonic and density logs, we can then theoretically compute the anisotropy. This computed anisotropy is an estimate if the shear velocities have to be estimated. Also, the fine layering on a scale smaller than the sampling rate of the logs is not seen and thus not accounted for. But despite of these shortcomings it is worth computing at least a part of the total anisotropy. With this "known" part included in the modelling, the remaining anisotropy can be better interpreted.

The equivalence between fine layering and anisotropy is valid in the long-wavelength limit, but what if the wavelength is not infinitely long? How thin must a set of layers be to be effectively homogeneous and anisotropic? And is this 'maximum thickness' dependent on the layer properties or on the wave propagation direction? The answer to these questions has to be known if one wants to replace the finely sampled depth model obtained from well logs by its equivalent anisotropic model with thicker homogeneous units (Hsu et al. 1988). A choice has to be made for the length l' over which the appropriate averaging of the log readings takes place. It is obvious that an infinitely small l', as prescribed by the theory, does not result in the objective of thicker units. By using a finite l' the equivalence is violated and it is desirable to have an understanding for the severity of this violation.

Most theoretical studies on how fine layering results in anisotropy (Riznichenko 1949, Postma 1955, Helbig 1956, Backus 1962) use the long-wavelength approximation. They make use of the property that the stress-strain state in a volume element small compared to the wavelength is approximately homogeneous. An alternative way is to first solve the wave equation for the

model and then take the low frequency limit. This was done by Rytov (1956) and Helbig (1984). Rytov looked at the wave field in a periodic structure consisting of two distinct media. He obtained very complex mathematical expressions. He therefore restricted himself in the final discussion to the determination of the asymptotic elastic parameters for specific propagation directions. He showed that these were identical to those determined with quasi-static approximations. Helbig (1984) considered a periodically layered medium with two constituents and used propagator matrices to derive the dispersion equation for SH-waves. He showed that a not long enough wavelength results in dispersion. In the evaluation of his results he restricted himself to numerical tests. His conclusion that the long-wavelength approach is strictly valid for wavelengths larger than three times the spatial period of layering is based on the models he used.

All workers before Backus (1962) derived their theory for periodic models. Backus showed that media containing layers of two or more kinds of rock when there is no vertical periodicity of properties, are effectively anisotropic over a distance l', where l' is small compared to the seismic wavelength. This means that a set of thin layers without periodicity is homogeneous and anisotropic over each distance l', and that the total set is effectively inhomogeneous and anisotropic. So it does not require periodicity to be effectively anisotropic. Lack of vertical periodicity results in inhomogeneity, i.e. the anisotropy is depth dependent.

Still, many authors studying layer-induced anisotropy consider periodic models (for instance Bachman 1979, Berryman 1979, Levin 1979, 1980, Schoenberg 1983, 1988, Helbig 1984). One apparent reason for this is that one does not want the model to be inhomogeneous. To study wave properties one likes a model with a thickness of several wavelengths. Hence, to keep it effectively homogeneous, one needs to repeat the layers with total thickness l' several times. Periodicity in the models is used in so many publications that one might (erroneously) think that it is a necessary condition for producing anisotropy. For instance, the terms PTL (Periodic Thin Layering) anisotropy (Bush and Crampin 1988) and TPM (Thinly layered Periodic media) anisotropy (Lyakhovitskiy 1984) have been used to refer to layer induced anisotropy. Others (Levshin and Ratnikova 1984) have stated: "The S-wave pulse transmitted through an arbitrary shuffle of thin layers has no special qualitative differences from one in a periodic thin layered model, as the same kind of splitting is observed. However, this non-periodic structure cannot be effectively described as

transversely isotropic".

The objective of this chapter is to study the equivalence between fine layering and anisotropy. The discussion is not restricted to infinitely thin layers but also deals with thin layers of finite thickness. An expression for the similarity between layering and anisotropy shows the dependence on the elastic parameters, the direction of wave propagation and the dependence on frequency. The model that is used is periodically layered. But, provided the period thickness is small, the response is independent on the number of periods. This emphasizes that periodicity is not a necessary condition for producing anisotropy. It implies for instance that also the extremest case of one single thin layer imbedded in a thick homogeneous medium results in effective anisotropy; a wave propagating through this model will have all the anisotropic characteristics.

Following Helbig, I use the technique of propagator matrices to compute the wave field in a periodically layered medium. The discussion is restricted to shear waves. More specifically, it is restricted to S1-waves, which are uncoupled from the P-waves. Also, the model is confined to two constituents. This is done to limit the complexity of the problem. The results, however, provide the insight to predict the results for more complex models and for the P- and S2-waves.

The propagator matrix for a sequence of layers consisting of N periods, each of thickness d, is expanded around $d/\lambda = 0$, where λ is the seismic wavelength. The first order terms form the propagator matrix of the anisotropic replacement medium. The higher order terms account for the effects of finite layer thicknesses. I use a model that consists of an anisotropic half-space on top of the sequence of layers with underneath another anisotropic half-space. This model is refered to as the ASA model. The reflectivity of this ASA model expresses the similarity between the sequence and its long-wavelength equivalent anisotropic medium. The reflectivity indicates whether the sequence of layers is effectively anisotropic, dispersive or inhomogeneous.

3.2 The seismic response of a sequence of thin layers

Propagator Matrix

Let us consider an anisotropic medium with hexagonal symmetry. I choose the coordinate system such that the axis of rotation symmetry is vertical i.e. along the x_3 - axis. For sake of convenience the x_3 - axis will be referred to as the z-axis. Wave propagation is in the x_1 - x_3 plane.

The propagator matrix $\underline{P}$ relates the displacement-stress vector $\underline{W}$ at depth z_1 to the displacement-stress vector at depth z_2 (Gilbert and Backus 1966, Aki and Richards 1980):

$$\underline{W}(z_2) = \underline{P}(z_2,z_1) \, \underline{W}(z_1) \tag{3.1}$$

where for S1-waves the displacement-stress vector is

$$\underline{W} = \begin{bmatrix} u_2 \\ \sigma_{23} \end{bmatrix} \tag{3.2}$$

with u_2 the displacement and σ_{23} the stress component acting on the plane $x_3=0$ in the x_2 direction. Because of continuity of displacement and stress across the interface (the boundary conditions) the propagator matrix for a stack of layers is formed by the product of the propagator matrices of all the layers:

$$\underline{P}(z_{N+1},z_1) = \prod_{i=1}^{N} \underline{P}(z_{i+1},z_i) \tag{3.3}$$

The propagator matrix for S1-waves of a homogeneous transversely isotropic medium between depths z_1 and z_2 is

$$\underline{P}(z_2,z_1) = \begin{bmatrix} \cos(\phi) & \sin(\phi)/m \\ -m\sin(\phi) & \cos(\phi) \end{bmatrix} \tag{3.4}$$

with

$$\phi = \omega \, s_3 \, (z_2 - z_1) \tag{3.5}$$

$$m = \omega \, c_{44} \, s_3 \tag{3.6}$$

where ω is the angular frequency, s_3 the vertical component of the slowness, and c_{44} an element of the elastic stiffness tensor. The slowness is determined by (see (2A.4))

$$(c_{66}/\rho) \, s_1^2 + (c_{44}/\rho) \, s_3^2 = 1 \tag{3.7}$$

The periodic model

Consider a periodically layered model as shown in Fig. 3.1. Each period consists of two layers a and b. Layer a has thickness d_a and layer b has thickness d_b. The period thickness d is therefore

$$d = d_a + d_b \tag{3.8}$$

Parameter h is the thickness fraction of layer a.

$$h = d_a / d \tag{3.9}$$

and thus

$$d_b = (1-h)d \tag{3.10}$$

The model consists of N periods in total. The total thickness, H, is therefore N.d. According to equation (3.3) the propagator matrix for this model is

$$\underline{P}(z_{N+1}, z_1) = (\underline{P}_b \underline{P}_a)^N \tag{3.11}$$

with $\underline{P}_a$ the propagator matrix for layer a and $\underline{P}_b$ for layer b.

The Objective

The objective is to find an expression for $(\underline{P}_b \underline{P}_a)^N$. In Appendix 3A the full derivation is given that leads to the desired expression. Here I outline the major
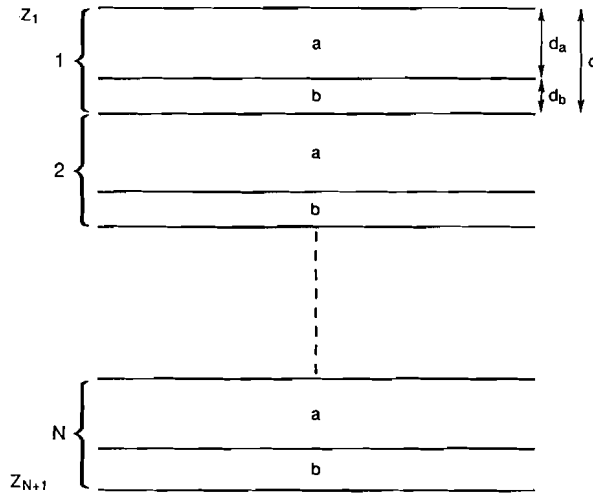
Fig. 3.1 The periodic model

steps of this derivation. For sake of convenience I have derived the expressions for isotropic layers a and b. They can however easily be updated to anisotropic constituents a and b by replacing shear modulus μ by c_{44}.

First I write $(\underline{P}_b \underline{P}_a)$ as the sum of the identity matrix $\underline{I}$ multiplied by a scalar and a matrix called $\underline{J}$. I then apply Newton's binomium to obtain an expression for $(\underline{P}_b \underline{P}_a)^N$ as the sum of $\underline{I}$ multiplied by a scalar, say A_1, and $\underline{J}$ multiplied by another scalar, A_2, (equation 3A.18 of the Appendix)

$$(\underline{P}_b \underline{P}_a)^N = A_1 \underline{I} + A_2 \underline{J} \qquad (3.12)$$

Both scalars A_1 and A_2 contain expressions that are to be taken to the N-th power. Next I prove that equation (3.12) only converges for N to infinity if the total sequence thickness is kept constant. Since the total thickness equals N.d this means that $(\underline{P}_b \underline{P}_a)^N$ converges if the period thickness d goes to zero. $(\underline{P}_b$ It converges to the propagator matrix of the anisotropic replacement medium. This

proves the validity of the long-wavelength approximation as used by Backus and others.

By writing the expressions in scalars A_1 and A_2 as series expansions, I obtain (equation 3A.40 of the Appendix)

$$(\underline{P}_b \, \underline{P}_a)^N = \underline{P}_{repl} + \underline{\Delta P} \tag{3.13}$$

with $\underline{P}_{repl}$ the propagator matrix of the anisotropic replacement medium, and $\underline{\Delta P}$ the matrix that represents the difference between the seismic response of the sequence of layers and the response of the anisotropic replacement layer

$$\underline{\Delta P} = \begin{bmatrix} \Omega_1 N^{-1} + \Omega_4 N^{-2} + O(N^{-3}) & -\Omega_3 N^{-2} + O(N^{-4}) \\ \Omega_2 N^{-2} + O(N^{-4}) & -\Omega_1 N^{-1} + \Omega_4 N^{-2} + O(N^{-3}) \end{bmatrix} \tag{3.14}$$

Ω_1, Ω_2, Ω_3 and Ω_4 are functions of the elastic parameters of layers a and b (shear modulus and density), the thickness of these layers and the wave propagation direction. Their explicit expressions are given in Appendix 3A. Note that the elements of $\underline{\Delta P}$ go to zero for infinite N, or, what is equivalent, for the period thickness approaching zero.

Our interest is the case where the layers are not infinitely thin. It is difficult to interpret $\underline{\Delta P}$ in terms of how its elements affect the wavefield. The elements of a propagator matrix, and thus of $\underline{\Delta P}$, have different dimensions. It is not obvious how each element affects the seismic response. We would like to have a single parameter that expresses the difference between the layered model and the anisotropic model. Therefore I introduce the ASA-model.

3.3 The effective medium for a sequence of fine layers

ASA-model

The ASA-model (Anisotropic-Sequence-Anisotropic) consists of the layered

sequence in between two anisotropic half-spaces, see Fig. 3.2. The anisotropy of the half-spaces equals the anisotropy of the sequence in the long wavelength approximation. By considering an incident wave from the upper half-space into the sequence and computing the wavefield that is reflected back into the upper half-space, we have a measure for the inhomogeneity of the whole model. If the sequence of layers is effectively anisotropic the incident wave will propagate without any loss of energy into the lower half-space. The weaker the resemblance with an anisotropic medium, the more energy is reflected.
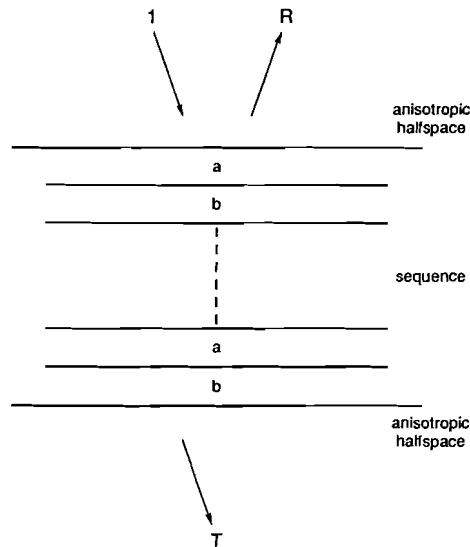

Fig. 3.2 The ASA model

Reflected field

The search for solutions of the elastic wave equation in a homogeneous medium in terms of plane waves can lead to a matrix notation for displacements and stresses (Aki and Richards 1980), that can be written as

$$\underline{W} = \underline{E}\,\underline{J}\,\underline{F} \qquad\qquad\qquad (3.15)$$

In the S1-wave case and an anisotropic medium (hexagonal symmetry), we have

$$\underline{E} = \begin{bmatrix} 1 & 1 \\ -im & im \end{bmatrix},$$

(3.16)

$$\underline{J} = \exp[-i\phi] \, \underline{I}$$

(3.17)

with ϕ and m defined in (3.5) and (3.6).

$\underline{F}$ is a vector whose elements represent the relative amplitudes of down- and upgoing field (weighting factors). For the ASA-model the incident field is scaled to amplitude 1, and the reflected field amplitude is denoted by R. We then have

$$\underline{F}(z_1) = \begin{bmatrix} 1 \\ R \end{bmatrix}$$

(3.18)

In the lower half-space no energy is propagating upwards and the downgoing field is denoted by T.

$$\underline{F}(z_N) = \begin{bmatrix} T \\ 0 \end{bmatrix}$$

(3.19)

If we define

$$\underline{Y} = \underline{E} \, \underline{J}$$

(3.20)

we thus have

$$\underline{W}(z_1) = \underline{Y}(z_1) \begin{bmatrix} 1 \\ R \end{bmatrix}$$

(3.21)

and

$$\underline{W}(z_N) = \underline{Y}(z_N) \begin{bmatrix} T \\ 0 \end{bmatrix}$$

(3.22)

If we now recall that

$$\underline{W}(z_N) = (\underline{P}_b \underline{P}_a)^N \, \underline{W}(z_1)$$

(3.23)

we can write

$$\underline{Y}(z_N) \begin{bmatrix} T \\ 0 \end{bmatrix} = (\underline{P}_b \underline{P}_a)^N \, \underline{Y}(z_1) \begin{bmatrix} 1 \\ R \end{bmatrix}$$

(3.24)

or

$$\begin{bmatrix} 1 \\ R \end{bmatrix} = \underline{Y}^{-1}(z_1) \ \{(\underline{P}_b \underline{P}_a)^N\}^{-1} \ \underline{Y}(z_N) \begin{bmatrix} T \\ 0 \end{bmatrix} \tag{3.25}$$

which, for simplicity, I write as

$$\begin{bmatrix} 1 \\ R \end{bmatrix} = \underline{A} \begin{bmatrix} T \\ 0 \end{bmatrix} \tag{3.26}$$

From (3.26) it follows that

$$R = A_{21}/A_{11} \tag{3.27}$$

I can without loss of generality take $z_1 = 0$ so that $\underline{J}(z_1)$ becomes the unit matrix and

$$\underline{Y}^{-1}(z_1) = 1/2 \begin{bmatrix} 1 & i/m_1 \\ 1 & -i/m_1 \end{bmatrix} \tag{3.28}$$

In this notation $m_1 = \omega \, c_{44} \, s_3$ of the upper half-space ($z < z_1$).

Note that the determinant of the propagator matrix is equal to 1 and thus in general

$$\underline{P}^{-1} = \begin{bmatrix} P_{22} & -P_{12} \\ -P_{21} & P_{11} \end{bmatrix} \tag{3.29}$$

When I now combine the equations given above, I obtain the expression for R:

$$R = \frac{P_{22} - \dfrac{m_N}{m_1} P_{11} + i(m_N P_{12} + \dfrac{P_{21}}{m_1})}{P_{22} + \dfrac{m_N}{m_1} P_{11} + i(m_N P_{12} - \dfrac{P_{21}}{m_1})} \tag{3.30}$$

where $m_1 = \omega \, c_{44} \, s_3$ of the upper half-space ($z < z_1 = 0$), $m_N = \omega \, c_{44} \, s_3$ of the lower half-space ($z > z_N$) and $\underline{P} = (\underline{P}_b \underline{P}_a)^N$.

Note that R is complex and frequency dependent. The propagator matrix for the sequence of layers is given in equations (3.13) and (3.14). Taking for each element of ΔP only the first term and ignoring the higher order terms leads to

$$R = \sin(\phi_{repl}) \, A \, B^{-1} \tag{3.31a}$$

with

$$\phi_{repl} = \omega \, s_{3_{repl}} \, H, \tag{3.31b}$$

where $s_{3_{repl}}$ is the vertical slowness component in the anisotropic replacement medium,

$$A = \omega \, d \, s_{3_{repl}}^{-1} \{ \frac{\mu_b}{\mu_a} s_{3_b}^2 - \frac{\mu_a}{\mu_b} s_{3_a}^2 \} \, h(1-h) \{ 1 + i \, \omega \, d \, \frac{(1-h)^2 s_{3_b}^2 - h^2 s_{3_a}^2}{3 \, s_{3_{repl}}} \}$$

$$(3.31c)$$

$$B = 2 \cos(\phi_{repl}) + i \{ (\omega^2 d^2 \xi - 2) \sin(\phi_{repl}) + \frac{1}{3} \omega^3 d^3 N s_{3_{repl}} \, \xi \, \cos(\phi_{repl}) \}$$

$$(3.31d)$$

where

$$\xi = \frac{-1}{4 \, (s_{3_{repl}})^2} \left[\frac{h(1-h)}{\mu_a \mu_b} \right]^2 (\mu_b s_{3b} + \mu_a s_{3a})^2 (\mu_b s_{3b} - \mu_a s_{3a})^2 \tag{3.31e}$$

Condition for the validity of reflectivity R

The expression for R as given in equation (3.31) is an approximation since I abbreviated the elements of $\underline{\Delta P}$. Let us consider the second term of ΔP_{11} as well, i.e.

$$\Delta P_{11} = \Omega_1 N^{-1} + \Omega_4 N^{-2} \tag{3.32}$$

and let us assume that the expression for R is a good approximation if

$$\Omega_4 N^{-2} << \Omega_1 N^{-1} \tag{3.33}$$

Then, by inserting the expressions for Ω_1 and Ω_4 into this inequality, I find

$$h(1-h) \, N \, \omega^2 \, d^2 \, \frac{1}{12} \left| \frac{\mu_b}{\mu_a} s3_b{}^2 - \frac{\mu_a}{\mu_b} s3_a{}^2 \right| \ll 1 \tag{3.34}$$

which is equivalent to

$$h(1-h) \, N \, (\frac{d^2}{\lambda^2})(2\pi V)^2 \frac{1}{12} \left| \frac{\mu_b}{\mu_a} s3_b{}^2 - \frac{\mu_a}{\mu_b} s3_a{}^2 \right| \ll 1 \tag{3.35}$$

where λ is the wavelength in the anisotropic replacement medium and V the replacement velocity (for convenience the subscript "repl" is omitted in the annotation of wavelength and velocity in the replacement medium).

So, the condition for the validity of the expression for R can be read as

$$N \, (\frac{d^2}{\lambda^2}) \ll \text{constant}, \tag{3.36}$$

in which the constant depends on the elastic parameters of layers a and b, their thicknesses, and the direction of wave propagation.

Numerical testing of reflectivity R

Figure 3.3 illustrates the reflectivity of the ASA model, where the contrast in elastic properties of layers a and b is large. The reflectivity is computed in two ways: the curve annotated by 'true' is obtained after 2N matrix multiplications, the other curve is from the derived expression for the reflectivity (equation 3.31). The reflectivity is displayed versus the number of periods N. The total sequence thickness is kept constant. Therefore a larger number of periods N means a smaller period thickness d (and hence a smaller d/λ). According to the validity condition, equation (3.35), R is for this example valid for N>>57. The curves show that for N well above 57 the two curves indeed approach each other.

For small values of N the reflectivity strongly fluctuates, for intermediate values of N it varies more smoothly and for large N values the reflectivity is almost constant and slowly approaches zero. These characteristics of the curve correspond to three different effective media: for small N the sequence of layers is effectively inhomogeneous, for intermediate N values it is effectively
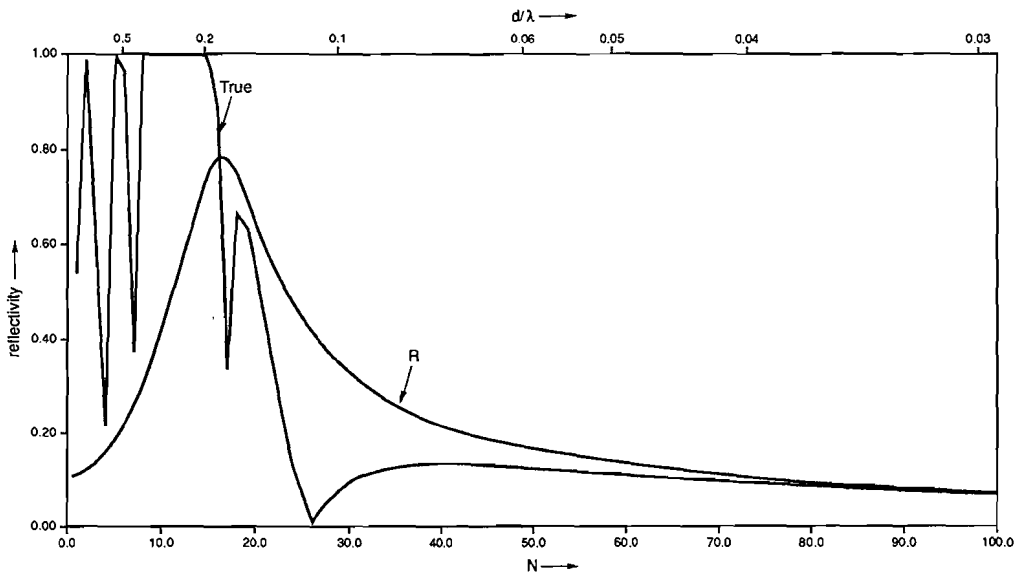
Fig. 3.3 The magnitude of the reflectivity of the ASA model as a function of the number of periods N. The reflectivity is either calculated by means of matrices multiplication ("true") or from equation (3.31) ("R"). The model parameters V_a = 1200 m/s , ρ_a = 2.4 g/cm^3 V_b = 500 m/s , ρ_b = 1.6 g/cm^3, H = 100 m, h = 0.5 , f = 17.6 Hz, λ = 34.2 m, s_1 = 0. According to (3.35) the approximation is valid for N>>57.

dispersive and for large N the sequence is effectively homogeneous and anisotropic.

Figure 3.4 is similar to Fig. 3.3, but the layers in the sequence have a smaller contrast. The validity condition here is that R is valid for N>>9. Compared to the previous example R is smaller for a given d/λ. It means that for smaller contrasts between the layers the period thickness can be larger to be still effectively homogeneous and anisotropic.
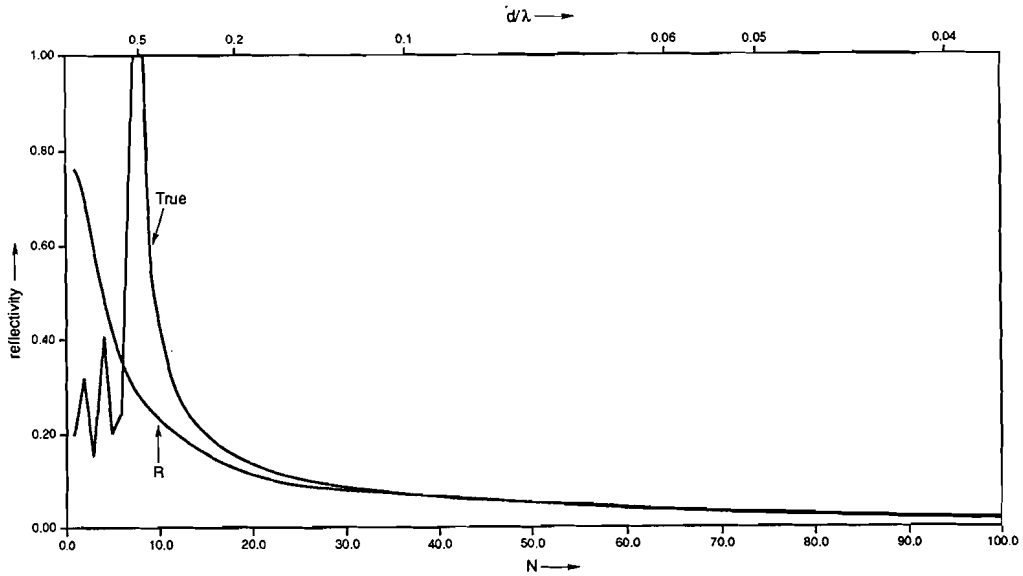
Fig. 3.4 The same as in Fig. 3.3, but now for V_a = 1200 m/s , ρ_a = 2.0 g/cm^3 V_b = 800 m/s , ρ_b = 2.0 g/cm^3, H = 200 m, h = 0.5 , f = 17.6 Hz, λ = 53.4 m, s_1 = 0. According to (3.35) the approximation is valid for N>>9.

Discussion on reflectivity R

The reflectivity of the ASA model is a measure for the difference in seismic response of the sequence of layers and its anisotropic replacement medium. The derived expression is an approximation since only the first two terms of each element of the sequence propagator matrix were used, where the propagator matrix was derived by means of a series expansion for d/λ approaching zero. If we replace ωd in (3.31) by $2\pi V d/\lambda$ we see that the nominator in the expression contains a $(d/\lambda)^3$ term. It is this term that contains the parameter N, the number of periods. Thus the dependence on the number of periods is only a higher order

effect. If we restrict to the first order terms, the expression for R simplifies to

$$R = \sin(\phi_{repl}) \, A \, B^{-1} \tag{3.37a}$$

$$A = 2\pi V \frac{d}{\lambda} \, (s_{3_{repl}})^{-1} \left| \frac{\mu_b}{\mu_a} s_{3_b}^{2} - \frac{\mu_a}{\mu_b} s_{3_a}^{2} \right| \, h \, (1\text{-}h) \tag{3.37b}$$

$$B = 2 \, (\cos(\phi_{repl}) - i \, \sin(\phi_{repl})) \tag{3.37c}$$

This shows that in the first order approximation the reflectivity is independent on the number of periods, and that it is linearly proportional to the ratio of period thickness d and wavelength λ.

For a homogeneous layer between two equal half-spaces constructive or destructive interference of the multiples in the layer occurs for specific wavelengths. For $\omega s_3 H = L\pi$ (L=1,2,3,etc.,) all reflections from the base of the layer are in phase, and 180° out of phase with the reflection from the top (see Appendix 3B). The total reflected energy is zero. For $\omega s_3 H = \frac{1}{2}\pi + L\pi$ (L=0,1,2,3,etc.,) the reflection from the top of the layer and the primary reflection from the base are in phase and the multiples alternating in phase and 180° out of phase. The amplitude of the reflected field is approximately twice the amplitude of the single ray reflected at the top of the layer. In the long-wavelength approximation the ASA model resembles a homogeneous layer in between two equal half-spaces and therefore the reflectivity has the $\sin(\phi_{repl})$ modulation (see Fig 3.5 and Fig 3.6).

Figures 3.7 and 3.8 illustrate the dependence on the direction of wave propagation. The angle of incidence is the angle between the vertical and the phase direction in the anisotropic half-space. Displayed are again the two curves "true" and "R". The dashed line, R', is $R/\sin(\phi_{repl})$.

The figures show that there is a strong angle dependence for the reflectivity. In a specific direction (in these examples just above 60 degrees) the reflectivity is zero. It means that there the sequence is exactly equal to a homogeneous anisotropic medium, despite the finite thickness of the layers. This phenomenon occurs when no multiples are generated in the sequence of layers, i.e. when the plane wave reflection coefficient is zero. This is discussed in the next section.
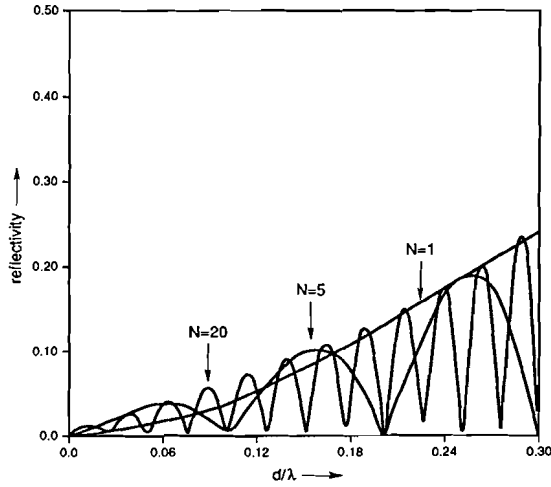
Fig. 3.5 The magnitude of the reflectivity of the ASA model as a function of d/λ. The three curves are for N=1, N=5 and N=20. The reflectivity is calculated with matrices multiplication. The model parameters are: V_a=1200 m/s, ρ_a=2.0 g/cm^3, V_b=800 m/s, ρ_b=2.0 g/cm^3

Fig. 3.6 The reflectivity magnitude, from matrices multiplication ("true") and according to equation (3.31) ("R") for model parameters: V_a=1200 m/s , ρ_a=2.0 g/cm^3 V_b=800 m/s , ρ_b=2.0 g/cm^3

Fig. 3.7 The reflectivity magnitude as a function of the angle of incidence. $V_a = 1200$ m/s , $\rho_a = 2.0$ g/cm^3 $V_b = 800$ m/s , $\rho_b = 2.0$ g/cm^3, H = 100 m, h = 0.5 , f = 17.6 Hz, $\lambda = 53.4$ m, N = 10. $R'=R/\sin(\phi_{repl})$
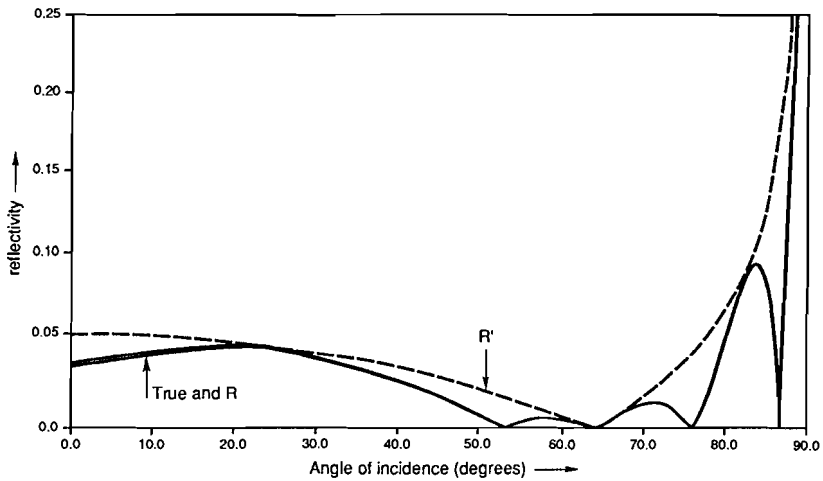
Fig. 3.8 As in Fig. 3.7, now for N = 20

The sequence reflectivity in terms of the intrinsic plane wave reflection coefficient

The underlying physical phenomenon of the effective homogeneity and anisotropy of a stack of thin layers is the interference of the many peg-leg multiples. As a measure for the effective homogeneity and anisotropy of the medium I used the sequence reflectivity. This reflectivity must therefore in some way be related to the peg-leg multiples. One of the parameters that affects multiple generation is the intrinsic reflection coefficient, i.e. the plane wave reflection coefficient between two individual layers. Therefore the objective is to express the sequence reflectivity in terms of the intrinsic reflection coefficient. The reflection coefficient for a wave incident from layer a on layer b is opposite to that for the wave incident from layer b on layer a. In our model of two distinct layers (a and b) the obvious choice is to use the absolute value of the reflection coefficient r.

$$r = \left| \frac{\mu_a\, s_{3_a} - \mu_b\, s_{3_b}}{\mu_a\, s_{3_a} + \mu_b\, s_{3_b}} \right| \qquad (3.38)$$

The sequence reflectivity is given in equation (3.37). Notice that we can write

$$\frac{V}{s_3} = \frac{\cos(\beta)}{s_3^2} \qquad (3.39)$$

where β is the angle between phase direction and the vertical. The reflectivity depends on the shear moduli of layers a and b and the vertical slownesses in these layers, but also on the vertical slowness in the anisotropic replacement medium. We can express this last quantity in terms of constituent quantities by using some of Backus' equations:

$$c_{44}\, s_{3_{repl}}^2 = h\, \mu_a\, s_{3_a}^2 + (1\text{-}h)\, \mu_b\, s_{3_b}^2 \qquad (3.40)$$

where

$$c_{44} = \left\{ \frac{h}{\mu_a} + \frac{(1\text{-}h)}{\mu_b} \right\}^{-1} \qquad (3.41)$$

From equations (3.37) and (3.39) - (3.41) we obtain

$$| R' | = \pi \, d/\lambda \, \cos(\beta) \, A/B \qquad\qquad (3.42a)$$

where

$$A = h(1-h) \left| \mu_b^2 s_{3_b}^2 - \mu_a^2 s_{3_a}^2 \right|, \qquad\qquad (3.42b)$$

$$B = ((1-h) \, \mu_a + h \, \mu_b)(h \, \mu_a \, s_{3_a}^2 + (1-h) \, \mu_b \, s_{3_b}^2) \qquad\qquad (3.42c)$$

and

$$R' = R/(\sin\phi) \qquad\qquad (3.42d)$$
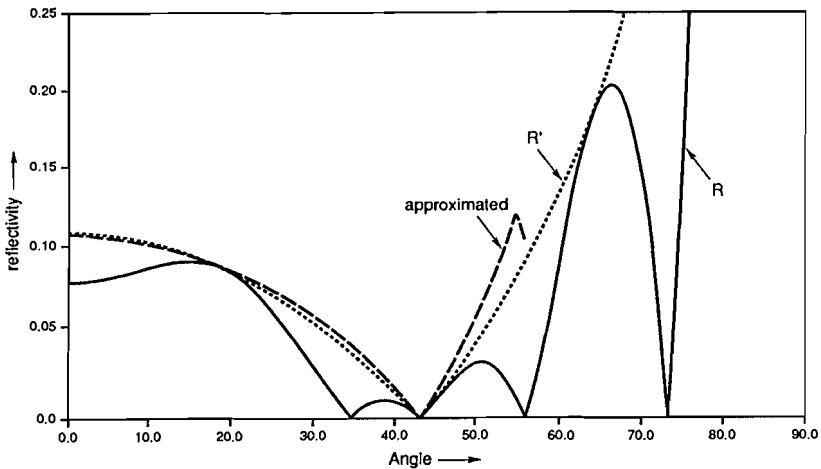
Fig. 3.9 Approximation for the reflectivity magnitude in terms of the intrinsic reflection coefficient.

Comparison of equations (3.38) and (3.42) shows that r and R' have the same zero-solutions. However, this comparison also shows that in general it is not possible to express R' in r. The reason is that the multiple interference not only depends on the layer contrast but also on the layer thicknesses. However, if we restrict ourselves to weak layer contrasts and moderate angles for β, or to be more precise, under the restrictions

$$\rho_a \cong \rho_b \qquad\qquad (3.43)$$

and

$$|V_b - V_a| << V_b + V_a \qquad\qquad (3.44)$$

we can derive

$$|R'| \cong \pi \, d/\lambda \, \cos(\beta) \, 4h(1-h) \, r \, \{1 - \frac{r^2 - r(4h-2)}{1 - r(4h-2)}\} \qquad (3.45)$$

This approximation becomes inaccurate for large angles of β, where the propagation angle in layer a or b is close to the critical angle (Fig. 3.9). In case layers a and b are equally thick (h=0.5) equation (3.45) reads

$$|R'_{h=0.5}| \cong \pi \, d/\lambda \, \cos(\beta) \, r(1-r^2) \qquad\qquad (3.46)$$

3.4 Examples

I use the reflectivity technique (Fuchs and Muller 1971) to generate some synthetic data in the tau-p domain.

The first example, Fig. 3.10, is to illustrate the weak dependence on the number of periods. The top figure is the tau-p response for a model with one single interface between an isotropic upper half-space and a transversely isotropic lower half-space. The seismic source is 50 meters above the interface in the isotropic half-space with a shear velocity of 1000 m/s. In the lower figures, a sequence is positioned between two isotropic half-spaces. The seismic response is compared with the response for the sequence replaced by its long-wavelength equivalent anisotropic medium. Note that $d/\lambda \cong 0.1$ For N=1 (the sequence consists of only one layer a and one layer b) there are no visible differences in response. This is also the case for N=5. If N becomes larger, e.g. N=10, we start to see small differences.

In an other example, Fig. 3.11, the sequence is again between two isotropic half-spaces. The seismic source is 25 meters above the sequence. The total thickness of the sequence is kept constant. Synthetics are computed for several
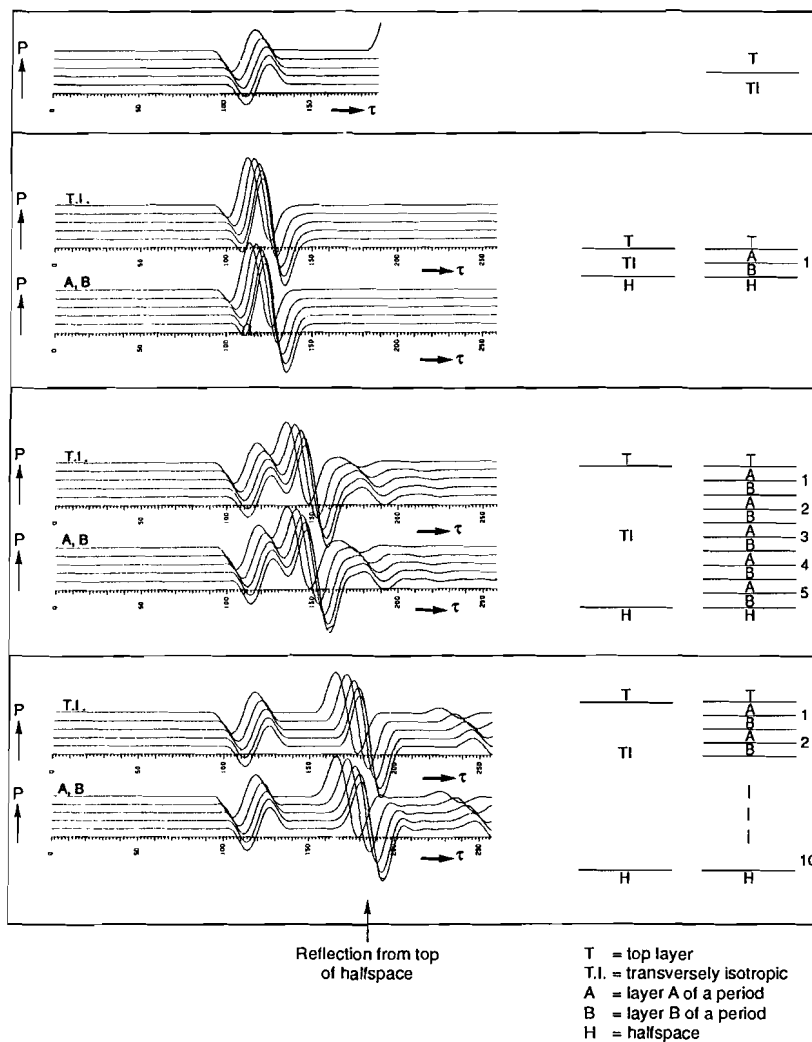
Fig. 3.10 Comparison between layered models and anisotropic models, showing the independence of the equivalence on the number of periods N. top-layer: V = 1000 m/s, ρ = 2.0 g/cm^3, thickness = 25 m , sequence a: V = 500, ρ = 1.6, b: V = 1250, ρ = 2.4,   h = 0.5, H = 40 m. half-space: V = 2000 ρ = 3.0

N-values. In this way we demonstrate the effectively inhomogeneous response, the dispersive response and the effectively homogeneous anisotropic response. In Fig. 3.11a the sequence contains one period and is clearly inhomogeneous. We see the individual reflections from respectively the top of layer a, the top of layer b and the bottom of layer b. This is no longer the case in Figs. 3.11c - 3.11h, where N is 5 and larger. For N=15, for example, we start seeing the sequence as one unit but with strongly dispersive reflections from top and bottom. Notice the dependence of the dispersion on the ray-parameter (angle of incidence). For $p \cong 7 * 10^{-4}$ s/m, the intrinsic reflection coefficient is zero. For all values of N this trace resembles the trace in the anisotropic case. For $p > 8.33 * 10^{-4}$ s/m the waves propagate super-critically in layers b. This means that the vertical slowness is imaginary and the amplitude decays exponentially during propagation. Super-critical waves in the anisotropic medium occur for $p > 9.8 * 10^{-4}$ s/m . Hence, for 8.33<p<9.8 and small d/λ values, the inhomogeneous waves in layers "b" have a real contribution to the effective medium, where this effective medium contains homogeneous waves.

Figure 3.12 is an example for S2-waves (the source emits only S2-waves). The recorded signal is the total amplitudes of S2- and P-waves. The sequence is a simplified model for a coal sequence (alternating coal and other rock) in a former mining area in the Netherlands (Veltmeyer and de Voogd 1982). In the top figure we see the S2 reflection from the top of the sequence, a S2-to-P converted wave, converted at the sequence base, and the S2 reflection from the sequence base (and weaker their multiples). The average seismic frequency in the upper figure is lower than that in the lower figure. In the upper figure d/λ $\cong$ 0.16 for the S2-wave and d/λ $\cong$ 0.09 for the P-wave. The constituent layer contrast between rock and coal is larger than in the example shown in Fig. 3.11.
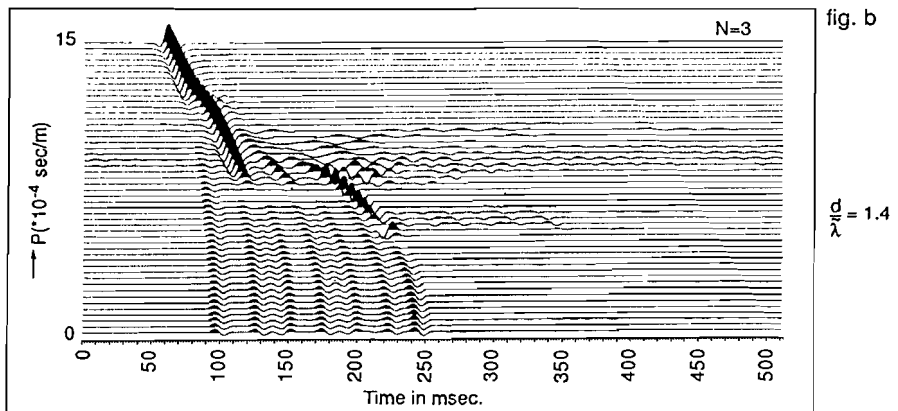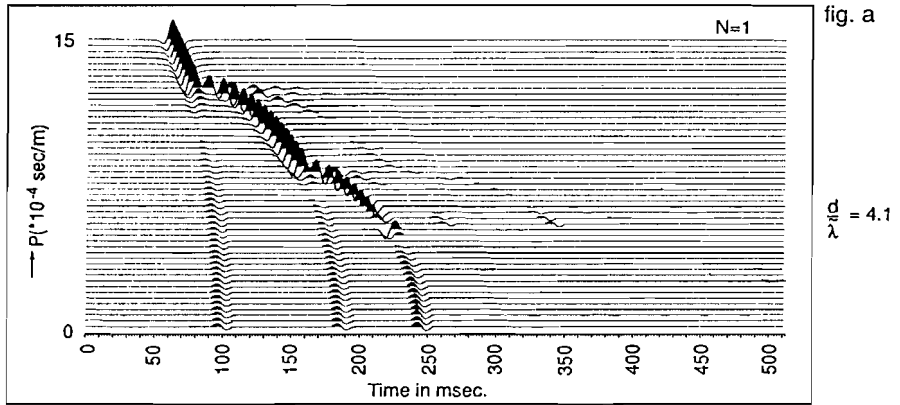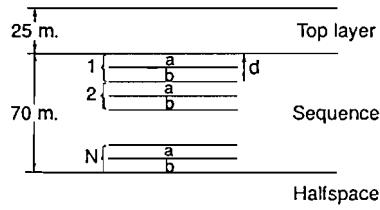
Fig 3.11 Tau-p curves. Layered sequence below isotropic top layer and above isotropic halfspace. Model parameters are: top-layer: $V = 550$ m/s, $\rho = 2.0$ g/cm^3 sequence a: $V = 800$, $\rho = 2.0$, b: $V = 1200$, $\rho = 2.0$, half-space: $V = 2000$ $\rho = 2.4$
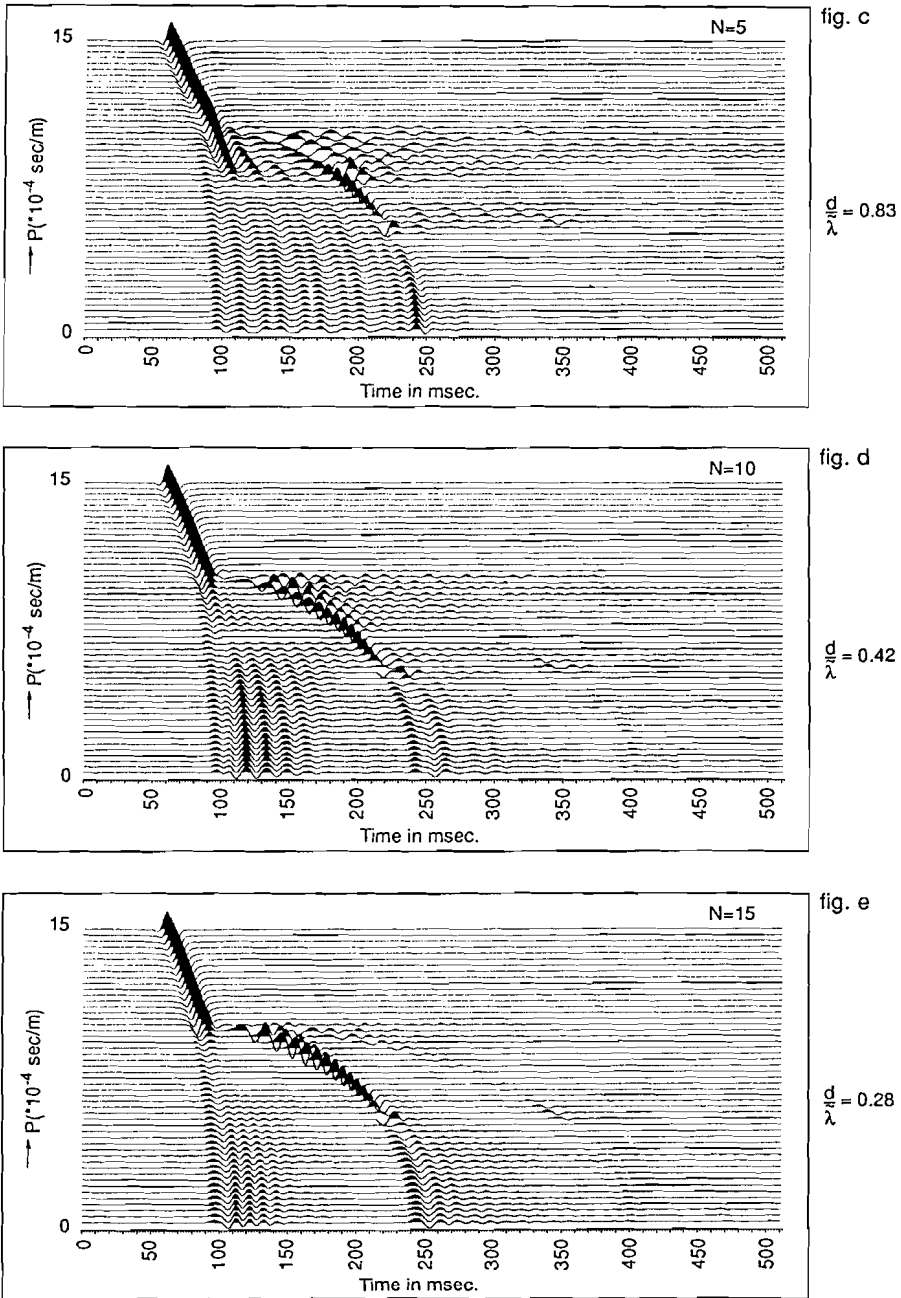
Fig 3.11 c, d, e
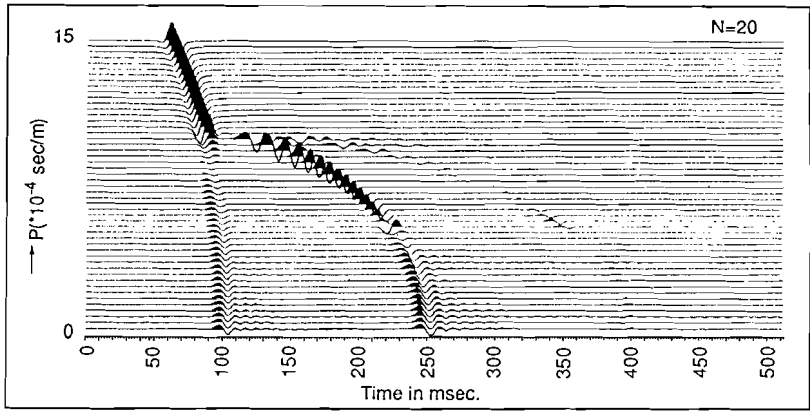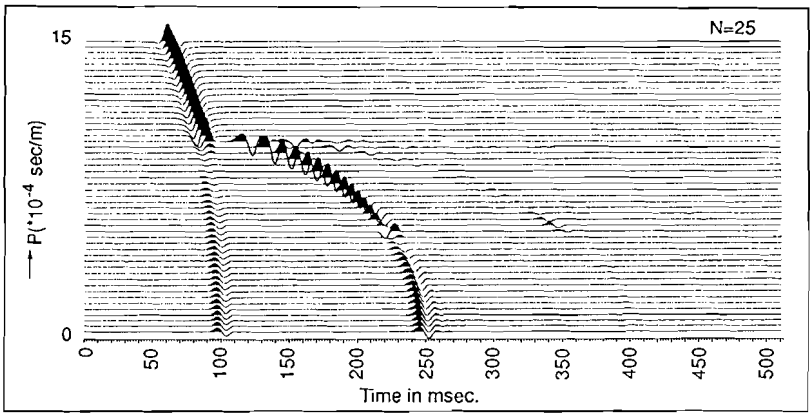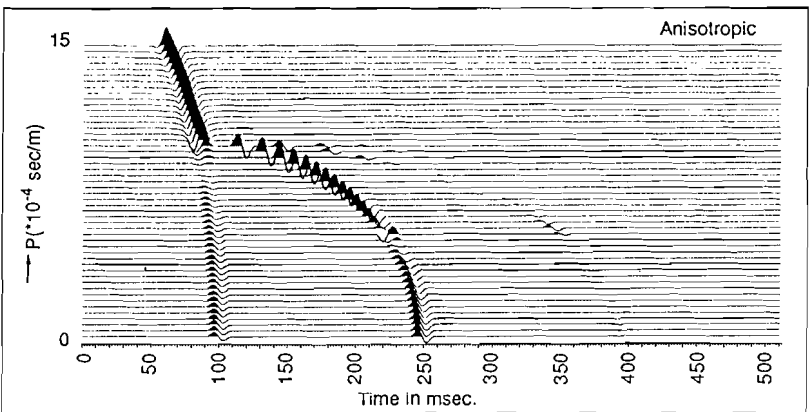
Fig 3.11 f, g, h
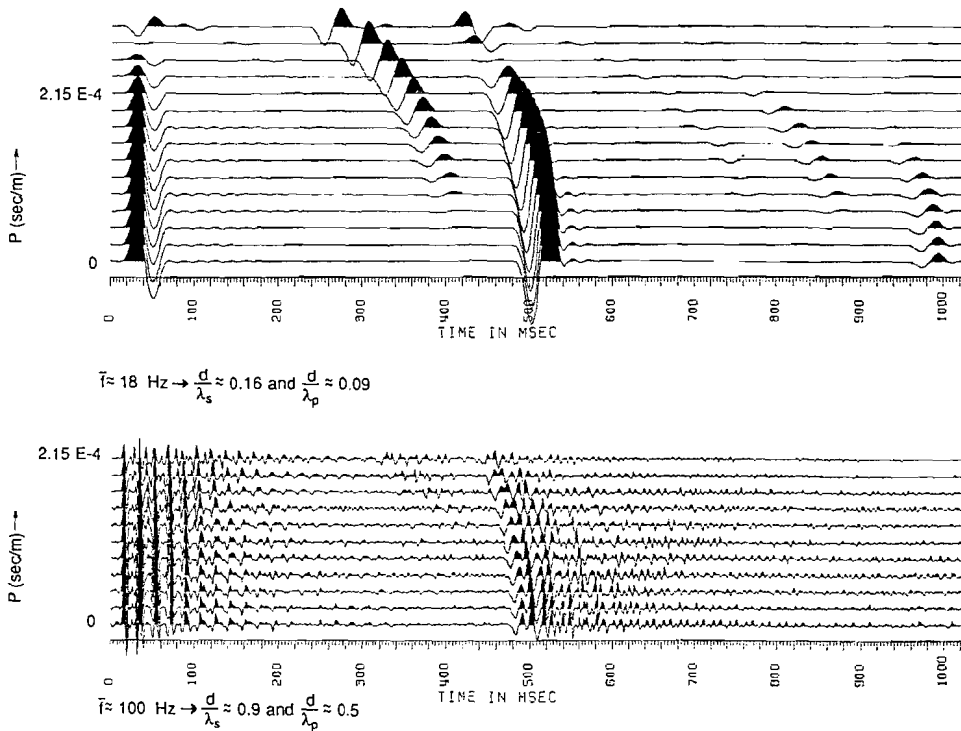
Fig. 3.12 Tau-p curves for a model similar as in Fig. 3.11. The sequence consists of alternating rock and coal. The seismic source in the isotropic top layer emits SV-waves. Model parameters; top-layer: $Vp=2500$ m/s, $Vs=1369$ m/s, $\rho=2.0$ g/cm^3, source 10 m above sequence; sequence "rock" $Vp=3302$, $Vs=1809$, $\rho=2.5$, thickness = 15.7 m , "coal" $Vp=2000$, $Vs=1095$, $\rho=1.5$, thickness = 0.5 m, total sequence thickness = 406 m; half-space: $Vp=2000$, $Vs=1095$, $\rho=1.5$. Upper figure: average frequency is 18 Hz. Lower figure: average frequency is 100 Hz.

Compared to Fig. 3.11g one would therefore perhaps expect to see more dispersion in the top figure of 3.12. However, the coal layer is relatively thin compared to the rock layer. This reduces the multiple effect (see the term "h(1-h)" in equation 3.31) and makes the size of the anisotropy smaller than when both layers would have had equal thicknesses. The bottom figure is the seismic response for an average frequency of 100 Hz.

3.5 **Dispersion**

The dispersion equation for the sequence of layers reads (Helbig 1984)

$$\cos(\omega\, s_3\, N\, d) = \frac{1}{2}(P_{11} + P_{22}), \tag{3.47}$$

where $\underline{P} = (\underline{P}_b \underline{P}_a)^N$.

With (3.13) and (3.14) this becomes

$$\cos(\omega\, s_3\, N\, d) = \cos(\omega\, s_{3_{repl.}}\, N\, d) + \Omega_4\, N^{-2}, \tag{3.48}$$

where

$$\Omega_4\, N^{-2} = \sin(\phi_{repl})\left[\frac{d}{\lambda}\right]^3 \frac{1}{6}\, (2\pi V_{repl})^3\, N\, (s_{3_{repl}})\, \xi, \tag{3.49}$$

with ξ defined in (3.31e).

The term $\Omega_4\, N^{-2}$ describes the dispersion, i.e., it makes the effective phase a function of wavelength. We see that the dispersion has a third order dependence on d/λ. Note that the effective phase as given in (3.48) is the phase for the total wavefield. For specific frequencies $\Omega_4\, N^{-2}$ is zero, namely when $\sin(\phi_{repl})=0$. For these frequencies the one-way ray path is half the wavelength. The phase of the primary ray (from top to base of the sequence) and all multiple rays have equal phase at top and bottom of the sequence. The phase for the sequence-case is

　
hence equal to the phase for the replacement-layer-case. For $\sin(\phi_{repl}) = 1$ the primary ray (from top to base of the sequence) and all multiple rays have equal phase at the bottom of the sequence, and their phase differs from the phase at the top of the sequence. This explains the $\sin(\phi_{repl})$ dependence of (3.48). As an example I take Fig. 3.10, for N=10, and compare the phase spectra (of the whole trace) for p=0 (Fig. 3.13).
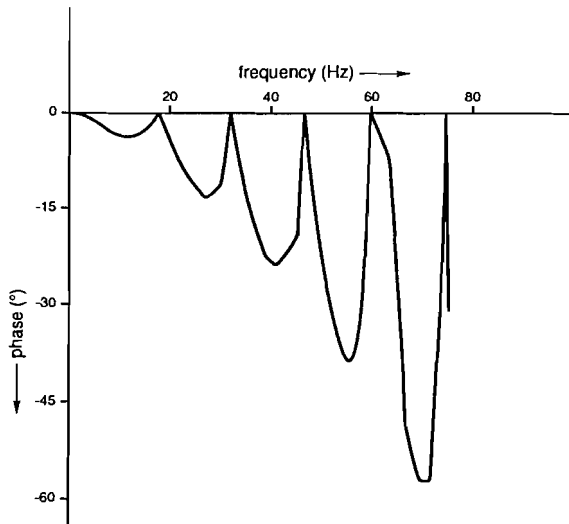
Fig 3.13 Phase difference ($\phi_{repl} - \phi_{sequence}$) for the model as in Fig. 3.10, with N=10 (p=0).

The phase for the sequence-case is always larger than (or equal to) the phase for the replacement-layer-case. The two spectra are equal at specific frequencies, for this model at f = L. 15 Hz, L=0,1,2,3 etc., which is when $\sin(\phi_{repl}) = 0$. To find the effective velocity of the sequence we have to select an isolated event as, for example, the reflection from the sequence base. If $\sin(\phi_{repl}) = 1$ the primary reflection from the sequence base and all its multiples are in-phase. Hence, by selecting those frequencies for which $\sin(\phi_{repl}) = 1$ equation (3.48) gives the effective velocity of the sequence. The envelope of Fig. 3.13 is the true dispersion

curve for the sequence. It follows from the term $\Omega_4 \, N^{-2}$ that the effective velocity is always smaller than the Transversely Isotropic replacement velocity.

Attenuation is the consequence of dispersion. I select in Fig. 3.10, N=10, a time window around the reflection from the base of the sequence, respectively base of the replacement layer, and compare energy spectra (Fig. 3.14).
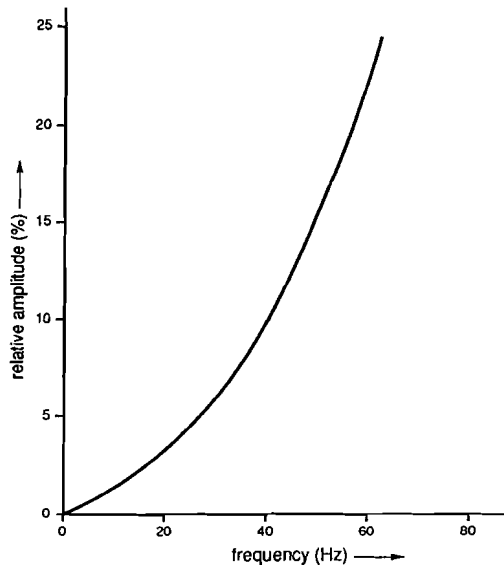
Fig. 3.14 Relative amplitude for the reflection from the top of the lower half-space in Fig. 3.10, N=10 (p=0) ; $(A_{repl} - A_{sequence}) / A_{repl}$ * 100%

At all frequencies the amplitude of the reflected signal is lower for the sequence case. For f=70 Hz the energy ratio is about -2.2 dB. This means the attenuation is 2.2/70 = 0.031 dB/Hz. To scale for the interval thickness we divide by the interval travel time. We then obtain ε, the attenuation over the time interval of one period (1/f) or cycle. For f=70 Hz we have ε=0.47 dB/cycle. The quality factor Q is

$$Q = (20 \, \pi \, ^{10}\log(e))/ \varepsilon \approx 27/\varepsilon \qquad\qquad (3.50)$$
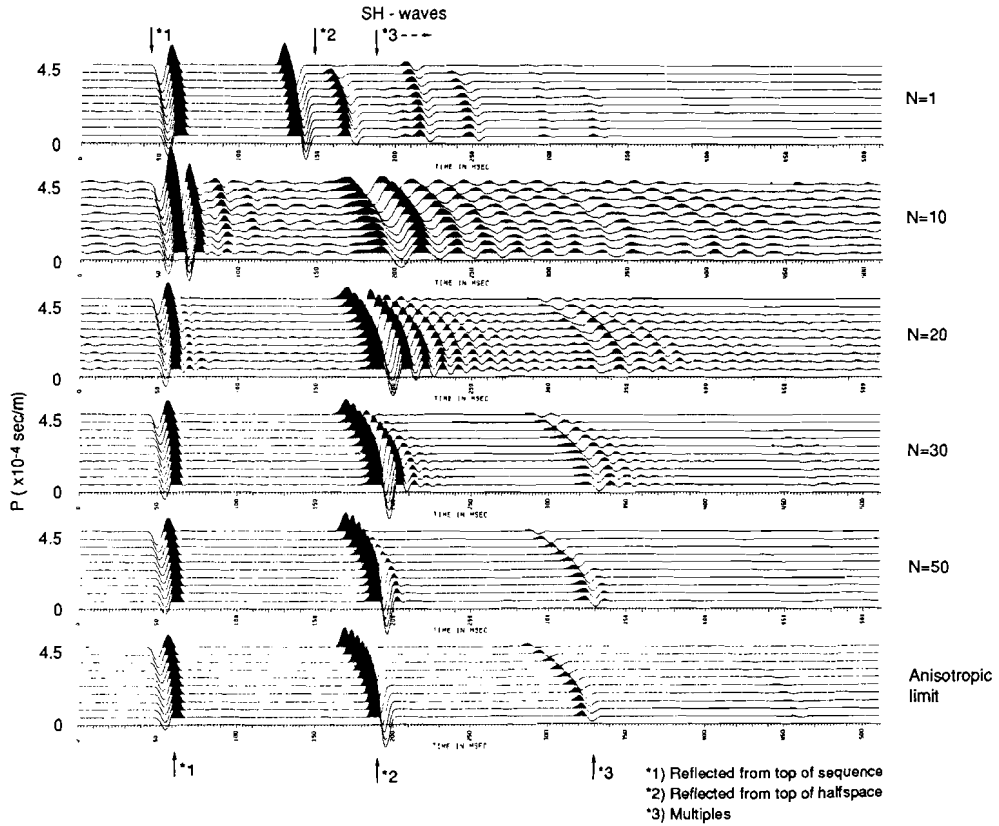
Fig. 3.15. Tau-p curves for a model as in Fig. 3.11. Model parameters are: top-layer: V=1000 m/s, ρ=2.0g/cm^3, thickness = 25 m ; sequence a: V=500, ρ=1.6, b: V=1250, ρ=2.4,   h=0.5, H=40 m. ; half-space: V=2000, ρ=3.0

For f=70 Hz this gives Q = 57. In a similar way we have for, for example, f = 30 Hz: ε = 0.25 dB/cycle, Q = 108.

The same example as discussed above, with the same dispersion, is shown in Fig. 3.15 for N=20, only with the total sequence thickness twice as large. We can see the dispersion in the ringy character of the wavelet. For thinner layers, thus smaller d/λ, the dispersion becomes smaller (Fig. 3.16).
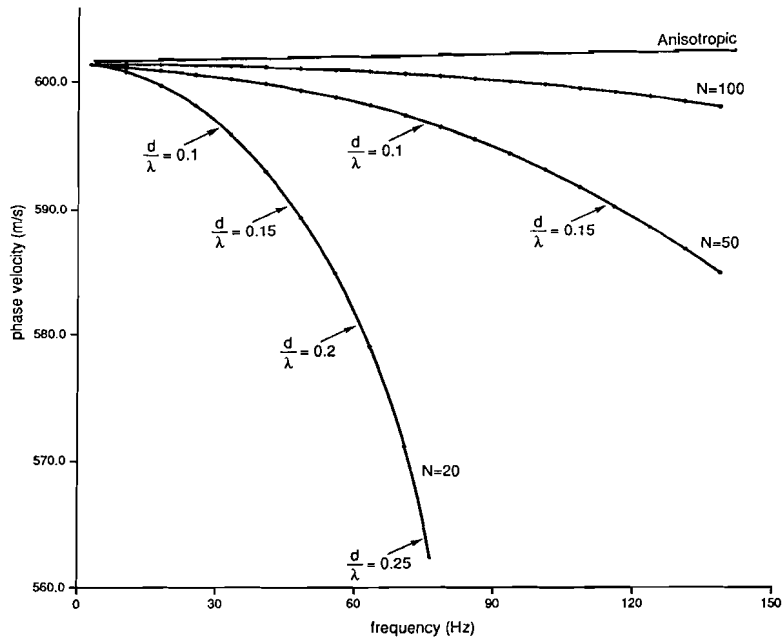
Fig. 3.16 Dispersion curves for the reflection from the base of the sequence in Fig. 3.15 (p=0)

I use well data to illustrate the attenuation due to dispersion in a real earth situation. The impedance log is shown in Fig. 3.17. I select the interval with the larger impedance contrasts (52 ms one-way time) and compute the seismic wavefield that has propagated trough this interval. Fig. 3.18 shows the amplitude spectrum. Although the selected interval is not perfectly periodic, we see the characteristic spectrum. Amplitude decreases with frequency.
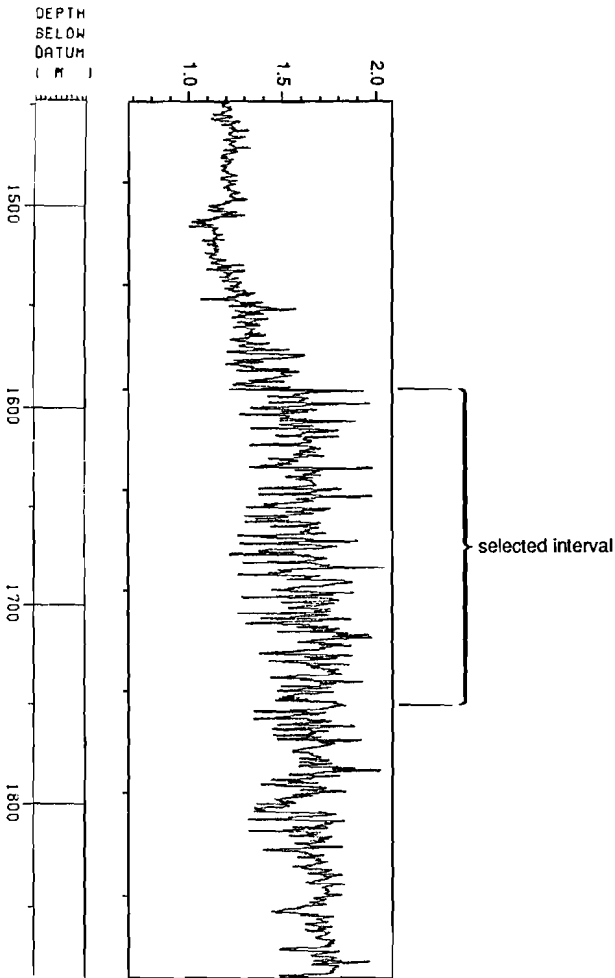
Fig. 3.17 Specific acoustic impedance log $(\ln (\frac{\rho V}{(\rho V)_{water}}))$

Zero attenuation occurs at more or less regular frequency intervals of 10 Hz, which correspond to $\sin(\phi_{repl}) = 0$. For f=180 Hz we obtain : ϵ=0.21 dB/cycle, Q=126.

No attenuation measurements have been made on the field data. It is therefore unknown how large the total attenuation is, where inelastic damping is included. Typical values of measured ε range from below 0.1 to 1.0 (Hauge, 1981, Schoenberger and Levin 1974, 1978, 1979). We can therefore conclude that dispersion caused by thin layers can account for an appreciable fraction of the total observed attenuation.
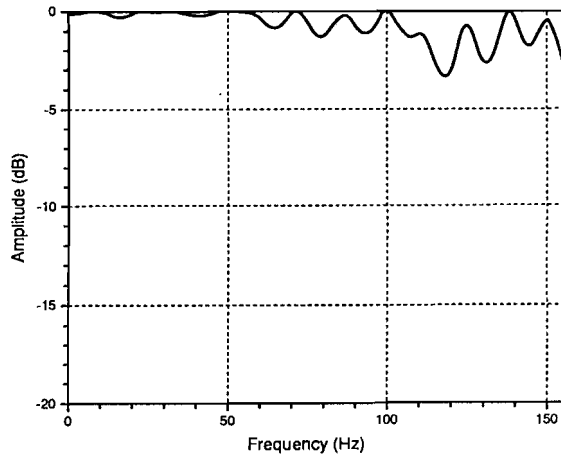
Fig. 3.18 Amplitude spectrum of an isolated reflector placed below the interval selected in Fig. 3.17.

3.6 Conclusions

A set of layers is, strictly speaking, only effectively homogeneous and anisotropic for infinitely large seismic wavelengths. The criterion of reflectivity can be used to decide when the equivalence is acceptable. This reflectivity is the fraction of the wavefield that is back-scattered when the sequence of layers is imbedded in the anisotropic replacement medium.

The reflectivity R is linearly proportional to d/λ, where d is the spatial periodicity and λ the seismic wavelength. Also, R is approximately linearly proportional to the plane wave reflection coefficient for the constituent layers. Since this reflection coefficient is a function of the angle of incidence, the effective medium, or the wavelength for which the equivalence is acceptable, will vary with angle of incidence. Finally, R depends on the relative thicknesses of the constituent layers. Maximum reflectivity is obtained if, for a two-constituent sequence of layers, the layers have equal thicknesses.

As a criterion for acceptance of the sequence of layers as effectively homogeneous we can use $R < 0.15$. For frequencies that satisfy this criterion the dispersion is less than 0.5% and the attenuation is less than 0.22 dB/cycle (Q larger than 120). This attenuation should be added to the homogeneous replacement medium since it is not small.

Examples: If r, the plane wave reflection coefficient, is 0.05, the criterion $R < 0.15$ implies $d/\lambda < 0.96$ (the seismic wavelength must at least be $1/0.96 = 1.04$ times as large as the period thickness), for r=0.1: $d/\lambda < 0.5$, for r=0.2: $d/\lambda < 0.24$, for r=0.3: $d/\lambda < 0.17$. These examples are for two constituents with equal thicknesses. The critical wavelength may be smaller if one of the constituents is much thicker than the other. If, for example, one layer is nine times as thick as the other layer, the criterion requires for r=0.05 that $d/\lambda < 2.67$ (the wavelength should be at least 0.37 times the period thickness). For a fixed d/λ the dispersion decreases with angle of incidence if the reflection coefficient decreases with angle of incidence and vice versa. There is no dispersion if r=0.

There is no requirement for periodicity in a sequence of fine layers for it be effectively anisotropic. Over each distance d satisfying the condition $R<0.15$ the layers can be regarded as effectively homogeneous and anisotropic.

The conclusions were derived for S1-waves (in isotropic media called SH-waves). The effective anisotropy results from the interference of peg-leg multiples in the thin layers. This interference depends on reflection coefficient and layer thicknesses. The conclusions stated above are therefore equally valid for P- and S2-waves.

Appendix 3A: <u>Series expansion for a product of propagator matrices</u>

The objective is to find an expression for the propagator matrix of a sequence of layers, consisting of n periods in which each period is formed by a layer a and a layer b, and to prove that in the limit of very thin layers this matrix approaches the propagator matrix of an homogeneous Transversely Isotropic (TI) medium. I only look at the shear-wave mode that has the elliptical slowness surface in the TI medium. i.e. the S1-wave. So the shear wave is uncoupled from the P-wave.

The following symbols are used for:

P   Propagator matrix

ω angular frequency

s_3 vertical slowness

s_1 horizontal slowness

d   thickness of one period (formed by layer a and layer b)

h   the thickness fraction of layer a

H   the total sequence thickness

n   number of periods

μ shear modulus

c_{ij} element of elastic stiffness tensor

subscripts a, b and TI refer to the layer type, where TI stands for Transversely Isotropic.

I consider matrices of the form

$$\underline{P} = \begin{bmatrix} \cos(\phi) & (1/M)\sin(\phi) \\ -M\sin(\phi) & \cos(\phi) \end{bmatrix} \tag{3A.1}$$

and more specifically

$$\underline{P}_a = \begin{bmatrix} \cos(\phi_a) & (1/M_a)\sin(\phi_a) \\ -M_a\sin(\phi_a) & \cos(\phi_a) \end{bmatrix} \tag{3A.2}$$

where

$$\phi_a = \omega s_3 h d \tag{3A.3}$$

$$M_a = \omega \mu_a s_{3a} \tag{3A.4}$$

I have chosen to make layers a and b isotropic but the derivation can easily be updated for transversely isotropic layers by changing μ in (3A.4) into c_{44}.

The expression for $\underline{P}_b$ is similar to (3A.2), only now with

$$\phi_b = \omega s_3 (1 - h) d \tag{3A.5}$$

The product of $\underline{P}_b$ and $\underline{P}_a$ is

$$\underline{P}_b\underline{P}_a = \begin{bmatrix} \varepsilon + \delta & \pi_2 \\ -\pi_1 & \varepsilon - \delta \end{bmatrix} \tag{3A.6}$$

with

$$\varepsilon = \cos(\phi_a)\cos(\phi_b) - \frac{1}{2}\left(\frac{M_a}{M_b} + \frac{M_b}{M_a}\right)\sin(\phi_a)\sin(\phi_b) \tag{3A.7}$$

$$\delta = \frac{1}{2}\left(\frac{M_b}{M_a} - \frac{M_a}{M_b}\right)\sin(\phi_a)\sin(\phi_b) \tag{3A.8}$$

$$\pi_1 = M_b\cos(\phi_a)\sin(\phi_b) + M_a\cos(\phi_b)\sin(\phi_a) \tag{3A.9}$$

$$\pi_2 = (1/M_b)\cos(\phi_a)\sin(\phi_b) + (1/M_a)\cos(\phi_b)\sin(\phi_a) \tag{3A.10}$$

Note that

$$\pi_1 \pi_2 = 1 + \delta^2 - \varepsilon^2 \quad (\det(\underline{P}_a \underline{P}_b) = 1) \tag{3A.11}$$

I write:

$$\underline{P}_b \underline{P}_a = \varepsilon \underline{I} + \underline{J} \tag{3A.12}$$

with

$$\underline{I} = \begin{bmatrix} 1 & 0 \\ 0 & 1 \end{bmatrix} \tag{3A.13}$$

and

$$\underline{J} = \begin{bmatrix} \delta & \pi_2 \\ -\pi_1 & -\delta \end{bmatrix} \tag{3A.14}$$

Note that

$$\underline{J}^2 = (\varepsilon^2 - 1) \underline{I} \tag{3A.15}$$

Because $\underline{J}\underline{I} = \underline{I}\underline{J} \; (=\underline{J})$, I can use Newton's binomium:

$$(\underline{P}_b \underline{P}_a)^n = \sum_{k=0}^{n} \varepsilon^{n-k} \begin{bmatrix} n \\ k \end{bmatrix} \underline{J}^k \tag{3A.16}$$

Let me choose a parameter ξ, such that $(\varepsilon^2 - 1) = (i\xi)^2 = -\xi^2$ and split the sum in (3A.16). I obtain

$$(\underline{P}_b \underline{P}_a)^n = \{ \sum_{k=0 \,(k \text{ even})}^{n} \varepsilon^{n-k} \begin{bmatrix} n \\ k \end{bmatrix} (i\xi)^k \} \underline{I} + \{ \sum_{k=0 \,(k \text{ odd})}^{n} \varepsilon^{n-k} \begin{bmatrix} n \\ k \end{bmatrix} (i\xi)^{k-1} \} \underline{J} \tag{3A.17}$$

or

$$(\underline{P}_b \underline{P}_a)^n = \frac{(\varepsilon + i\xi)^n + (\varepsilon - i\xi)^n}{2} \underline{I} + \frac{(\varepsilon + i\xi)^n - (\varepsilon - i\xi)^n}{2i\xi} \underline{J} \tag{3A.18}$$

So (3A.7) - (3A.10), (3A.13), (3A.14), (3A.18) and $\varepsilon^2 + \xi^2 = 1$ determine $(\underline{P}_b \underline{P}_a)^n$.

case 1: $\varepsilon^2 > 1$

I now consider the case $\varepsilon^2 > 1$. I write $i\xi = \Theta$ and choose the sign of Θ equal to the sign of ε. If ϕ_i and M_i do not depend on n then the diagonal elements of $(P_bP_a)^n$ behave as $(\varepsilon + \Theta)^n \{(1/2 \pm \delta/(2\Theta)\}$, since $\varepsilon^2 - \Theta^2 = (\varepsilon + \Theta)(e - \Theta) = 1$, so

$$|\varepsilon + \Theta| > 1 > |\varepsilon - \Theta| > 0 \text{ and } (\varepsilon - \Theta)^n \to 0$$

This shows that in general $(P_bP_a)^n$ does not converge if $n \to \infty$

case 2: $\varepsilon^2 \leq 1$

If $\varepsilon^2 \leq 1$ then there is a (unique) ψ in $[0, \pi]$ such that

$$\varepsilon = \cos(\psi) \qquad (3A.19)$$

and

$$\xi = \sin(\psi) \qquad (3A.20)$$

(I may choose $\xi \geq 0$)

Equation (3A.18) becomes:

$$(P_bP_a)^n = \cos(n\psi)\,I + \frac{\sin(n\psi)}{\sin(\psi)}\,J \quad (\psi = 0,\pi) \qquad (3A.21)$$

If, again, ϕ and M do not depend on n, convergence in general is impossible because $Tr((P_bP_a)^n) = 2\cos(n\psi)$.

I have thus shown that convergence of $(P_bP_a)^n$ is not possible if ϕ and M are independent of n. But in my model ϕ depends on n. The total sequence with thickness H consists of n periods with thickness d, thus H = n d, and thus

$$\phi_a = \omega\, s_3\, h\, H/n \qquad (3A.22)$$

With H fixed, $(P_bP_a)^n$ converges for $n \to \infty$

I write

$$\phi_a = \psi_a/n, \quad \psi_a \geq 0 \tag{3A.23}$$

$$\phi_b = \psi_b/n, \quad \psi_b \geq 0, \tag{3A.24}$$

so that ψ_a and ψ_b do not depend on n.

First of all it can now been shown that (using (3A.7) - (3A.10))

$$\varepsilon \uparrow 1 \text{ for } n \to \infty \tag{3A.25}$$

and

$$\delta, \pi_1, \pi_2 \to 0 \text{ for } n \to \infty \tag{3A.26}$$

Thus for n sufficiently large I can introduce ψ with the help of (3A.19) and (3A.20) (now is $\psi \in [0, \pi/2]$).

I now derive asymptotic expressions for ε, δ, π_1, and π_2. If I define

$$M_+ = \frac{1}{2}\left(\frac{M_a}{M_b} + \frac{M_b}{M_a}\right) \tag{3A.27}$$

$$M_- = \frac{1}{2}\left(\frac{M_b}{M_a} - \frac{M_a}{M_b}\right) \tag{3A.28}$$

then the result is

$$\varepsilon = 1 - \frac{1}{2n^2}(\psi_a^2 + \psi_b^2 + 2M_+\psi_a\psi_b) +$$

$$\frac{1}{24n^4}[\psi_a^4 + \psi_b^4 + 6\psi_a^2\psi_b^2 + 4M_+\psi_a\psi_b(\psi_a^2 + \psi_b^2)] +$$

$$\frac{-1}{720n^6}[\psi_a^6 + \psi_b^6 + 15\psi_a^2\psi_b^2(\psi_a^2 + \psi_b^2) +$$

$$6M_+\psi_a\psi_b(\psi_a^4 + \psi_b^4) + 20M_+\psi_a^3\psi_b^3] + \quad O(n^{-8}) \tag{3A.29}$$

$$\delta = \frac{1}{n^2} M_- (\psi_a\psi_b) + \frac{-1}{6n^4} M_- (\psi_a\psi_b)(\psi_a^2 + \psi_b^2) +$$

$$\frac{1}{120n^6} M_- [\psi_a\psi_b(\psi_a^4 + \psi_b^4) + \frac{10}{3}\psi_a^3\psi_b^3] +$$

$$O(n^{-8}) \qquad\qquad (3A.30)$$

$$\pi_1 = \frac{1}{n}(M_a\psi_a + M_b\psi_b) + \frac{-1}{6n^3}[M_a(\psi_a^3 + 3\psi_a\psi_b^2) + M_b(\psi_b^3 + 3\psi_b\psi_a^2)] +$$

$$\frac{1}{120n^5}[M_a(\psi_a^5 + 10\psi_a^3\psi_b^2 + 5\psi_a\psi_b^4) + M_b(\psi_b^5 + 10\psi_b^3\psi_a^2 + 5\psi_b\psi_a^4)]$$

$$+ \frac{-1}{5040n^7}[M_a(\psi_a^7 + 21\psi_a^5\psi_b^2 + 35\psi_a^3\psi_b^4 + 7\psi_a\psi_b^6)$$

$$+ M_b(\psi_b^7 + 21\psi_b^5\psi_a^2 + 35\psi_b^3\psi_a^4 + 7\psi_b\psi_a^6)] + O(n^{-9}), \qquad (3A.31)$$

and

π_2 as π_1 but with M_i^{-1} instead of M_i, (i=a,b).

Finally I have to find an expression for ψ, with the help of (3A.19), (3A.20) and (3A.29) and the 'ansatz'

$$\psi = \frac{\chi_1}{n} + \frac{\chi_2}{n^2} + \frac{\chi_3}{n^3} + \frac{\chi_4}{n^4} + \frac{\chi_5}{n^5} + \frac{\chi_6}{n^6} + \frac{\chi_7}{n^7} + O(n^{-8}) \qquad (3A.32)$$

Because of the singular behaviour of $x \to \arccos(x)$ for $x = 1$, I have to use the implicit relationship

$$\varepsilon = \cos(\psi) \left(= 1 - \frac{\psi^2}{2!} + \frac{\psi^4}{4!} - \dots \right) \qquad (3A.33)$$

I substitute (3A.29) and (3A.32) and set the terms with equal powers of n equal to each other. In this way I find

$$\chi_2 = \chi_4 = \chi_6 = 0 \qquad\qquad (3A.34)$$

$$\chi_1 = (\psi_a^2 + \psi_b^2 + 2 M_+ \psi_a\psi_b)^{1/2} \qquad\qquad (3A.35)$$

$$\chi_3 = (M_+^2 - 1)\ \psi_a^2 \psi_b^2 / (6\chi_1) \tag{3A.36}$$

$$\chi_5 = \chi_3\ (\psi_a^2 + \psi_b^2 + 4\ M_+\ \psi_a\psi_b)\ /\ 15 \tag{3A.37}$$

Now that I have derived the asymptotic expression I can substitute them into (3A.21). Some useful expressions are

$$\cos(n\psi) = \cos(\chi_1) - \frac{\chi_3 \sin(\chi_1)}{n^2} - \frac{2\chi_5 \sin(\chi_1) + \chi_3^2 \cos(\chi_1)}{2n^4} + O(n^{-6}) \tag{3A.38}$$

$$\frac{\sin(n\psi)}{n \sin(\psi)} = \frac{\sin(\chi_1)}{\chi_1} + \left[\frac{\chi_3 \cos(\chi_1)}{\chi_1} - \frac{6\chi_3 - \chi_1^3}{6\chi_1} \cdot \frac{\sin(\chi_1)}{\chi_1} \right] \frac{1}{n^2} + O(n^{-4}) \tag{3A.39}$$

The final result is

$$(\underline{P}_b \underline{P}_a)^n = \begin{bmatrix} \cos(\chi_1) + \dfrac{\Omega_1}{n} + \dfrac{\Omega_4}{n^2} + O(n^{-3}) & \dfrac{1}{\chi_3}\sin(\chi_1) - \dfrac{\Omega_3}{n^2} + O(n^{-4}) \\[3mm] -\chi_3 \sin(\chi_1) + \dfrac{\Omega_2}{n^2} + O(n^{-4}) & \cos(\chi_1) - \dfrac{\Omega_1}{n} + \dfrac{\Omega_4}{n^2} + O(n^{-3}) \end{bmatrix}$$
$$\tag{3A.40}$$

$$\chi_1 = \left(\psi_a^2 + \psi_b^2 + \left(\frac{M_a}{M_b} + \frac{M_b}{M_a}\right)\psi_a\psi_b\right)^{1/2} \tag{3A.41}$$

$$\chi_3 = (M_a\psi_a + M_b\psi_b)\ /\ \chi_1 \tag{3A.42}$$

$$\Omega_1 = \frac{1}{2}\left(\frac{M_b}{M_a} - \frac{M_a}{M_b}\right) \psi_a\psi_b\ \frac{\sin(\chi_1)}{\chi_1} \tag{3A.43}$$

$$\Omega_2 = \chi_3\ \{\ \sin(\chi_1)\ [\ \frac{1}{6}(\psi_a^2 + \psi_b^2) + \frac{6\chi_3 - \chi_1^3}{6\chi_1} +$$
$$\frac{1}{3}\frac{M_a\psi_a\psi_b^2 + M_b\psi_b\psi_a^2}{M_a\psi_a + M_b\psi_b}\ ] - \chi_3\ \cos(\chi_1)\} \tag{3A.44}$$

$$\Omega_3 = \frac{1}{\chi_3} \{ \sin(\chi_1) [\frac{1}{6}(\psi_a{}^2 + \psi_b{}^2) + \frac{6\chi_3 - \chi_1{}^3}{6\chi_1} +$$

$$\frac{1}{3} \frac{M_a{}^{-1}\psi_a\psi_b{}^2 + M_b{}^{-1}\psi_b\psi_a{}^2}{M_a{}^{-1}\psi_a + M_b{}^{-1}\psi_b}] - \chi_3 \cos(\chi_1)\} \qquad (3A.45)$$

$$\Omega_4 = - \sin(\chi_1) [\omega^2 H^2 \psi_a\psi_b (M_+{}^2 - 1)]/(96 \chi_1 h (1-h)) \qquad (3A.46)$$

where

$$\psi_a = \omega s_{3_a} h H \qquad (3A.47)$$

$$\psi_b = \omega s_{3_b} (1-h) H \qquad (3A.48)$$

The last step is to prove that the first terms of the elements of $(\underline{P}_b\underline{P}_a)^n$ as given by (3A.40) are equal to the elements of the propagator matrix of the Transversely Isotropic replacement medium. More specifically it has to be shown that

$$\chi_1 = \phi_{TI} = \omega s_{3_{TI}} H \qquad (3A.49)$$

and

$$\chi_3 = M_{TI} = \omega c_{44} s_{3_{TI}} \qquad (3A.50)$$

This proof is straight forward with the help of the following equations;

the equation for the slowness of the shear wave:

$$c_{66} s_1{}^2 + c_{44} s_3{}^2 - \rho = 0, \qquad (3A.51)$$

the elastic stiffness tensor elements according to Backus:

$$c_{66} = h \mu_a + (1-h) \mu_b \quad (= \langle\mu\rangle \text{ in Backus' notation}) \qquad (3A.52)$$

and

$$c_{44} = h \mu_a{}^{-1} + (1-h) \mu_b{}^{-1} \quad (= \langle\mu^{-1}\rangle^{-1} \text{ in Backus' notation}), \qquad (3A.53)$$

and Snell's law, stating a constant horizontal slowness:

$$s1_{TI} = s1_a = s1_b \tag{3A.54}$$

Thus

$$\lim_{n \to \infty} (\underline{P}_b \underline{P}_a)^n = \begin{bmatrix} \cos(\phi_{TI}) & \dfrac{1}{M_{TI}} \sin(\phi_{TI}) \\ -M_{TI} \sin(\phi_{TI}) & \cos(\phi_{TI}) \end{bmatrix} \tag{3A.55}$$

Appendix 3B: <u>Reflectivity expressed as an infinite series of rays</u>

The reflected field for a single homogeneous layer between two boundaries is formed by an infinite series of rays (Fig. 3.B1). When the two half-spaces are equal we have

$$R = r - r \sum_{k=0}^{\infty} r^{2k} \exp[i(k+1)\, 2\phi]\, t_1\, t_2, \tag{3B.1}$$

where

r = the plane S1-wave reflection coefficient between half-space and layer,

t_1 = the transmission coefficient from half-space to layer,

t_2 = the transmission coefficient from layer to half-space,

$\phi = \omega\, s_3\, H$, with H the layer thickness.

For $\phi = L \pi$ (L=1,2,3,...) the reflection from the top of the layer is 180° out-of-phase with the reflections from the base of the layer. The sum of the amplitudes of all reflections from the base equals the amplitude from the reflection from the top; $A = r - r \sum_{k=0}^{\infty} r^{2k}\, t_1\, t_2 \ = 0$. Hence, for $\phi = L \pi$ the magnitude of reflectivity R

is zero.

For $\phi = \frac{1}{2} \pi + L \pi$ (L=0, 1,2,3,...) the reflection from the top of the layer is in-phase with the primary reflection from the base of the layer. The multiples are alternating $180°$ out-of-phase and in-phase. The total amplitude is approximately 2r:

$$A = r + r \sum_{k=0}^{\infty} (-1)^k r^{2k} t_1 t_2 \approx 2r.$$
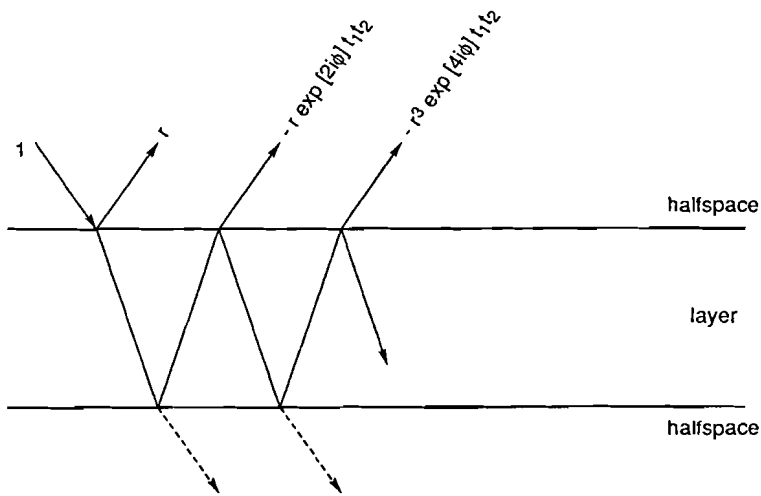
Fig. 3.18 The infinite series of rays that are equivalent to the reflection obtained for a single layer between two boundaries via the propagator matrix

CHAPTER 4:

THREE-TERM TAYLOR SERIES FOR t^2 - x^2-CURVES OF P- AND S-WAVES OVER LAYERED TRANSVERSELY ISOTROPIC GROUND

This chapter is a modified version of the paper: Three-term Taylor series for t^2 - x^2-curves of P- and S-waves over layered transversely isotropic ground, by Hake, J.H., Helbig, K. and Mesdag, C.S., 1984, Geophysical Prospecting 32, 828-850.

Abstract

The arrival time curve of a reflection from a horizontal interface, beneath a homogeneous isotropic layer, is a hyperbola in the x-t domain. If the subsurface is one-dimensionally inhomogeneous (horizontally layered) or if a few or all of the layers are transversely isotropic with a vertical axis of symmetry, the statement

is no longer strictly true, though the arrival time curves are still hyperbola-like. In the case of transverse isotropy, however, classical interpretation of these curves fails. Interval velocities calculated from t^2 - x^2-curves do not always approximate vertical velocities and therefore cannot be used to calculate depths of reflectors.

To study the relationship between velocities calculated from t^2 - x^2-curves and the true velocities of a transversely isotropic layer, we approximate t^2 - x^2-curves over a vertically inhomogeneous transversely isotropic medium by a three-term Taylor series and calculate expressions for these terms as a function of the elastic parameters. It is shown that both inhomogeneity and transverse isotropy affect slope and curvature of t^2 - x^2-curves. For P-waves the effect of transverse isotropy is that the t^2 - x^2-curves are convex upwards; for S2-waves (quasi-shear waves polarised in the plane of propagation) the curves are convex downwards. For S1-waves (shear waves polarised perpendicular to the plane of propagation) transverse isotropy has no effect on curvature.

4.1 Introduction

Stacking is a major step in the processing of seismic reflection data. To image the subsurface, i.e. to obtain c_{ijkl} as a function of space, the pre-stack t-x data are summed along hyperbolae to simulate zero-offset data. This stack may then form the input for post-stack migration or can be used as initial model for, for example, pre-stack migration. The bulk of currently acquired seismic data consists of P-waves. The use of shear waves is small and still mainly experimental. However, their contribution to seismic exploration is rapidly growing, judging from the ever-increasing number of publications dealing with shear waves. There is a change in the industry from exploration applications to reservoir characterization applications. Shear waves play an important role in

this. Stacking is not only for P-wave data a significant processing step but also for S-wave data. Although for S-waves the focus may be more on abstracting lithology information from the data, there will always be a need for imaging (positioning) and for improvement of signal-to-noise ratio by means of stacking.

Many sedimentary rocks are finely layered. The thickness of individual layers is small compared to the seismic wavelength and hence the compound layers are effectively anisotropic. The anisotropy has hexagonal symmetry. We may expect that often the axis of rotation symmetry is vertical, as generally layers are horizontal. This means that we may expect that sedimentary rocks are transversely isotropic. Stresses acting on the rock can cause microcracks and fractures. These are most likely vertically oriented because the weight of the overburden orientates the principle stress with the largest magnitude in the vertical direction. The anisotropy resulting from vertical cracks and fractures is called azimuthal anisotropy. The combination of the fine layering and the stress results in a rock that is effectively anisotropic with orthorhombic symmetry.

Although both are likely to occur, the fine layering is more important for stacking than the vertical cracks or fractures. Observations have been made that the azimuthal anisotropy is weak compared to the transverse isotropy (Serrif 1987, Sriram 1987). Fine layering is expected to be present over large vertical distances. Stresses may vary with depth and the reaction of a rock to applied stress is lithology dependent. Hence we may expect that azimuthal anisotropy varies with depth (see observations made by Winterstein and Meadows 1991). Azimuthal anisotropy may locally be large. However, for a kinematic parameter as stacking velocity, which is only sensitive to the average properties of a thick interval, the azimuthal anisotropy may appear weak. Another argument why transverse isotropy is more important for stacking than azimuthal anisotropy is found in the characteristics of both types of anisotropy at far offsets. The stacking velocity is most sensitive to the far offset data where the Normal Move Out is the largest. It is at the larger offsets where transverse isotropy dominates azimuthal anisotropy concerning splitting and polarization of the shear waves (chapter 7).

The objective of this chapter is to find the relationship between velocities calculated from reflection-time curves and the true velocities of a transversely

isotropic layer. Levin (1979, 1980) computed t^2 - x^2-curves for a known transversely isotropic layer and compared the velocities calculated from the slope of these curves with the known velocities of the layer. Radovich and Levin (1982) gave expressions for velocities calculated from the tangents to the slope of t^2 - x^2-curves in terms of the plane-wave velocity as a function of the plane-wave angle in the layer. It is more useful to describe t^2 - x^2 curves in terms of the elastic parameters of the layer, and not just for homogeneous medium but also for a vertically inhomogeneous medium. Such relationships can be used to interpret seismic data in terms of a layered and partially or completely transversely isotropic ground.

To evaluate the effect of transverse isotropy on t^2 - x^2-curves, we approximate these curves by a three-term Taylor series and calculate expressions for these terms as functions of the elastic parameters. We do this for the three wave types: P-waves, S1-waves and S2-waves. The distinction between S1- and S2-wave is based on polarization. The quasi-shear wave called S2 is polarised in the x-z plane, the plane of propagation. The other shear wave, the S1-wave, is polarised in the y-direction.

4.2 Wave surface and t^2-x^2 curve

The arrival time curve observed at the surface is directly related to the wave surface of the waves propagating in the medium above the reflecting interface. For a homogeneous isotropic medium the wave surface is a sphere (two-dimensionally a circle). For a horizontal reflecting interface the t-x-curve is a centred hyperbola. This means that the t^2 - x^2-curve is a straight line. The slope of this line corresponds to the squared slowness of the medium. The intercept with the t^2-axis is the square of the two-way vertical travel time and the intercept with the x^2-axis is the square of twice the reflector depth (multiplied

with -1). If the wave surface is elliptical, the t^2 - x^2-curve is - as for a spherical wave surface - a straight line. This follows immediately from the equation for an elliptical wave surface at time t:

$$t^2 = \left[\frac{z}{g_z}\right]^2 + \left[\frac{x}{g_x}\right]^2 \qquad\qquad (4.1)$$

where g_x is the ray velocity in the horizontal direction and g_z the ray velocity in the vertical direction (Fig. 4.1a).
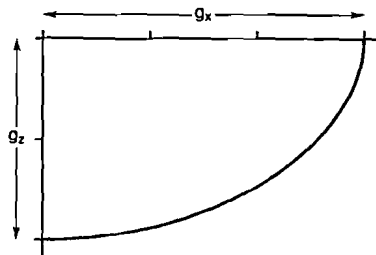
Fig. 4.1 (a) Elliptical wave surface at unit time: g_x is the velocity in horizontal direction, g_z the velocity in vertical direction.
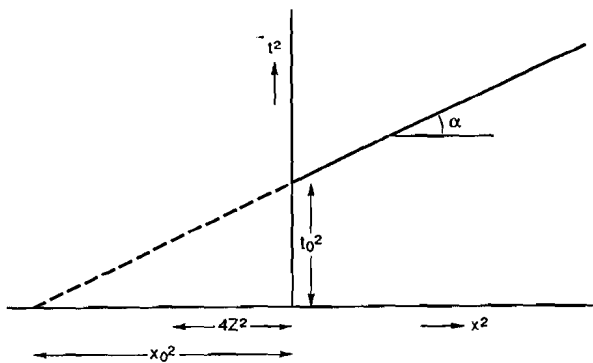
Fig. 4.1 (b) t^2- x^2 curve corresponding the wave surface of Fig. 4.1(a).

The slope of the t^2 - x^2-curve now corresponds to the square of the horizontal

slowness. The intercept with the t^2-axis is still the square of the two-way vertical travel time, but the intercept with the x^2-axis is not equal to the square of twice the reflector depth (Fig. 4.1b).
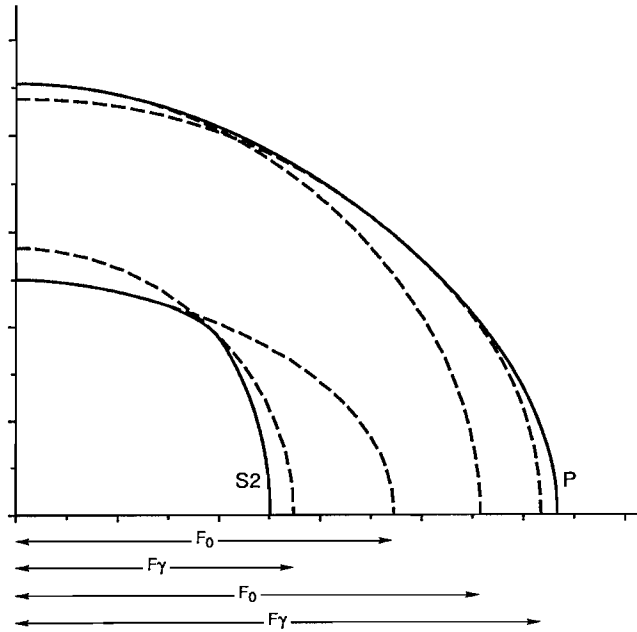
Fig. 4.2 Wave surfaces of P- and S2-waves for a homogeneous transversely isotropic medium with λ=0.7, τ=0.3, h=0 and k=0. Dashed lines represent the best-fit ellipse at the wave surface for vertical direction and for an arbitrary direction γ. F_0 is the horizontal axis of the ellipse fitted at the vertical, F_γ for direction γ.

In general, if the wave surface differs from an ellipse, the t^2-x^2-curve is not a straight line. For an arbitrary wave surface the corresponding t^2-x^2-curve can be constructed by fitting an ellipse to every point of the wave surface (the axes of this ellipse being horizontal and vertical). The slope of the tangent to the t^2-x^2 curve in the corresponding point is then given by the horizontal axis of this best-fit ellipse. The intercept with the t^2-axis of this tangent is given by the

vertical axis of the ellipse. The effect of transverse isotropy on t^2 - x^2-curves can therefore be deduced from the wave surface. For S1-waves the wave surface is always elliptical and therefore the t^2 - x^2-curve is always a straight line. For P- and S2-waves the wave surfaces are generally not elliptical and therefore the t^2 - x^2-curves generally differ from a straight line.

To illustrate this we have calculated wave surfaces for P- and S2-waves in a medium with transverse isotropy due to fine layering (see Fig. 4.2).

We fitted an ellipse to the wave surfaces for vertical direction and a second ellipse for an arbitrary direction, making an angle with the vertical. For P-waves, the horizontal axis of the best-fit ellipse for vertical direction is smaller than the horizontal axis of the ellipse for an off-vertical direction. Hence, the velocity calculated from the slope of the t^2 - x^2-curve increases with offset. This means that the t^2 - x^2-curve is convex upwards. (Convex upwards means that the slope of the curve decreases for increasing ray-parameter. Convex downwards means that the slope increases with ray-parameter. As long as no cusps occur - as might be the case for S2-waves - an increase in ray-parameter corresponds to an increase in offset.) For S2-waves it is just the opposite: the horizontal axis of the best-fit ellipse for vertical direction is larger than the horizontal axis of the best-fit ellipse for the second direction. Thus in this example the t^2 - x^2-curve for S2-waves is convex downwards. It will be shown that this is correct not just for the particular example used here but for all t^2 - x^2-curves of media with transverse isotropy due to layering.

4.3 The parameters of a transversely isotropic medium

First we define the parameters which are used to describe transversely isotropic media. Because of the hexagonal symmetry, the elastic tensor has five distinct non-vanishing elements. These five elements are represented as elements of a 6x6 matrix: c_{11}, c_{13}, c_{33}, c_{44} and c_{66}. If the transverse isotropy is

due to fine layering these five elements are related to the parameters of the constituent layers as shown by Backus (1962). These five elements together with density are the parameters which describe wave propagation in transversely isotropic media. To reduce the number of parameters Helbig (1981) introduced a normalised, dimensionless set of four parameters which he called λ, τ, h and k. The relationship between this new set of parameters and the original set is

$$\lambda = c_{44}/c_{66}, \quad \tau = \frac{1}{2}(1 - c_{13}/c_{33}), \quad h = \frac{1}{2}(2c_{44} - c_{33} + c_{13})/c_{33}$$

and

$$k = \frac{1}{4}\{c_{13}(c_{13} + 2c_{66}) + c_{33}(2c_{66} - c_{11})\}/(c_{66}c_{33}) \qquad (4.2)$$

Note that throughout this chapter the symbol λ stands for a dimensionless parameter and not for wavelength. It is used as a parameter to indicate the amount of anisotropy.

For transverse isotropy due to fine layering the relationship between the anisotropy parameters and the layer parameters can be expressed in terms of θ, the squared ratio of shear and compressional velocity and μ, the shear modulus of the, intrinsically isotropic, constituent layers:

$$\lambda = \frac{1}{<\mu> <1/\mu>}$$

$$\tau = <\theta>$$

$$h = \frac{<\theta/\mu> - <\theta> <1/\mu>}{<1/\mu>} \qquad (4.3)$$

$$k = \frac{<\theta \mu> - <\theta> <\mu>}{<\mu>}$$

where the symbol $< >$ denotes a weighted average (weighted by layer thickness).

These averaging equations give some insight into the meaning of the anisotropy parameters. Parameter τ is an average of the squared ratio of shear and compressional velocity of the individual layers. If μ is constant, then, from the averaging equations, $\lambda = 1$ and $h = k = 0$. In this case the medium is isotropic. For θ constant and μ variable we have $\lambda < 1$ and $h = k = 0$. Such a medium is called a K-medium and is described by density and three instead of five distinct

elastic parameters. In many sedimentary rocks the ratio of shear to compressional velocity varies only over a small range and therefore a K-medium is often a good approximation.

4.4 Three-term Taylor series approximation for t^2-x^2 curves

To describe t^2 - x^2-curves, we approximate these curves by a Taylor series. We restrict ourselves to the first three terms of this series and calculate expressions for these terms as a function of the elastic parameters of the medium.

First we consider a Taylor series approximation at zero offset:

$$t^2 = \lim_{x \to 0} \sum_k B_k \, x^{2k} \tag{4.4}$$

with

$$B_k = \frac{1}{k!} \frac{d^k (t^2)}{(dx^2)^k} \tag{4.5}$$

Consider a horizontally layered medium. Each layer is homogeneous and either isotropic or transversely isotropic. The expressions for the terms B_k (k=0,1,2) are (Appendix A):

$$\lim_{x \to 0} B_0 = \left[\sum \Delta t_i \right]^2 \tag{4.6}$$

$$\lim_{x \to 0} B_1 = \frac{\sum \Delta t_i}{\sum F_i^2 \Delta t_i} \tag{4.7}$$

with

$$F^2 = g_1/s_1 \qquad\qquad (4.8)$$

$$\lim_{x \to 0} B_2 = \frac{\left[\sum F_i^2 \Delta t_i\right]^2 - \sum \Delta t_i \cdot \sum (F_i^4 + H_i)\, \Delta t_i}{4\left[\sum F_i^2 \Delta t_i\right]^4} \qquad (4.9)$$

with

$$H = \frac{1}{s_1}\, \frac{d(F^2)}{ds_1} \qquad\qquad (4.10)$$

(all summations are over index i)

where

i = 1,...,Q, when Q is the total number of (gross) layers above the reflector;

Δt_i = the two-way vertical travel time in layer i;

g_1 = the horizontal component of wave velocity $\underline{G}$;

s_1 = the horizontal component of slowness $\underline{S}$, equal to the ray-parameter p.

The wave velocity $\underline{G}$ (or group velocity) is the velocity of a wave emanating from a point source. Normal velocity $\underline{V}$ (or phase velocity) is the velocity with which planes equal phase propagate perpendicular to the wave front. The slowness $\underline{S}$ has the same direction as the normal velocity vector $\underline{V}$, and the magnitude of $\underline{S}$ is the reciprocal of the magnitude of $\underline{V}$:

$$s_1 = \frac{v_1}{v_j\, v_j} \qquad\qquad (4.11)$$

With the equations for the velocity variations of P-, S1- and S2-waves in transversely isotropic media, F and H can be expressed in terms of the elastic parameters.

With the two parameter sets (i) $c_{11}, c_{13}, c_{33}, c_{44}, c_{66}$ and (ii) h, k, λ, τ, c_{44} (c_{44} is used for scaling), the density ρ, and the abbreviations

$J = c_{13} + c_{44}$, $L = c_{11} - c_{44}$, $M = c_{33} - c_{44}$ and $N = (L.M - J^2)$, one has:

For P-waves:

$$\lim_{x->0} F^2 = \frac{1}{\rho}\left[c_{11} - \frac{N}{M}\right] = \frac{c_{44}}{\rho(h+\tau)}\left\{1 + \frac{4h(1-\tau)}{1-h-\tau}\right\} \tag{4.12}$$

$$\lim_{x->0} H = \frac{1}{\rho^2}\frac{4\,N\,(J)^2\,c_{33}}{(M)^3} = \frac{(4\,c_{44})^2}{\rho^2(h+\tau)}\frac{(1-\tau+h)^2}{(1-\tau-h)^2}\left\{\frac{1-k-\tau}{\lambda} - \frac{(1-\tau)^2}{1-h-\tau}\right\} \tag{4.13}$$

For S2-waves:

$$\lim_{x->0} F^2 = \frac{1}{\rho}\left[c_{44} + \frac{N}{M}\right] = \frac{c_{44}}{\rho}\left\{\frac{4(1-k-\tau)}{\lambda} + \frac{(1-\tau)(4\tau-3) - h}{1-h-\tau}\right\} \tag{4.14}$$

$$\lim_{x->0} H = -\frac{1}{\rho^2}\frac{4\,N\,(J)^2\,c_{44}}{(M)^3} = -\frac{(4\,c_{44})^2}{\rho^2}\frac{(1-\tau+h)^2}{(1-\tau-h)^2}\left\{\frac{1-k-\tau}{\lambda} - \frac{(1-\tau)^2}{1-h-\tau}\right\} \tag{4.15}$$

For S1-waves

$$F^2 = \frac{c_{44}}{\rho\lambda} = \frac{c_{66}}{\rho} \tag{4.16}$$

and

$$H = 0 \tag{4.17}$$

From (4.6) we see that B_0, the intercept with the t^2-axis, is the square of the sum of the vertical travel times. This is the same as for isotropic media, but the second term B_1 is different. For isotropic media, B_1 is the reciprocal of the time average of the squared velocity; B_1(isotropy) = $1/v^2_{rms}$ (= $\sum \Delta t_i$ / $\sum v_i^2 \Delta t_i$). From (4.7) we see that for transversely isotropic media B_1 is the reciprocal of the time average of F^2, the ratio of the horizontal components of wave velocity and slowness.

4.5 Interpretation of the moveout velocity F

The question arises how F has to be interpreted for the three wave types. Equations (4.12), (4.14) and (4.16) give the relationship between F and the elastic parameters.

S1-waves:

The horizontal ray- and phase-velocity of S1-waves in a transversely isotropic medium is $(c_{66} / \rho)^{1/2}$. From (4.16) it follows therefore that for S1-waves F equals the horizontal velocity.

P-waves:

For P-waves the expression for F is more complicated. If the medium can be modelled by a K-medium one has

$$F = (c_{44} / \rho\tau)^{1/2} = (c_{33} / \rho)^{1/2} \qquad\qquad (4.18)$$

This is just the vertical velocity $G_{vertical}$ ($\underline{G}_{vertical}=(0,0,g_3)$). This result agrees with the theorem established by Krey (Krey and Helbig 1956).

How much can F deviate from the vertical velocity when the medium cannot be modelled by a K-medium?

We define the anisotropy factor A,

$$A = F/G_{vertical}, \qquad\qquad (4.19)$$

as the ratio of the velocity computed from the reflection time curve and the vertical velocity.

From (4.12) we have

$$A = \left[1 + \frac{4h(1-\tau)}{1-h-\tau}\right]^{1/2} \qquad\qquad (4.20)$$

From the stability constraints for θ and μ (0 < θ < 3/4 and 0 < μ) and equations (4.3), the stability constraints for λ, τ, h and k can be calculated (see Helbig 1981).

These stability constraints limit the values h and τ can attain and therefore limit the range of A. To illustrate by how much A can deviate from 1, we give some examples.

If λ = 4/9 and 0 < θ < 3/4 (θ is the squared ratio of S- and P-velocity of the constituent layers) and τ= 0.3, we have 0.44 < A < 1.94. λ = 4/9 is a rather low value and corresponds to a strong anisotropy, implying that the horizontal S1-velocity is 50% higher than the vertical velocity. For media of more moderate anisotropy the range of possible values for the anisotropy factor becomes smaller with the limit (for λ = 1, i.e., for isotropy) A = 1. For a more realistic range of θ, e.g. 0.2 < θ < 0.42, and for λ = 4/9, the anisotropy factor is between 0.77 and 1.25.

S2-waves:

For S2-waves the expression for F is given by (4.14). The ratio between F and the vertical S2-wave velocity is for a K-medium:

$$A = \left[\frac{4(1-\tau)}{\lambda} + 4\tau - 3 \right]^{1/2} \tag{4.21}$$

In Fig. 4.3 the anisotropy factor is plotted as a function of τ for several values of λ. If λ = 1 the medium is isotropic and F is equal to the velocity of the medium. If λ < 1, F is always larger than the vertical velocity. If the medium cannot be described by a K-medium, A is constrained by the ranges of λ, τ, h and k. For example, according to the stability constraints we have for λ = 4/9, 0.2<θ< 0.42 and τ = 0.3 that A satisfies 1.95 < A < 2.25. We see that for S2-waves the anisotropy factor can achieve much higher values than for P-waves.
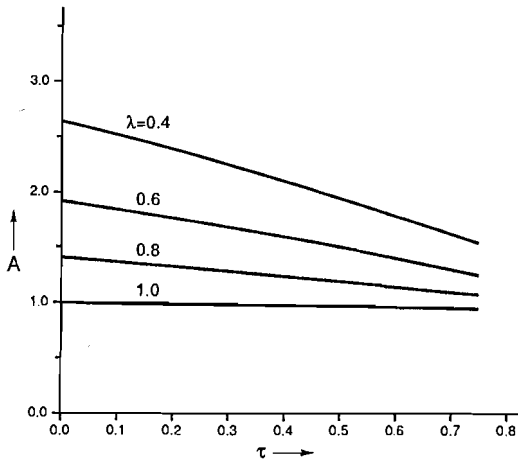
Fig. 4.3 Anisotropy factor A for S2-waves , zero offset.

4.6 The third Taylor series term

The third term of the Taylor series, B_2, describes the deviation of the t^2-x^2 curve from a straight line. The expression for B_2 is given by (4.9). B_2 can be split into one part due to inhomogeneity and one due to transverse isotropy.: $B_2 = (I) + B_2(TI)$, with

$$B_2(I) = \frac{\left[\sum F_i^2 \Delta t_i\right]^2 - \sum \Delta t_i \cdot \sum (F_i^4)\, \Delta t_i}{4\left[\sum F_i^2 \Delta t_i\right]^4} \qquad (4.22)$$

and

$$B_2(TI) = \frac{-\sum \Delta t_i \cdot \sum H_i \Delta t_i}{4\left[\sum F_i^2 \Delta t_i\right]^4}$$
(4.23)

$B_2(I)$ is a well-known expression. It is the contribution to B_2 of the inhomogeneity of the medium (Al-Chalabi 1973). $B_2(TI)$ is the effect of the transverse isotropy. Thus both inhomogeneity and transverse isotropy cause the t^2 - x^2-line to be curved. Using the Cauchy-Schwartz inequality it can be shown that $B_2(I) \leq 0$. This means the effect of inhomogeneity is qualitatively the same for all three wave types; if inhomogeneity alone would affect the curvature of the t^2 - x^2-curve, then it would be convex upwards.

The sign of $B_2(TI)$ depends on the sign of H. We restrict the discussion to transversely isotropic media for which N > 0 (this is always true for media with transverse isotropy due to periodic layering (Berryman 1979)). Because all other terms of (4.13) and (4.15) are positive, H is positive for P-waves and negative for S2-waves. Thus for P-waves the t^2 - x^2 will always be convex upwards. Whether for S2-waves the t^2 - x^2-curve is convex upwards or convex downwards depends on the relative magnitude of the anisotropy and inhomogeneity effects.

4.7 Series approximation at non-zero offsets

So far the discussion has been restricted to a Taylor series approximation at zero offset. For an arbitrary offset x_0 we have (Appendix A):

$$t^2 = \lim_{x \to x_0} \sum_k B_k (x^2 - x_0^2)^k$$
(4.24)

with

$$\lim_{x \to x_0} B_0 = \left[\sum \Delta t_i\right]^2 ,$$ (4.25)

$$\lim_{x \to x_0} B_1 = \frac{\sum \Delta t_i}{\sum F_i^2 \Delta t_i}$$ (4.26)

with

$$F_i^2 = g_1/s_1$$ (4.27)

where t_i is the two-way travel time along the ray in layer i and F_i the ratio of the horizontal components of wave velocity and slowness for this particular ray in layer i, arriving at the surface at offset x_0.

Inhomogeneity and F (which depends on the angle of incidence) determine the slope of a t^2 - x^2-curve at a certain offset. To study the effect of transverse isotropy we restrict the discussion in the following to homogeneous media.
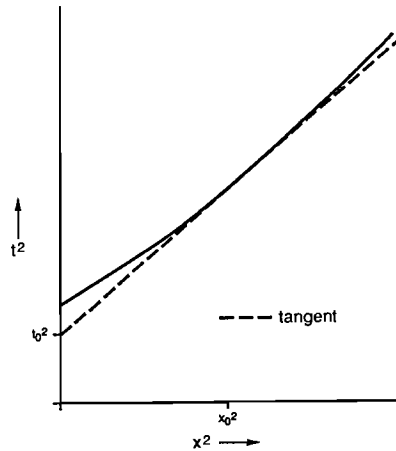
Fig. 4.4 The intercept with the t^2 axis of the tangent to the t^2-x^2curve at offset x_0

We have characterised t^2 - x^2-curves by Taylor series terms. Another characterising parameter is the intercept with the t^2-axis (t_0) of the tangent to the t^2 - x^2-curve at offset x_0 (see Fig. 4.4).

The derivation of the expression for t_0 as a function of the elastic parameters is simple. In Fig. 4.1 we saw that the slope of the tangent was given by the horizontal axis of the ellipse and the intercept with the t^2-axis by the vertical axis of the ellipse. We found that the horizontal axis of the ellipse is $F = (g_1/s_1)^{1/2}$. Thus for reasons of symmetry the vertical axis is $(g_3/s_3)^{1/2}$ and the intercept with the t^2-axis is therefore

$$t_0^2 = \frac{4\,z^2}{g_3/s_3} \tag{4.28}$$

where z is the depth of the reflector.

For $x_0 = 0$, g_3/s_3 is the squared vertical velocity. For infinite offset we have for g_3/s_3:

P-waves:

$$\lim_{x_0 \to \infty} g_3/s_3 = \frac{1}{\rho}\left\{c_{44} + \frac{(c_{13} + c_{44})^2}{c_{11} - c_{44}}\right\} \tag{4.29}$$

S2-waves:

$$\lim_{x_0 \to \infty} g_3/s_3 = \frac{1}{\rho}\left\{c_{33} - \frac{(c_{13} + c_{44})^2}{c_{11} - c_{44}}\right\} \tag{4.30}$$

4.8 <u>Examples</u>

Figure 4.5 shows t^2 - x^2-curves for P-waves. The curves are calculated for a homogeneous layer with the properties of a K-medium, reflector depth 1, and unit vertical P-wave velocity. The curves are calculated for offsets out to 4 and for several values of λ.

Figure 4.6 shows the velocity F calculated from the slope of the curves in Fig. 4.5. For zero offset, F is for all curves identical to the vertical velocity because the layer is a K-medium. For increasing offsets, F increases towards the horizontal velocity. Figure 4.7 shows t_0 as a function of the offset. Figure 4.8 shows $B_2(TI)$, calculated from the curves of Fig. 4.6. $B_2(TI)$ is always negative, and because increasing offset corresponds to an increasing ray-parameter, this means the t^2 - x^2-curve is convex upwards for all offsets. For increasing offset the absolute value of $B_2(TI)$ becomes smaller and quickly goes to zero. This means that the curvature of the t^2 - x^2-curve is strongest at small offsets. For media with stronger transverse isotropy (smaller λ), the t^2 - x^2-curve is more strongly curved.

Figure 4.9 shows t^2 - x^2-curves for S2-waves. The homogeneous layer (K-medium) has again unit thickness but now the vertical S2-wave velocity is taken as unity. The curves are calculated for several values of λ. The curves for λ= 0.6 and λ= 0.4 show cusps. Figure 4.10 shows F as a function of the offset. For small offsets, F increases for increasing anisotropy (compare to Fig. 4.3). For large offsets, F approaches the horizontal velocity, which for S2-waves is equal to the vertical velocity. Figure 4.11 shows t_0 as a function of the offset. In Fig. 4.12, where $B_2(TI)$ is displayed, we see that for small offsets $B_2(TI)$ is positive. As long as no cusps occur, $B_2(TI)$ remains positive for larger offsets and approaches zero. If the wave surface has cusps, $B_2(TI)$ can be negative for some offsets. If we take the example of λ= 0.6, $B_2(TI)$ has two vertical asymptotes, namely for the offsets $x_0 \cong 1.65$ and $x_0 \cong 1.9$. Between these two offsets, $B_2(TI)$ has positive and negative values. Furthermore, the behaviour of $B_2(TI)$ for small offsets as a function of λ should be noted: if $\lambda = 1$, the medium is isotropic and thus $B_2(TI)=0$.
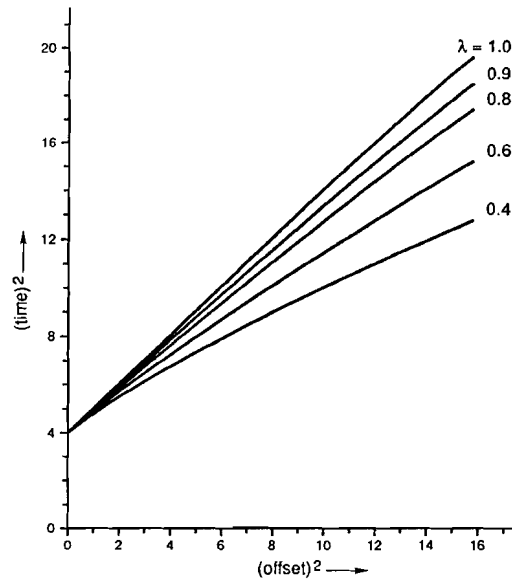
Fig. 4.5 t^2-x^2 curves of P-waves for a homogeneous K-medium. Reflector depth and vertical P-wave velocity are taken as units, $\tau=0.3$
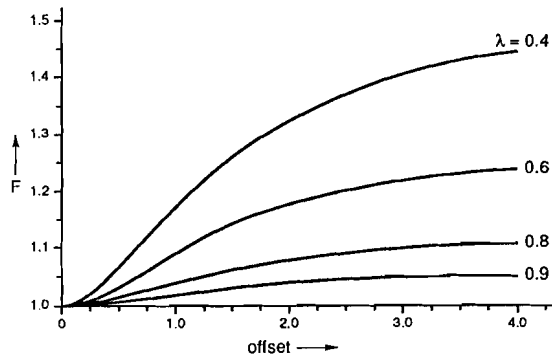
Fig. 4.6 Velocity F for the curves in Fig. 4.5, as a function of offset
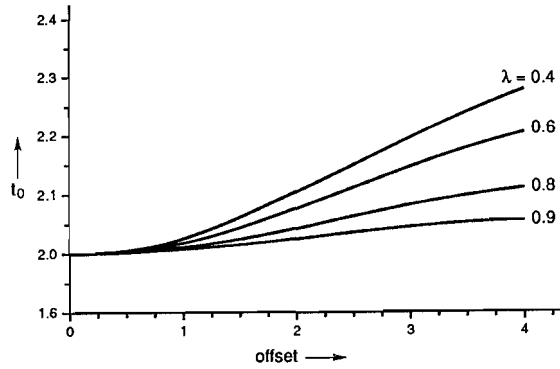
Fig. 4.7 Intercept time t_0 for the curves in Fig. 4.5, as a function of offset.
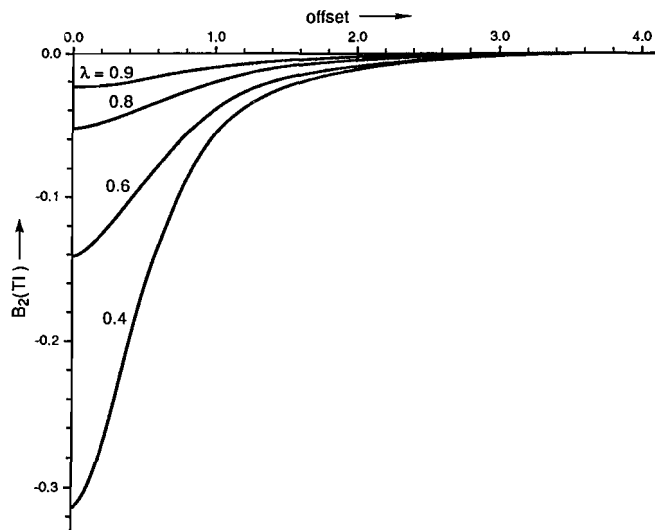
Fig.4.8 The third Taylor series term due to anisotropy, for the curves in Fig. 4.5
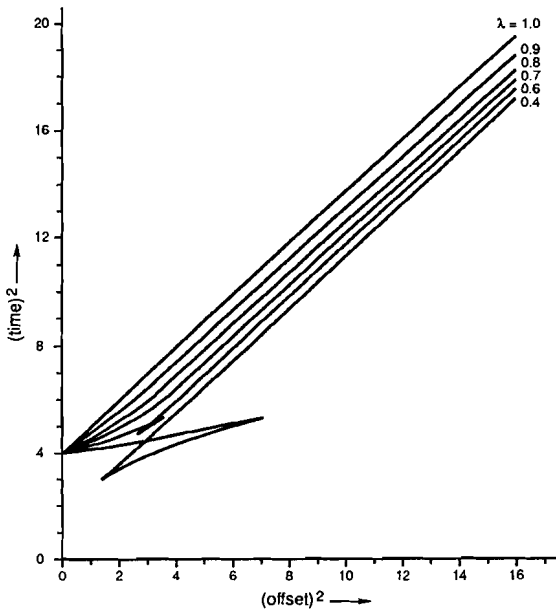
Fig. 4.9 t^2-x^2 curves of S2-waves for a homogeneous K-medium. Reflector depth and vertical S2-wave velocity are taken as units, $\tau=0.3$
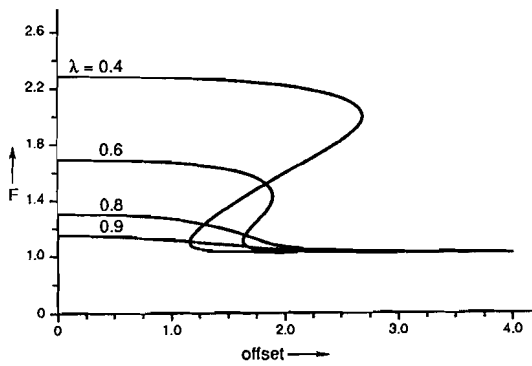
Fig. 4.10 Velocity F for the curves in Fig. 4.9, as a function of offset.
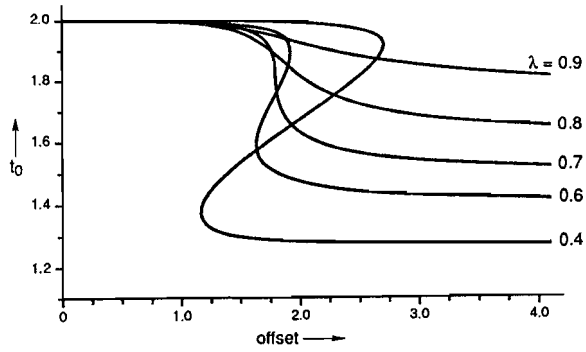
Fig. 4.11 Intercept time t_0 for the curves in Fig. 4.9, as a function of offset.
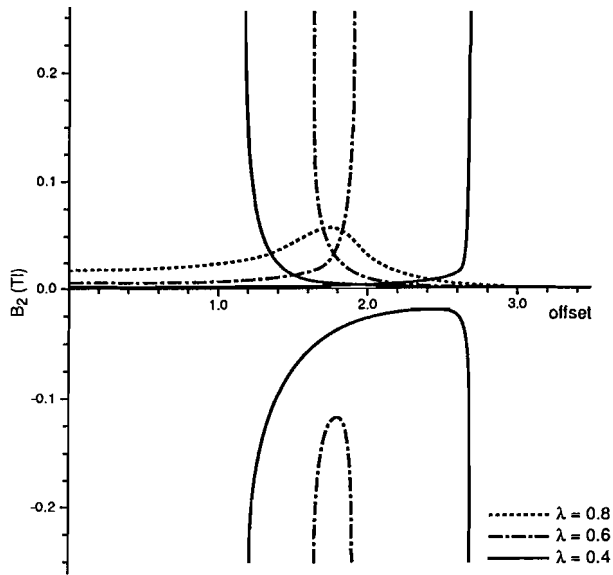
Fig.4.12 The third Taylor series term due to anisotropy, for the curves in Fig. 4.9

A decrease in λ, i.e. an increase in anisotropy, causes an increase of $B_2(TI)$ until a certain value of λ where $B_2(TI)$ reaches a maximum. Further decrease of λ leads to a decrease of $B_2(TI)$. The curve for $\lambda = 0.4$, for example, shows that for $x_0 < 1$ (offset smaller than the reflector depth) $B_2(TI)$ is almost zero. Thus with S2-wave data and with a maximum geophone offset smaller than the reflector depth one could "miss" the cuspidal behaviour. If the t^2 - x^2-curve would be a straight line it would mean that either the medium is isotropic or "very transversely isotropic"!
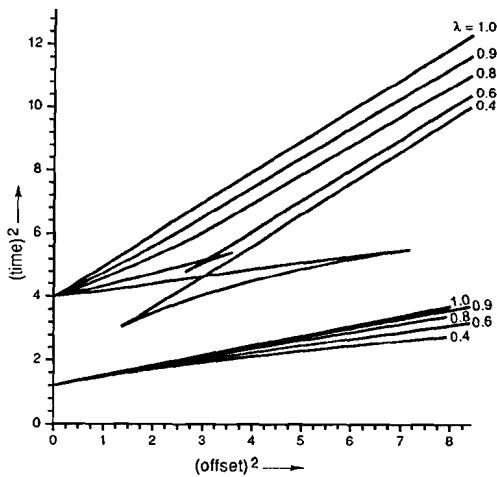
Fig. 4.13 t^2-x^2 curves of S2-waves (upper curves) and for P-waves (lower curves) for the medium as in Fig. 4.9

Figure 4.13 shows t^2 - x^2-curves for P- and S2-waves for the medium of Fig. 4.9. The difference between the respective curves are obvious. The curves are convex downwards for the S2-waves and convex upwards for P-waves. At small offsets the slope for P-waves is independent of λ, but for S2-waves strongly dependent on λ. For large offsets the slope is approximately constant for S2-waves while this is not true for P-waves. The time difference between two S2-wave curves is larger than that between the corresponding P-wave curves. Deviation from a straight line is in general larger for S2-waves than for P-waves. For P-waves this deviation is strongest for small offsets (vertical rays) while for S2-waves the

strongest deviation from a straight t^2 - x^2-curve occurs for offsets between 1.2 and 2.4 (for angles between 30 and 50 degrees against the vertical).

4.9 Time-to-depth conversion

To convert arrival times to depths in a correct way, vertical travel times and vertical velocities should be used. We have seen that these velocities are in general not obtained from t^2 - x^2 curves of transversely isotropic media by routine application of the Dix-Krey equation (Dix 1955, Krey 1951). Hence, when anisotropy effects are ignored, calculated depths may be in error. If the same reflector has been observed with different wave types, different depths can be calculated for each wave type. The mismatch between P-, S1- and S2-events corresponding to the same reflector is sometimes called the "P-S-event tie problem". For small offsets, the mismatch between the true depth of a reflector and the calculated depth (using F) is relatively small for P-waves. The calculated depth of the reflector can be larger, equal to or smaller than the true depth. The effect of mismatch for S-waves is larger than for P-waves: for S1-waves the calculated depth is true depth multiplied by $(1/\lambda)^{1/2}$; the effect for S2-waves is even larger.

4.10 Conclusions

We studied interval velocities F derived from reflection curves, for

horizontal reflectors and layers that possess transverse isotropy caused by fine layering. We found that F is in general not the same as the vertical velocity. The exception is for P-waves when the intrinsic fine layers all have the same Poisson ratio and the velocity is obtained from (near-) zero offset data. We defined the anisotropy factor A as the ratio of F and the vertical velocity. This factor depends for P-waves and S2-waves (polarised in the sagittal plane) on offset. The derived velocity is an apparent horizontal velocity. It is the horizontal velocity of the best-fit ellipse through the wave surface. The wave surface is only for the S1-wave a true ellipse. For S1-waves F and A are therefore independent of offset.

(i) Small offsets: For P-waves A is in the vicinity of unity. For S-waves A can reach much higher values, for example values around 2. The anisotropy factor for S2-waves is always larger than for S1-waves.

(ii) Larger offsets: For P-waves F increases with offset. The same effect can be caused by a vertical velocity gradient in the layer. For S2-waves F decreases with offset, opposite to the effect of vertical inhomogeneity.

The deviation from an hyperbola is of relevance, as in practice stacking velocities are computed from hyperbolic fits. For P-waves this deviation is largest at small offsets. Remarkable is that for S2-waves, although F strongly deviates from the vertical velocity, the reflection curve is more hyperbolic than for P-waves. Only at large offsets, where ray directions are round about 40° against the vertical, the S2-wave reflection curve can be strongly non-hyperbolic.

Erroneous interpretation of reflection curves (i.e. acceptance of the derived velocity as vertical velocity) can lead to an erroneous reflector depth. It leads to a mismatch in depth between P-, S2- and S1-events belonging to the same

reflector.

If a sufficient number of independent observations of arrival time curves exist (e.g. if P-, S1- and S2-waves have been observed) the expressions for the Taylor series terms can be used to calculate the elastic parameters of the layers.

APPENDIX A: Derivation of the terms of the Taylor series for a t^2-x^2 curve

The relation between arrival time t and offset x is

$$t^2 = \lim_{x \to x_0} \sum_k B_k (x^2 - x_0^2)^k \qquad (A4.1)$$

with

$$B_k = \frac{1}{k!} \frac{d^k(t^2)}{(dx^2)^k} \qquad (A4.2)$$

Consider a horizontally layered medium, each layer being homogeneous and either isotropic or transversely isotropic.

Define

γ the angle between wave velocity vector $\underline{G}$ and the vertical axis,

$\underline{S}$ the slowness vector,

$\underline{V}$ the phase (or normal) velocity vector.

Assume the ray travels in the vertical plane (1-3 plane or x-z plane). The two-way travel time along the ray is (Fig. A4.1):

$$t = \sum_{i=1}^{Q} \Delta t_i \qquad\qquad (A4.3)$$

with

$$\Delta t = \frac{2\,\Delta z}{|G|\,\cos(\gamma)} = \frac{2\,\Delta z}{g_3} \qquad\qquad (A4.4)$$
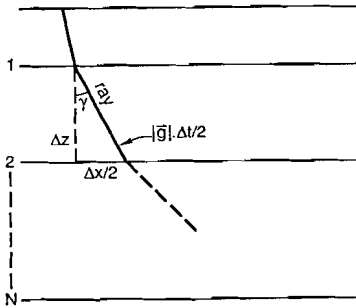
Fig. 4.A1 Geometry of a ray segment

The corresponding offset x is

$$x = \sum_{i=1}^{Q} \Delta x_i \qquad\qquad (A4.5)$$

with

$$\Delta x = 2\,\Delta z\,\tan(\gamma) = \Delta t\,g_1 \qquad\qquad (A4.6)$$

From (A4.2) we have

$$B_0 = \left(\sum_{i=1}^{Q} \Delta t_i \right)^2 \tag{A4.7}$$

and

$$B_1 = \frac{d(t^2)}{d(x^2)} = \frac{t}{x} \frac{dt}{dx} \tag{A4.8}$$

The ray parameter p is: $p = dt/dx$, and equals the horizontal slowness component s_1. Thus

$$B_1 = p \sum_{i=1}^{Q} \Delta t_i \bigg/ \sum_{i=1}^{Q} g_{1i} \, \Delta t_i \tag{A4.9}$$

Define

$$F^2 = g_1 / s_1 \tag{A4.10}$$

One thus gets

$$B_1 = \sum_{i=1}^{Q} \Delta t_i \bigg/ \sum_{i=1}^{Q} F_i^2 \, \Delta t_i \tag{A4.11}$$

Because

$$s_1 = \frac{v_1}{|V|^2} \tag{A4.12}$$

equation (A4.10) can be written as

$$F^2 = \frac{g_1}{v_1} |V|^2 \tag{A4.13}$$

In the case of isotropy, wave velocity $\underline{G}$ and phase velocity $\underline{V}$ are equal and thus $g_1 = v_1$. So in case of isotropy $F^2 = |V|^2$. From (A4.2) we have

$$B_2 = \frac{1}{2}\frac{d}{dx^2}\left[\frac{dt^2}{dx^2}\right] \tag{A4.14}$$

$$= \frac{1}{2}\frac{d}{dx^2}\sum_{i=1}^{Q}\Delta t_i \Big/ \sum_{i=1}^{Q}F_i^2\,\Delta t_i \tag{A4.15}$$

For convenience we drop indices i in the following. Equation (A4.15) becomes

$$B_2 = \frac{1}{4x}\left\{\frac{\Sigma F^2\Delta t\ \frac{d}{dx}(\Sigma\Delta t) - \Sigma\Delta t\ \frac{d}{dx}(\Sigma F^2\Delta t)}{(\Sigma F^2\Delta t)^2}\right\}, \tag{A4.16}$$

with

$$\frac{d}{dx}(\Sigma\Delta t) = p \tag{A4.17}$$

and

$$\frac{d}{dx}(\Sigma F^2\Delta t) = \frac{d}{dx}\left[\frac{x}{p}\right], \tag{A4.18}$$

since $x = p\,\Sigma\,F^2\,\Delta t$. Equation (A4.18) can be written as

$$\frac{p - \dfrac{x}{dx/dp}}{p^2} = \frac{\dfrac{d}{dp}(\Sigma\,F^2\Delta t)}{\Sigma\,F^2\,\Delta t + p\,\dfrac{d}{dp}(\Sigma F^2\Delta t)} \tag{A4.19}$$

with

$$\frac{d}{dp}(\Sigma\,F^2\Delta t) = \Sigma\left\{\Delta t\,\frac{dF^2}{dp} + F^2\,\frac{d\Delta t}{dp}\right\} \tag{A4.20}$$

If we take the limit for zero offset, the expression for B_2 becomes

$$\lim_{x\to 0} B_2 = \frac{(\Sigma F^2\Delta t)^2 - \Sigma\Delta t \cdot \Sigma(F^4 + H)\,\Delta t}{4(\Sigma F^2\Delta t)^4} \tag{A4.21}$$

with $\quad H = \left[\frac{1}{p}\,\frac{d(F^2)}{dp}\right]$ \hfill (A4.22)

Chapter 5

Anisotropy factors: practical aspects

5.1 Introduction

In chapter 4 we looked at interval velocities computed from arrival time curves of reflected waves. It was shown how F, the velocity computed from the slope of t^2-x^2 curves, depends on the elastic medium parameters (equations (4.12), (4.14) and (4.16)). For anisotropic layers F is in general not the vertical velocity (equations (4.20) and (4.21)). Moreover, F varies with offset (Fig. 4.6 and 4.10). The anisotropy factor A was defined as the ratio of F and the vertical velocity.

Stacking velocities are derived from hyperbolic fits to reflection time (t-x) curves. The interval velocities computed from stacking velocities are hereafter called seismic velocities. In areas of seismic exploration there are mostly, next to seismic reflection data, check shot data (seismic source at surface, receiver down-hole). The velocities obtained from these check shots are vertical velocities, hereafter called well velocities. From seismic and well velocities the anisotropy factor can be derived. However, some practical problems arise. The seismic velocity is not exactly equal to F since the seismic velocity is derived from a fit over a certain offset range. Moreover, in structurally complex areas, such as for example several dipping and non-parallel layers, the computed interval velocity can not simply be corrected for subsurface geometry to obtain a geometry-free velocity (chapter 6). A correct F can then only be obtained by using velocity model

building and depth-migration techniques. Even for a flat subsurface geometry the seismic velocity may differ from F, namely when a layer has a vertical gradient in its elastic parameters. In practical situations all layers are somewhat inhomogeneous. The objective of this chapter is to estimate the magnitude of the effect of velocity gradients on differences between seismic and well velocities. It is found that this effect can be of the same magnitude as anisotropy effects. It is therefore relevant for interpretation of observed mismatches between seismic and well velocities.

5.2 Inhomogeneity factors

Imagine a single horizontal isotropic layer with a linear velocity function with gradient k,

$$k = \frac{v2-v1}{z2-z1}, \qquad (5.1)$$

where v1 is the velocity at z1, the top of the layer, and v2 is the velocity at the layer's base, z2.

The two-way vertical travel time is

$$t = \int_{z1}^{z2} \frac{1}{v(z)} dz = \frac{2}{k} \ln\left[\frac{v2}{v1}\right] \qquad (5.2)$$

The velocity obtained from a check shot, the well velocity v_w, is

$$v_w = 2 \, (z2-z1) / t \qquad (5.3)$$

The root-mean-square velocity v_{rms} is

$$v_{rms} = \left[\left[\int_{t1}^{t2} v^2 \, dt \right] / t \right]^{1/2} \qquad (5.4)$$

$$= \{ v_w \, (v1+v2)/2 \}^{1/2}, \qquad (5.5)$$

The well velocity v_w is always smaller than the velocity at mean depth if $k \neq 0$ (more time is spent in the slower part). The root-mean-square velocity is therefore larger than the well velocity.

Let me now define the inhomogeneity factor I as the ratio of seismic velocity v_s to well velocity v_w for an isotropic layer.

$$I = v_s / v_w \qquad (5.6)$$

Factor I depends on the offset range since the seismic velocity v_s depends on offset.

(i) lower limit for I :

For small offsets v_s is equal to the rms-velocity. This gives the lower limit for I.

$$I_{min} = \{ (v1+v2)/2 \ln(v2/v1) (v2-v1)^{-1} \}^{\frac{1}{2}} \qquad (5.7)$$

(ii) upper limit for I:

I use the theory of chapter 6 to find an upper limit for the inhomogeneity factor. In the intercept time τ – ray parameter p domain, reflection time curves for horizontal reflectors have a simple relationship with the slowness surfaces of the layers. Ray parameter p is the horizontal slowness component, which is constant along a ray path. Intercept time τ is the sum over all layers of vertical slowness component multiplied by layer thickness.

$$\tau = \sum_i s_{zi} z_i, \qquad (5.8)$$

where s_z is the vertical slowness component. If the velocity is a continuous function with depth this reads

$$\tau = \int s_z(z) \, dz \qquad (5.9)$$

Since $p = s_x$ (the horizontal slowness component) and $s_x^2 + s_z^2 = v^{-2}$, this can be written as

$$\tau(p) = \int \frac{(1 - p^2 v(z)^2)^{1/2}}{v(z)} \, dz \qquad (5.10)$$

With this expression we can compute the reflection time curve for an isotropic

interval with the velocity function given by equation (6.1). This τ-p curve can then be interpreted in terms of an effective slowness surface for the interval: $s_x=p$, $s_z=\tau/(2(z2-z1))$. The result is

$$s_z = \frac{1}{(v2 - v1)} \left\{ y - \frac{1}{2} \ln \left| \frac{1+y}{-1+y} \right| \right\} \quad \left| \begin{array}{l} (1-s_x^2 v2^2)^{1/2} \\ \\ (1-s_x^2 v1^2)^{1/2} \end{array} \right. \tag{5.11}$$

Let us assume v2>v1. Then s_z is complex for p>1/v2, representing the evanescent regime. For p<1/v2 the slowness curve is approximately an ellipse. This is illustrated in Fig. 5.1 by the approximately straight line in the squared slowness domain. The ratio of vertical and horizontal ellipse axis is equal to the ratio of seismic velocity and well velocity. It gives an upper limit for I, obtained for an offset range corresponding to the range from p=0 to p=1/v2. Numerical tests showed

$$I_{max} \cong 1 + 0.05 \left[\frac{v2}{v1} - 1 \right] \tag{5.12}$$
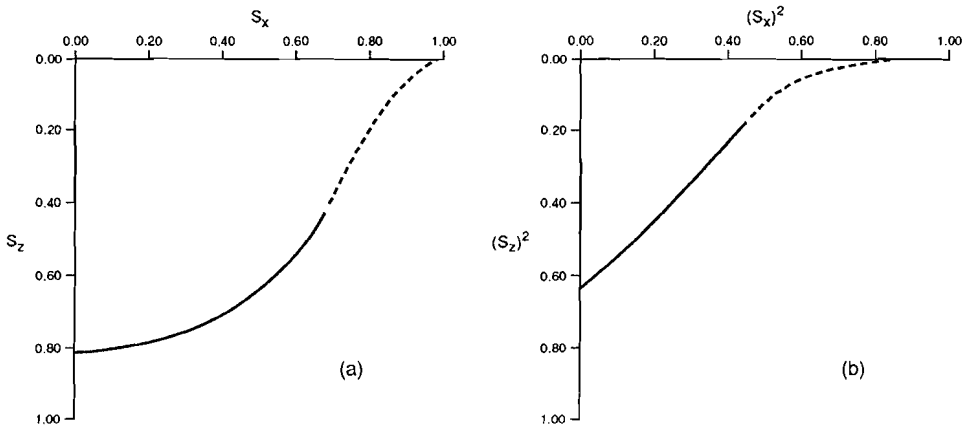
Fig 5.1 (a) Slowness surface derived from a τ-p curve for an isotropic layer with a linear vertical velocity gradient: v1 = 1, v2 = 1.5. The dashed part of the curve represents the evanescent regime. (b) The squared slowness surface to demonstrate its ellipse-like shape.

For typical offset ranges used in seismic exploration (the maximum offset about the same as the depth of the objective level), the inhomogeneity factor lies

approximately halfway between I_{min} and I_{max}.

We take, for example, the velocity function $v(z) = v(0) + k. z$, with $v(0) = 1500$ m/s and $k = 1$ s^{-1}. For $z1=0$ and $z2=1000$ m we have $I_{min} = 1.010$ and $I_{max} = 1.033$. When the stacking velocity is derived from an offset range between 250 and 2500 m we find $I_{250<x<2500} = 1.026$.

For $z1=0$ and $z2=2000$ m the results are $I_{min} = 1.029$, $I_{max} = 1.067$ and $I_{250<x<2500} = 1.039$.

5.3 Real data examples

P-waves

Figure 5.2 shows a real data example for P-waves from North Sea data. The seismic stacking velocities and two-way zero-offset travel times are from the Base Tertiary reflector. The data are from a block of 6x6 km^2 in which five wells are located. The seismic velocities are corrected for reflector dip, where the dip is estimated from the time-slope of the horizon (the slope in a time section) and the best-fitting linear velocity-time function.

The velocity-time function is used for time-to-depth conversion of the reflection times. The seismic velocities and the well velocities are displayed versus the mean depth of the interval. Figure 5.2 shows that the well velocities are lower than the seismic velocities. The ratio of seismic velocity to well velocity is for the five wells on average 1.025 ± 0.008 (the seismic velocity is taken from the best-fitting velocity function, the error is computed from the 95% confidence limit on the seismic data points). This ratio can, within the accuracy of the measurements, completely be explained by a vertical velocity gradient. The best-fitting velocity function for the seismic velocities gives $v(0)=1516$ m/s and $k=0.79$ s^{-1}. This results in an inhomogeneity factor $I_{min} = 1.02$. Hence the difference between well velocities and seismic velocities in this example are due to inhomogeneity and not due to anisotropy.
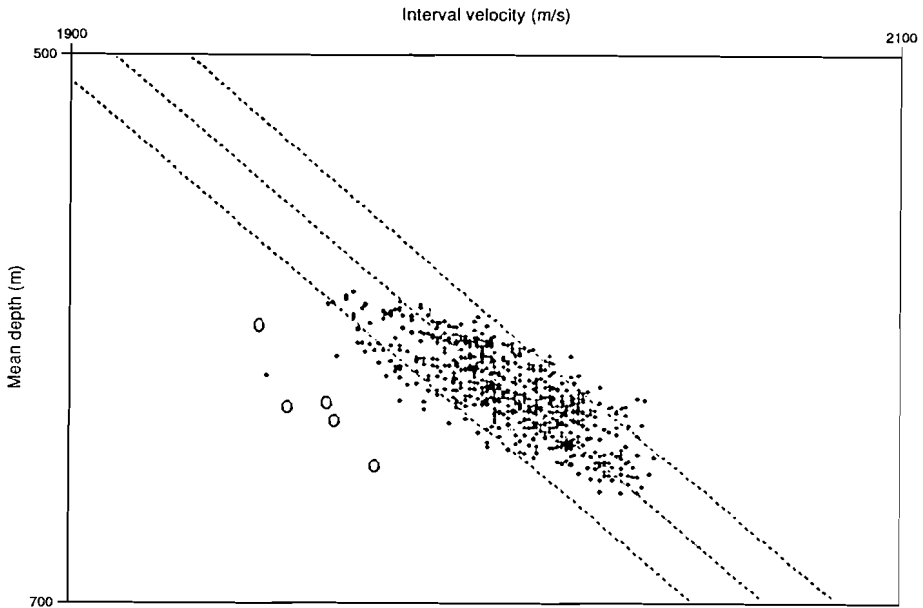
Fig. 5.2 P-wave interval velocities versus mean depth for the interval between datum and Base Tertiary. Open circles are well velocities, black dots are seismic velocities. The outer dashed lines give the 95% confidence limits, the middle dashed line the best fitting linear seismic velocity function: V(z) = 1516 + 0.79 * z (m/s). This velocity gradient accounts for the consistently lower well velocities.

S-waves

Table 1 gives the shear-wave velocity profile obtained from a seismic experiment in the northern part of the Netherlands.

The interval shear-wave velocities are calculated from stacking velocities. It is possible that the intervals are anisotropic. In that case the listed velocities are equal to the vertical velocity multiplied by an anisotropy factor. This does, however, not affect the calculation of the inhomogeneity factors I_{min} and I_{max}. In their expressions, (5.7) and (5.10), the anisotropy factor drops out. For the whole depth range, i.e. from zero to 820 m, we obtain I_{min} = 1.10 and I_{max} = 1.24. A smaller depth range reduces these factors ; for z=0-227 m

I_{max} = 1.07, for z = 0-462 m I_{max} = 1.16, for z= 462-820 m I_{max} = 1.02.

Table 1: shear-wave velocity profile

depth (m)	velocity (m/s)
0 - 218	380
218 - 277	540
277 - 462	740
462 - 583	886
583 - 820	1080

5.4 Conclusions

Vertical velocity gradients cause differences between seismic velocities and well velocities that can be of the same order of magnitude as those typical for layer-induced anisotropy. For P-waves the mismatch can be a few percent. For shear waves it can under realistic circumstances be up to 20%, especially in shallow sediments with a large shear-wave velocity gradient.

If seismic interval velocities, derived from stacking velocities, are compared with interval velocities from check shots, one should bear in mind that

(i) if the interval is thick, resulting in a large relative velocity difference between top and bottom of the interval, the larger seismic velocities may completely (or for a large part) be caused by inhomogeneity and not by anisotropy,

(ii) if for a thin interval the seismic velocity is found to be larger than the well velocity then this is likely due to anisotropy rather than due to inhomogeneity.

Chapter 6

Anisotropy and Tau-P transforms

Abstract

Slant stacking transforms seismic data, recorded as a function of source-receiver offset and travel time, into the domain of intercept-time τ and ray parameter p. The shape of τ-p curves is closely related to slowness surfaces. A layer-stripping operation in the τ-p domain removes the effects of the layers above a target layer. The resulting curve is the slowness surface of the target layer except for a scaling factor containing thickness and dip of the layer. The relationship between τ-p curves, slowness surfaces and geometry of the subsurface can be expressed analytically. Synthetic τ-p curves, calculated with the reflectivity method, show some of the difficulties that can arise in determining the shape of the curves and in applying the stripping operation.

6.1 Introduction

The analysis of seismic reflection and refraction data using tau-p transforms is done for a variety of applications. For example, tau-p filtering is applied in order to separate shear waves and compressional waves (Tatham et al. 1982). Analysis of dispersive ground roll in the p-f domain (McMechan 1980), velocity model determination in the tau-p domain (Diebold 1981, Stoffa et al. 1981 and Kennett 1981), migration (Bisset and Durrani 1984) and p-dependent deconvolution to compensate for source- and receiver directivity (Van der Schans and Ziolkowsky 1983) are other applications.

The tau-p transform, or slant stacking, is often mentioned as a plane wave decomposition of seismograms (Chapman 1981, Treitel et al. 1982). It means that after the transform has been applied, the data can be considered as originating from (a series of) plane-wave sources. This property of the transform is commonly known for isotropic media but also holds for anisotropic media, as will be shown later. The tau-p transform translates the data from the wave surface domain into the slowness surface domain. It has therefore additional significance for anisotropic media, where plane-wave velocities and ray velocities are in general different. The transform can make it easier to analyse and model the data with the eikonal equation, which relates phase velocities to the elastic parameters, not ray velocities. Also, the possible multi-valued-ness of the data due to cusps in the wave front is removed after the transform has been applied.

In the next paragraph I discuss the slant stack transform and show that it can be regarded as a plane wave decomposition. Then I apply the slant stack to analyse travel times of reflected waves. These arrival times depend on the geometry of the layers (thickness and dip) and on the elastic parameters of each layer. The tau-p curves are scaled slowness surfaces. The scaling depends on the geometry of the subsurface. I derive this scaling factor for horizontal layers and for dipping layers. The relationship between tau-p curves and slowness surfaces can be used to visualize the slowness surfaces of the layers.

6.2 The slant stack transform

Two types of transforms for transforming seismic data from the offset-time domain to the tau-p domain (and vice versa) exist. One is the slant stack or Radon transform, the other is called the 'proper slant stack' and is in essence almost equivalent to the Sommerfeld integral. Both transforms can be used for applications based on travel times of events. The difference between the two transforms is the way they handle amplitudes. The Radon transform is used for proper amplitude handling in case the seismic source is a line-source. For a point-source the 'proper slant stack' should be applied (see, for example, Chapman 1981). In the following the discussion is restricted to line-sources.

The forward slant stack transform is defined as (Chapman 1981)

$$u(p,\tau) = \int_{-\infty}^{\infty} u(x,\tau+px)\,dx \tag{6.1}$$

where $u(x,t)$ is the wave field as function of time t and horizontal spatial coordinate x. The inverse transform is

$$u(x,t) = \frac{1}{2\pi} \frac{d}{dt} H(\int_{-\infty}^{\infty} u(p,t-px)\,dp), \tag{6.2}$$

where H denotes the Hilbert transform.

The process of slant stacking can be represented in a graphical way. The slant stack of a panel of traces in the t-x domain is the sum of the sample values from each trace along a given slope. That is, for a given slope or slant of $p=dt/dx$ and a given intercept time τ of this slope, the sum of all points along that slope is attributed to the new sample at τ,p. The transform is formed by summing along numerous different slopes and intercept times. The inverse transform is again a slant stack, but now along slopes of $x=-d\tau/dp$.

The definition of the Fourier transform pair is:

$$G(\omega) = \int_{-\infty}^{\infty} e^{i\omega t} \, g(t) \, dt \tag{6.3}$$

with the inverse transform

$$g(t) = \frac{1}{2\pi} \int_{-\infty}^{\infty} e^{-i\omega t} \, G(\omega) \, d\omega \tag{6.4}$$

The temporal Fourier transform applied to the forward slant stack results in the frequency representation of this transform:

$$u(p,\omega) = \int_{-\infty}^{\infty} e^{-i\omega p x} \, u(x,\omega) \, dx \tag{6.5}$$

The spatial Fourier transform applied to the wave field results in:

$$u(\underline{K},\omega) = \int_{-\infty}^{\infty}\int_{-\infty}^{\infty} e^{i(k_x x + k_z z)} \, u(\underline{X},\omega) \, dxdz \tag{6.6}$$

A physical meaning can be assigned to the transform parameter $\underline{K}$. Plane waves satisfy the wave equation, see chapter 2, with their velocity given by the eikonal equation (2.16). For homogeneous media equation (6.6) satisfies the wave equation if $k_x{}^2 + k_z{}^2 = \omega^2 |\underline{S}|^2$. Then $u(\underline{K},\omega)$ is the wave field of a plane wave with slowness $\underline{S}$. For horizontally layered models we apply the spatial Fourier transform with respect to x only,

$$u(k_x,\omega) = \int_{-\infty}^{\infty} e^{ik_x x} \, u(x,\omega) \, dx, \tag{6.7}$$

and $u(k_x,\omega)$ satisfies the wave equation if $k_x{}^2 = \omega^2 |\underline{S}|^2 - k_z{}^2 = \omega^2 \, s_x{}^2$. The resemblance of equations (6.5) and (6.7) implies that $p^2 = s_x{}^2$. Hence, p is the horizontal slowness component, which is the same for all three wave modes in each horizontal layer.

6.3 Travel times

The travel time t along a ray in an isotropic medium is
$t = |\underline{L}| / |\underline{V}| = \underline{L} \cdot (\underline{V}^{-1})$, where $\underline{L}$ is the raypath and $\underline{V}$ the velocity along the
path. $\underline{V}^{-1}$ is the inverse velocity or slowness. In an anisotropic medium the travel
time is $t = |\underline{L}| / |\underline{G}| = \underline{L} \cdot \underline{S}$, where $\underline{G}$ is the ray velocity, $\underline{S}$ the slowness and
$\underline{S} \cdot \underline{G} = 1$, see (2.30). Because of the similarity between the expressions for the travel
time in isotropic and in anisotropic media, both being the inproduct of a distance
vector and a slowness vector, the equation for the travel time in a layered earth as
given by Diebold and Stoffa (Diebold and Stoffa 1981), can be generalized for an
anisotropic earth to

$$t = x_a\, s_{x;1}^{d} + x_b\, s_{x;1}^{u} + \sum_i Z_i(\, s_{z;i}^{d} + s_{z;i}^{u}\,) \qquad (6.8)$$

in which (see Fig. 6.1)

x_a is the offset between shot position A and an arbitrary but fixed reference point,

x_b is the offset between receiver position B and this reference point, ($X = x_a + x_b$,
the total offset),

$s_{x;1}^{d}$ is the x-component of slowness vector $\underline{S}$, belonging to the downgoing ray in
layer 1,

$s_{x;1}^{u}$ is the x-component of slowness vector $\underline{S}$, belonging to the upgoing ray in layer
1,

$s_{z;i}^{d}$ is the absolute value of the z-component of slowness vector $\underline{S}$, belonging to the
downgoing ray in layer i,

$s_{z;i}^{u}$ is the absolute value of the z-component of slowness vector $\underline{S}$, belonging to the
upgoing ray in layer i,

Z_i is the thickness of layer i, measured at the reference point and $Z_i \geq 0$.
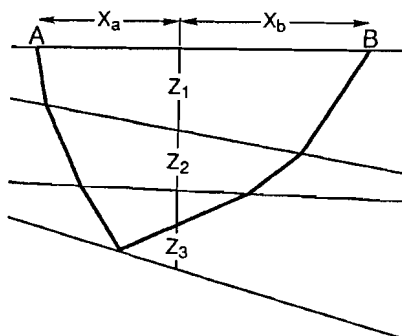
Fig. 6.1 Ray path in a dipping layer model.

The significance of equation (6.8) is not only that it gives the exact travel time for any recording geometry, but also that it relates horizontal and vertical components of slowness vectors to travel times. The relationship between offset X, travel time t, ray parameter p and intercept time τ is

$$t = pX + \tau \tag{6.9}$$

Hence, form (6.8) and (6.9) it follows that p is related to horizontal components of slowness vectors and τ is related to vertical components of slowness vectors. In other words, equation (6.8) relates τ-p curves to slowness surfaces. This relationship is further analysed in the next paragraphs for specific layer geometries.

Horizontal layers

Consider a set of horizontal layers, each being homogeneous and anisotropic (or isotropic as a special case of anisotropy). The slowness component along the interface is the same for all rays participating in the reflection-transmission process at the interface (Snell's law). Thus

$$s_{x;i}^{d} = s_{x;i}^{u} = s_x \tag{6.10}$$

and (6.8) becomes

$$t = X \, s_x + \sum_i Z_i (\, s_{z;i}^{d} + s_{z;i}^{u} \,)$$

(6.11)

It then follows for τ and p:

$$p = s_x$$

(6.12)

and

$$\tau = \sum_i Z_i (\, s_{z;i}^{d} + s_{z;i}^{u} \,)$$

(6.13)

For the first reflector the τ-p curve is equal to the average of down- and upward parts of the slowness surface of the first layer, except for a scaling factor 2Z in the τ-axis. This is illustrated in Fig.s 6.2, which show the relationship between wave surface (Fig. 6.2a), slowness surface (Fig. 6.2b), t-x curve (Fig. 6.2c) and τ-p curve (Fig. 6.2d).

For the N-th reflector the τ–p curve is the sum of all the average slowness surfaces of the layers above, with for each surface the vertical slowness component multiplied by twice the layer thickness. The $(\tau_N - \tau_{N-1})$ - p curve, which is obtained after subtraction of the N-th and (N-1)-th τ-p curve, equals the scaled average slowness surface of the layer between reflectors N and N-1. This so-called stripping operation (Schultz 1982) removes the effects of the upper layers. This $(\Delta\tau)$ - p curve is elliptical when the interval is isotropic. Calculating the layer thickness is then similar to calculating the stretching factor which transforms the ellipse into a circle. The $(\Delta\tau)$ - p curve is also elliptical when the interval possesses elliptical anisotropy, or to be more precise, when the average of the downward and upward parts of the slowness surface is elliptical.
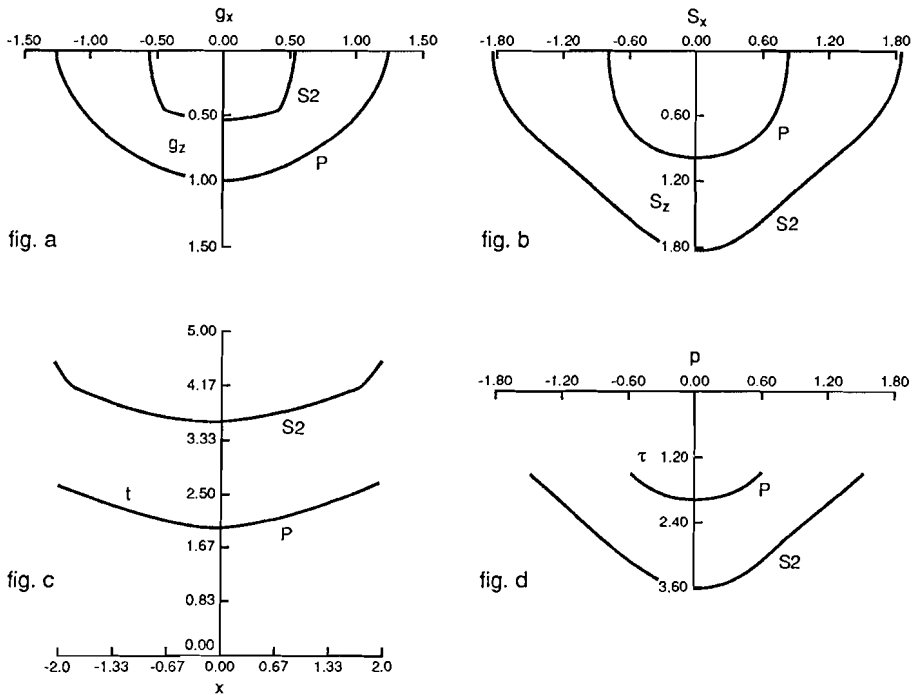
Fig. 6.2 Wave surfaces (Fig a), slowness surfaces (Fig. b), t-x curves (Fig. c) and τ-p curves (Fig d) of P- and S2 waves for a transversely isotropic medium with $c_{11}/\rho=1$,

$c_{44}/c_{66} = 0.6$, $c_{13}/c_{33} = 0.4$, $c_{44}/c_{33} = 0.3$ and $c_{66} = \frac{1}{2.8}(c_{11} - c_{13}{}^2/c_{33})$. The wave surface has small cusps. The reflector is horizontal at unit depth. The τ-p curves are obtained from slant stacking the t-x curves in Fig. c.

Dipping layers

In case of dipping reflectors the travel time curves depend on the recording geometry. For a Common-Shot-Point gather, shot-position A is kept constant and the natural choice for the reference point is $x_a = 0$ and $x_b = X$. For a Common-Mid-Point-gather the reference point is in the middle between shot position and receiver

position: $x_a = x_b = \frac{1}{2} X$.

CMP geometry

For the one-layer case (Fig. 6.3) equation (6.8) becomes for a CMP-gather:

$$t_{CMP} = \frac{1}{2} X (s_x^d + s_x^u) + Z_M (s_z^d + s_z^u) \qquad (6.14)$$

fig. a   fig. b
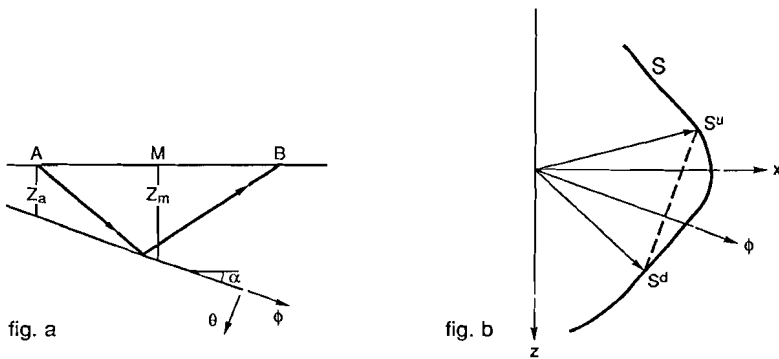
Fig. 6.3 Snell's law for a dipping layer. The downgoing and upgoing ray (Fig. a) correspond to a downgoing (s^d) resp. an upgoing (s^u) slowness vector (Fig. b), which lie on one and the same normal to the reflecting interface, the parameter line (dashed).

Ray parameter p is the average of the horizontal components of the slowness vectors while τ is the average of the vertical components, multiplied by twice the thickness at the CMP-point. Again the ($\tau/2z$) - p curve is an average slowness surface.

A special case is obtained for a reflector coinciding with a symmetry plane of the slowness surface. Anisotropy caused by, e.g., the alignment of small scale heterogeneities as elongated pores or grains, cracks or fine layering, has such symmetry if these alignments are parallel to the reflector. If the slowness surface in Fig. 6.3b would be symmetrical around the reflector it follows immediately that then the expressions for τ and p are

$$p_{sym} = \cos(\alpha)\, s_\phi \tag{6.15}$$

$$\tau_{sym} = 2Z_M \cos(\alpha)\, s_\theta \tag{6.16}$$

in which ϕ and θ are a new coordinate system as defined in Fig. 6.3a, α is the dip and $s_\theta \geq 0$. The τ-p curve is elliptical if the layer is either isotropic or elliptical anisotropic with respect to the ϕ-θ coordinate system. The τ-p curve is the slowness surface ($s_\phi - s_\theta$ curve) of the layer, stretched in the "ϕ" direction with $\cos(\alpha)$ and in the "θ" direction with $2Z_M \cos(\alpha)$.

<u>CSP geometry</u>

For a CSP gather equation (6.8) becomes for the one-layer case

$$t_{CSP} = X\, s_x^u + Z_A (\, s_z^d + s_z^u\,) \tag{6.17}$$

For the special case that the reflector coincides with a symmetry plane, we have

$$p_{sym} = \cos(\alpha)\, s_\phi \pm \sin(\alpha)\, s_\theta, \quad \begin{array}{l} \text{+ for shooting down-dip} \\ \text{- for shooting up-dip} \end{array} \tag{6.18}$$

$$\tau_{sym} = 2Z_A \cos(\alpha)\, s_\theta \tag{6.19}$$

The τ-p curve is not elliptical for either isotropic or elliptically anisotropic layers.

Figure 6.4 shows an example for a dipping reflector not coinciding with a symmetry plane of the slowness surface of the layer above.

Multi-layered subsurface

For a set of interfaces, each with arbitrary dip, the τ-p curves can be computed if for every layer the thickness at the reference point, dip and the slowness surface are known. The slowness vectors belonging to one ray can be constructed using Snell's law (Fig. 6.5a,b) and equation (6.8) gives the travel time. The parameter line is not straight but bent if not all interfaces are parallel (Fig. 6.5). The number of bends corresponds to the number of layers with a divergent top and base. This
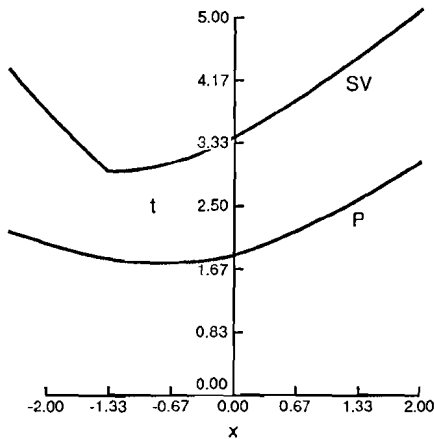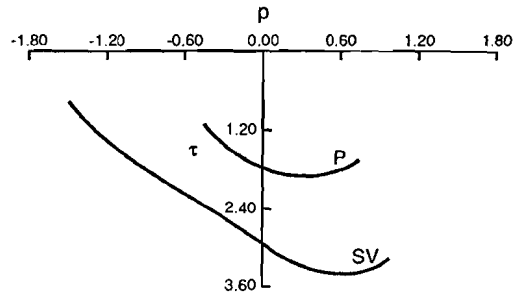
fig. a   fig. b

Fig. 6.4 t-x Curves (Fig. a) and τ-p curves of P- and S2 waves. The reflector dips 20° towards positive offsets. The elastic parameters are the same as in Fig. 6.3, with the symmetry axis perpendicular to the reflector. The layer thickness at the shot position is unity. The recording geometry is a CSP geometry. The τ-p curves are scaled slowness surfaces shown in Fig. 6.3. The scaling factors are given in equations (6.18) and (6.19).

complicates the interpretation of τ-p curves in terms of slowness surfaces.

Suppose the interval of interest is between interfaces N and N-1. The stripping operation is only useful if the two interfaces are parallel, because only then does ray parameter p in both τ-p curves have the same physical meaning. If top and bottom of the interval are parallel and stripping has been applied the result is $\tau = Z_N(s^d_{z;N} + s^u_{z;N})$ and, for a CMP geometry, $p = \frac{1}{2} (s^d_{x;1} + s^u_{x;1})$. Thus, p is related to horizontal slownesses of the shallowest layer and the question is how to relate these to the horizontal slownesses of the target interval. This relation depends on the shape of the parameter line. If for example the target layer is overlain by one divergent isotropic layer, then the meaning of the ray parameter in the Δτ-p curve is the same as in equation (6.15) or (6.18). This follows immediately from a construction similar to the one in Fig. 6.5b. Finally, it can be proven that the

$\Delta\tau$–p curve is not elliptical when all layers are isotropic and the target layer is overlain by two or more divergent layers with different slowness surfaces.

fig. a   fig. b
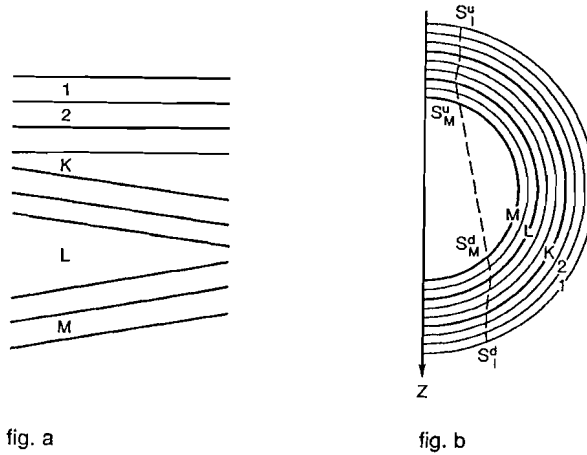
Fig. 6.5 Geometry (Fig. a) and slowness surfaces (Fig. b) of a multi-layered subsurface. Snell's law is illustrated for a ray reflected from the bottom of layer M; the slowness vector in each layer has its endpoint on the intersection of the parameter line and the slowness surface of that layer.

6.4 Synthetic tau-p curves

Figures 6.6 and 6.7 show synthetic τ-p curves calculated with the reflectivity method (Fuchs and Muller 1971) for a transversely isotropic model. The expression for the propagator matrix was calculated from the equations for wave propagation in transversely isotropic media (chapter 2). In the slant stack transform special care must be taken to avoid disturbing effects of aliasing and end-effects (Schultz and Claerbout 1978). The synthetics shown here are free of these artifact. This is
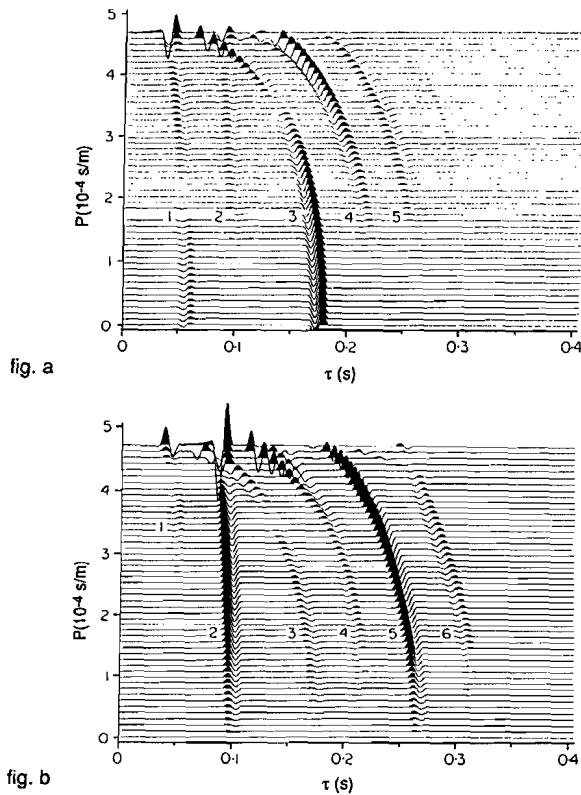
fig. a

fig. b

Fig. 6.6 Synthetic τ-p curves for a horizontal 3-layer model. Fig. a vertical displacements, Fig. b horizontal (x-direction) displacements. Layer 1: isotropic, z=40m, Vp=1600m/s, Vs=600m/s, ρ=2g/cm^3. Layer 2: hexagonal symmetry with vertical axis of symmetry, z=100m, c_{11}=9.057 [*10^{12} g/s^{2}m], c_{13}=2.322, c_{33}=5.807 , c_{44}=1.742 , c_{66}=2.903 , ρ=2 g/cm^3, (vertical S2-velocity=933 m/s, vertical P-velocity=1704 m/s, horizontal P-velocity=2128 m/s). Layer 3: isotropic half-space, Vp=1800 m/s, Vs=1000 m/s, ρ=2.5 gr/cm^3. The anisotropy parameters are an un-scaled version of those in Fig. 6.3. The source is an explosive point-source and the receivers are placed at the free surface.

Identification of the arrivals: 1 = P1P1 ; 2 = P1S1; 3 = P1P2P2P1 ; 4 = mixture of P1P2S2P1 + P1S2P2P1 and P1P2P2S1; 5 = P1P2S2S1 + P1S2P2S1 ; 6 = P1S2S2S1, in which for example P1S1 means a downward going P-wave in layer 1, reflected at the first interface and upward going in layer 1 as a S-wave (here S2- waves).

because the reflectivity method directly computes the response in the ray parameter domain.

The reflectivity zone, for which all primary reflections, multiples and converted waves are calculated, consists of a transversely isotropic layer with a vertical axis of symmetry. It is overlain by an isotropic layer, with an explosive point source and receivers at the free surface. Underneath the anisotropic layer is an isotropic half-space. The anisotropy parameters are an un-scaled version of those in Fig. 6.2. Travel time picking is needed for the stripping operation. It requires interpretation of the several events. In Fig. 6.6 for example, the P-wave slowness surface of the anisotropic layer, multiplied with 2Z, is obtained if the curves indicated with the numbers 1 and 3 are subtracted. These curves correspond to P-wave reflections from respectively the top and bottom of the anisotropic layer. The S2-slowness surface is obtained by subtracting curves 6 and 2.
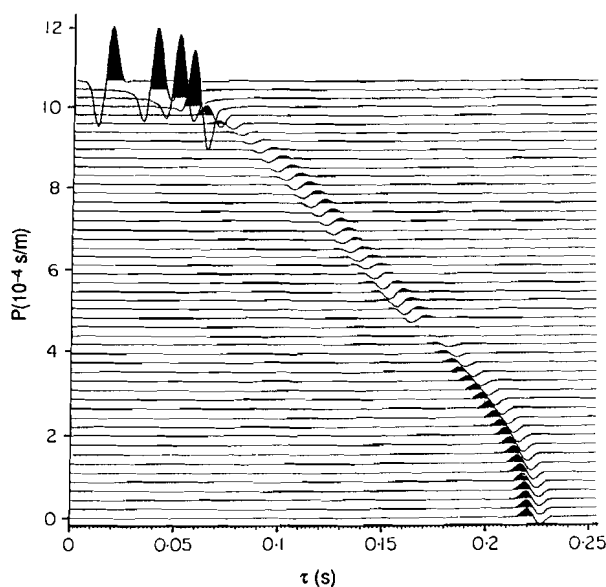
Fig. 6.7 Synthetic τ-p curve for the S2-wave reflected at the interface between layers 2 and 3 as described in Fig. 6.6. The input source signal is the same for all ray parameters. Displayed is the total displacement of the reflected wave. Z = 100 m.

Figure 6.7 illustrates the difficulties that can occur in the time picking due to phase- and amplitude changes of the wavelet. The figure gives the total displacement recorded inside the anisotropic layer due to a S2-wave reflected at the top of the half-space. The wavelet changes hamper the recognition of the typical shape of the slowness surface as in Fig. 6.2b.

6.5 Conclusions

The statement that the slant stack transform can be seen as a plane wave decomposition not only holds for isotropic media but also for anisotropic media. For horizontally stratified models each p-trace represents the model response of a plane wave for which the horizontal slowness component equals p. This transform from the wave surface domain (time-offset domain) to the slowness surface domain (τ-p domain) has special significance for anisotropic media where the characteristic surfaces have different properties.

If all layers are horizontal, a simple stripping operation in the τ-p domain results in the slowness surface of a selected interval, scaled in the vertical direction by twice the interval thickness. For dipping layers the scaling affects both the horizontal slowness and the vertical slowness. The scaling depends on the layer thickness, dip and on the recording geometry. If the subsurface consists of several dipping and non-parallel layers then the stripping operation does not result in a τ-p curve that can easily be scaled to a slowness surface. Practical difficulties may arise from identification of the events and from wavelet variations that hinder correct time picking.

Chapter 7

Polarizations in media with orthorhombic symmetry

Abstract

Approximate equations are derived for velocities and polarizations in general anisotropic media. These approximate equations are applied to anisotropy with orthorhombic symmetry caused by superposition of aligned vertical fractures, modeled as slip interfaces, and fine horizontal layering. The leading shear-wave polarization is parallel to the fractures for phase directions with angles up to 30° with the vertical if there is no fine layering. Fine layering in the fractured medium restricts the cone of propagation directions in which the fast shear-wave polarization is parallel to the fractures. An analytical expression is derived for the shear-wave polarizations, in terms of the contributions from the layering and the fractures. This expression is used in a real-data example (multi-component, multi-offset, multi-azimuth VSP) to explain the observed shear-wave polarizations.

7.1 **Introduction**

Rock is subject to stresses that engender fractures and micro-cracks to open normal to the minimum compressive stress. Large differential stresses lead to fracturing of the rock. Parallel micro-cracks or fractures, with properties that have rotation symmetry, result in anisotropy with hexagonal symmetry. Most likely the symmetry axis is horizontal as the cracks/fractures are most likely vertical due to the overburden weight. In the following we refer to this anisotropy as Horizontal Isotropy (HI) (*). This stress-induced anisotropy has attracted much attention in recent years. Cracks and fractures in rock are relevant in exploitation of hydro-carbon reservoirs. Measuring anisotropy is a means to obtain information about these features. The polarization of the faster shear is used to obtain the orientation of the cracks or fractures.

In exploring for stress-induced anisotropy one cannot ignore the other significant cause of anisotropy, i.e., fine layering. The common occurrence of fine layering in sediments makes it likely that formations overlaying the objective interval are anisotropic. This overburden anisotropy has to be removed prior to interpreting the anisotropy of the objective interval. This removing of overburden anisotropy is known as stripping (Winterstein 1990) and requires knowledge of splitting and the shear-wave eigendirections (polarizations of the eigen modes). It is also possible that the objective interval not only contains fractures or cracks but is in addition finely layered. Figure 7.1 shows an example of alternating layers of different lithology, of which one is fractured and the other finely layered.

Adding fine layering to a fractured interval complicates the interpretation of the shear-wave polarizations in terms of the fracture orientation. Within the seismic observation cone (say angles up to about 30 degrees with the vertical) the faster shear-wave polarization and the fracture strike in general no longer coincide. This is illustrated in the examples by Wild and Crampin (1991). A possible approach to interpret observed polarizations is by means of data base inversion (MacBeth 1991), in which measured polarizations are compared to polarizations for a range of models. The motivation for this approach is found in the complexity of the anisotropy. Adding fractures to layering makes the anisotropy orthorhombic or of even lower symmetry. For such anisotropy

polarizations and velocities must be computed numerically by solving the Christoffel equation.

Fig. 7.1 Alternation of fractured limestone and shale. Jurassic Blue Lias near Lilstock, Bristol Channel U.K. (courtesy KSEPL).

In this chapter we look at anisotropy with orthorhombic symmetry, caused by a superposition of horizontal layering (TI, (*)) and vertical fractures or thin micro-cracks (HI). The objective is to find an expression for the shear-wave polarizations in terms of the contributions of the two types of anisotropy. To overcome the problem of numerical solutions we use approximate equations. Existing approximate equations for P-waves (Backus 1965) are good approximations for weak anisotropy and even sometimes for comparatively strong anisotropy (Crampin 1982). Existing approximate equations for S-waves (Crampin 1977) are only applicable in planes of symmetry. This is because the assumption was made that the shear-wave polarizations are perpendicular to the plane of propagation and in this plane respectively. By not making this assumption we obtain approximate shear-wave equations with a validity for off-symmetry planes comparable to P-waves.

* Terminology

Based on symmetry properties of crystals, 7 symmetry systems (triclinic, monoclinic, orthorhombic, tetragonal, trigonal, hexagonal, cubic) exist. Hexagonal symmetry has a 6-fold axis of rotation. In addition to these crystal symmetry systems there is the transverse isotropy system: a symmetry system with an infinite-fold axis of rotation. For elastic waves hexagonal symmetry and transverse isotropy are synonyms. In this monograph the default orientation of the axis of 6- or infinite-fold rotation, simply called the symmetry axis, is taken to be vertical. The term Transverse Isotropy, abbreviated as TI, is exclusively used here for the situation of a vertical symmetry axis. Horizontal Isotropy, HI, refers to the situation where the axis of 6- or infinite-fold rotation is in a horizontal direction. Horizontal Isotropy is a special case of azimuthal anisotropy, which means that properties vary with azimuth.

7.2 Approximate equations for velocities and polarizations in weakly anisotropic media

A method to derive approximate equations for phase velocities in a weakly anisotropic medium was given by Backus (1965). Since he was interested in upper-mantle anisotropy in P-wave recordings, he gave in his paper the explicit expressions for the approximate P-wave velocity variation. Later Crampin (1977) used Backus' method to derive the approximate expressions for S-waves, but only for wave propagation in a plane of symmetry. Some symmetry systems have a number of symmetry planes, but one cannot rely on the assumption that the plane of recording is such a symmetry plane. Outside symmetry planes these

approximate equations are often not good (Crampin and Kirkwood 1981). Therefore I use Backus' method to derive the approximate equations for S-wave phase velocities and polarizations in an arbitrary plane of propagation.

We can write the stiffness tensor of an anisotropic medium as the sum of an isotropic tensor $\underline{C}^{(0)}$ and a tensor $\underline{C}^{(1)}$ expressing the anisotropy of the medium (Federov, 1968).

$$C_{jkmn} = C_{jkmn}^{(0)} + C_{jkmn}^{(1)} \tag{7.1}$$

The isotropic tensor describes an isotropic medium with P-wave velocity $V_p^{(o)}$ and S-wave velocity $V_s^{(o)}$

$$\rho^{-1} C_{jkmn}^{(0)} = \{V_p^{2(0)} - 2 V_s^{2(0)}\} \delta_{jk} \delta_{mn} + V_s^{2(0)} \{\delta_{jm} \delta_{kn} + \delta_{jn} \delta_{km}\} \tag{7.2}$$

We assume the anisotropy to be weak. This means that the anisotropic tensor must be small compared to the isotropic tensor, which implies

$$\rho^{-1} C_{jkmn}^{(1)} \ll V_s^{2(0)} \tag{7.3}$$

The velocities are computed from the eikonal equation

$$\rho^{-1} C_{jkmn} \beta_k \beta_n = V^2 \alpha_j \delta_{jm} \tag{7.4}$$

The solution of (7.4) can be written as

$$V^2 = V^{2(0)} + V^{2(1)} + V^{2(2)} + \dots \tag{7.5}$$

and

$$\underline{\alpha} = \underline{\alpha}^{(0)} + \underline{\alpha}^{(1)} + \underline{\alpha}^{(2)} + \dots \tag{7.6}$$

where $V^{2(0)}$ is the squared isotropic velocity and $\underline{\alpha}^{(0)}$ is the isotropic polarization vector. The higher order terms $V^{2(n)}$ and $\underline{\alpha}^{(n)}$ are of the n-th order in $\rho^{-1} C_{jkmn}^{(1)} \beta_k \beta_n$.

Since the anisotropy is assumed to be weak only the first order term has to be considered.

The isotropic solution for P-waves gives a polarization vector $\underline{\alpha}$ parallel to the wave propagation direction $\underline{\beta}$. Let us assume that this is, in the first order approximation, still valid. We then have for P-waves

$$V^{2(1)} = \rho^{-1} C_{jkmn}^{(1)} \beta_k \beta_m \alpha_j^{(0)} \alpha_n^{(0)} \qquad (7.7)$$

(To derive this result we use that α and β are unit vectors).

Thus in the first order approximation the P-wave velocity is

$$V_p^2 = V^{(0)2} + \rho^{-1} C_{jkmn}^{(1)} \beta_j \beta_k \beta_m \beta_n \qquad (7.8)$$

To specify a direction in 3 dimensions we need 2 angles, for example azimuth and dip. Alternatively we can look at the angular variation in a plane. To see how properties vary in the third dimension we can then rotate this plane. This plane rotation can be achieved by rotation of the coordinate system and involves therefore a transformation of the stiffness tensor (Appendix 7.A). Following Backus' approach we choose the angular variation within a plane. In the (x_1, x_2, x_3) coordinate system we consider the angular variation in the $x_1 - x_3$ plane. The propagation direction β is

$$\beta = (\cos(\theta), 0, \sin(\theta)), \qquad (7.9)$$

where θ is the angle with the x_1-axis, also called the dip of the phase velocity vector. After some algebraic manipulation we then find

$$V_p^2 = A + B \cos(2\theta) + D \sin(2\theta) + E \cos(4\theta) + F \sin(4\theta) \qquad (7.10)$$

where

$$A = \{ 3(c_{11} + c_{33}) + 2(c_{13} + 2c_{55}) \} / (8\rho) \qquad (7.11a)$$

$$B = (c_{11} - c_{33}) / (2\rho) \qquad (7.11b)$$

$$D = (c_{15} + c_{35}) / (2\rho) \qquad (7.11c)$$

$$E = \{ c_{11} + c_{33} - 2(c_{13} + 2c_{55}) \} / (8\rho) \qquad (7.11d)$$

$$F = (c_{15} - c_{35}) / (2\rho) \qquad (7.11e)$$

For the shear waves we assume that, in the first order approximation, the polarization is in the plane perpendicular to β. In this plane we can not arbitrarily choose the polarizations of the two shear modes since the anisotropy prescribes the polarizations.

Define

$$B_{jn} = \rho^{-1} C_{jkmn}^{(1)} \beta_k \beta_m$$

$\underline{\alpha}^{(SH)}$ the polarization of the SH-wave in the isotropic case,

$\underline{\alpha}^{(SV)}$ the polarization of the SV-wave in the isotropic case.

Let

$$\underline{\alpha} = \xi \; \underline{\alpha}^{(SH)} + \psi \; \underline{\alpha}^{(SV)}, \tag{7.12}$$

the polarization in the anisotropic medium.

The shear-wave equivalence of equation (7.7) is

$$\begin{bmatrix} \alpha_j^{(SH)} B_{jn} \alpha_n^{(SH)} & \alpha_j^{(SH)} B_{jn} \alpha_n^{(SV)} \\ \alpha_j^{(SV)} B_{jn} \alpha_n^{(SH)} & \alpha_j^{(SV)} B_{jn} \alpha_n^{(SV)} \end{bmatrix} \begin{bmatrix} \xi \\ \psi \end{bmatrix} = V^{2(1)} \begin{bmatrix} \xi \\ \psi \end{bmatrix} \tag{7.13}$$

We choose the isotropic shear-wave polarizations

$$\underline{\alpha}^{(SH)} = (0, 1, 0) \tag{7.14a}$$

$$\underline{\alpha}^{(SV)} = (-\sin(\theta), 0, \cos(\theta)) \tag{7.14b}$$

The solution for the shear-wave velocities is

$$V^2 = 0.5 \; \{a + d \; \pm \sqrt{(a - d)^2 + 4 \, b^2} \; \}, \tag{7.15}$$

where

$$a = (c_{66} + c_{44})/(2\rho) \; +$$

$$+ \cos(2\theta) \; (c_{66} - c_{44})/(2\rho) \; +$$

$$+ \sin(2\theta) \; c_{46}/\rho \tag{7.16a}$$

$$b = \; \sin(\theta) \; (c_{36} - 2c_{45} - c_{16})/(4\rho) \; +$$

$$+ \cos(\theta) \; (c_{34} + 2c_{56} - c_{14})/(4\rho) \; +$$

$$+ \sin(3\theta) \; (c_{36} + 2c_{45} - c_{16})/(4\rho) \; +$$

$$+ \cos(3\theta) \; (c_{14} + 2c_{56} - c_{34})/(4\rho) \tag{7.16b}$$

$$d = (4c_{55} + c_{11} - 2c_{13} + c_{33})/(8\rho) +$$

$$+ \cos(4\theta) \; (4c_{55} - c_{11} + 2c_{13} - c_{33})/(8\rho) +$$

$$+ \sin(4\theta) \; (c_{35} - c_{15})/(2\rho) \qquad\qquad (7.16c)$$

The shear-wave polarizations are determined by

$$\frac{\xi}{\psi} = \frac{-b}{a - V^2} = \frac{d - V^2}{-b} \qquad\qquad (7.17)$$

7.3 <u>Orthorhombic models</u>

We build orthorhombic models by adding fractures to a transversely isotropic medium. This adding is done by using the Schoenberg and Muir (1990) theory. The transversely isotropic background medium (vertical symmetry axis) has parameters

$c_{11b} \; (= c_{22b}), \quad c_{12b}, \quad c_{13b}(=c_{23b}), \quad c_{33b}, \; c_{44b}(=c_{55b}) \; \text{and} \quad c_{66b}, \; \text{with}$
$c_{66b} = 1/2 \,(c_{11b} - c_{12b})$.

The fractures are modelled by parallel slip interfaces (Schoenberg 1980). The fracture parameters are the normal compliance Z_N and the tangential compliance Z_T. Fracture compliances reveal the slip of the fractures as a linear function of the stress components acting across the fractures. The parameterization with compliances is useful since it also applies to thin micro-cracks (Schoenberg and Douma 1988). The case of fluid filled micro-cracks may be approximated by letting $Z_N = 0$ and $Z_T \neq 0$.

Adding the fractures to the background medium results in the effective parameters

$$c_{11} = c_{11b} \, (1 - \Lambda_N) \qquad\qquad 7.18)$$

$$c_{12} = c_{12b} \, (1 - \Lambda_N)$$

$$c_{13} = c_{13b} \, (\, 1 - \Lambda_N)$$

$$c_{22} = c_{11b} \, (\, 1 - \frac{c_{12b}^2}{c_{11b}^2} \, \Lambda_N)$$

$$c_{23} = c_{13b} \, (\, 1 - \frac{c_{12b}}{c_{11b}} \, \Lambda_N)$$

$$c_{33} = c_{33b} \, (\, 1 - \frac{c_{13b}^2}{c_{11b} \, c_{33b}} \, \Lambda_N)$$

$$c_{44} = c_{44b}$$

$$c_{55} = c_{44b} \, (\, 1 - \Lambda_3)$$

$$c_{66} = c_{66b} \, (\, 1 - \Lambda_2),$$

where

$$\Lambda_N = Z_N \, c_{11b} \, / \, (1 + Z_N \, c_{11b}), \qquad\qquad\qquad (7.19)$$

$$\Lambda_3 = Z_T \, c_{44b} \, / \, (1 + Z_T \, c_{44b})$$

$$\Lambda_2 = Z_T \, c_{66b} \, / \, (1 + Z_T \, c_{66b})$$

Note that $0 \leq \Lambda < 1$.

The specific fracture parameterization by compliances makes that the nine elastic stiffnesses of the orthorhombic model only depend on seven independent parameters.

Figure 7.2a

Figure 7.2b

Figure 7.2c
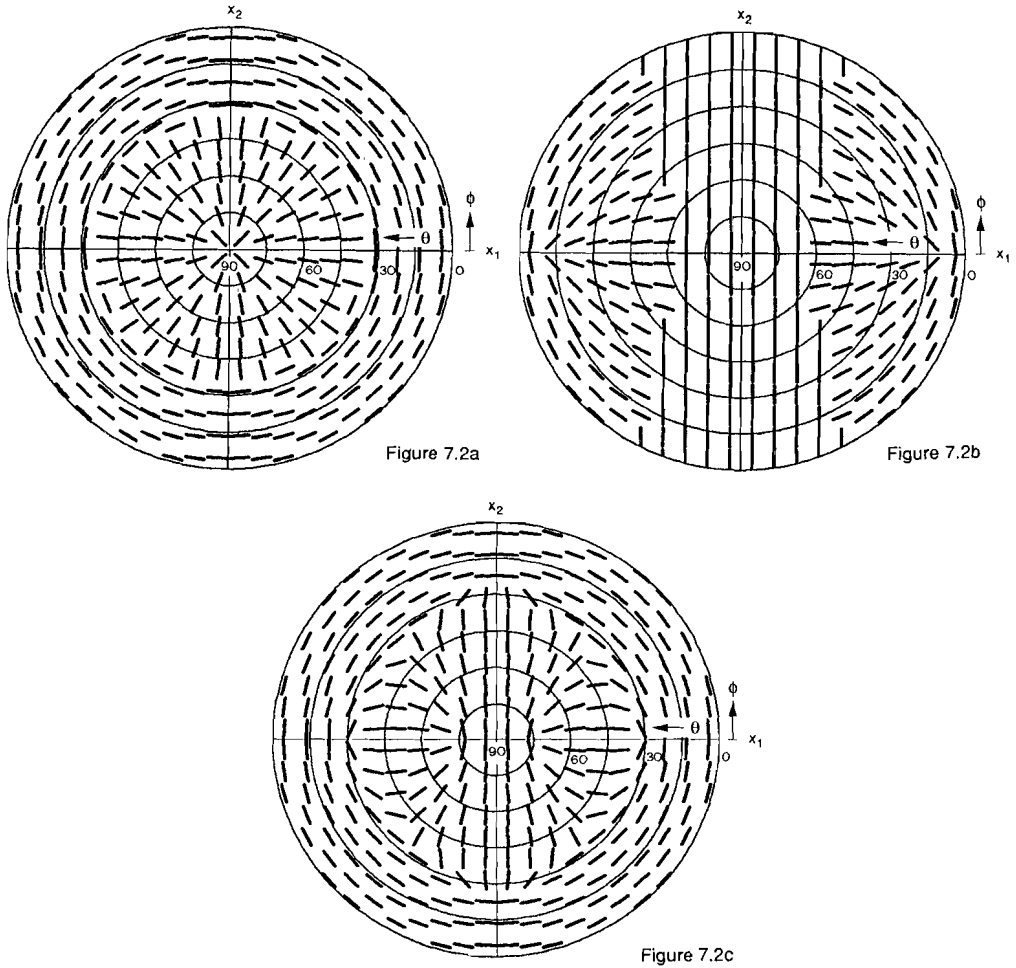
Fig. 7.2 Azimuth-dip displays of polarization vector of the fast shear wave (from the Christoffel equation) : (a) Transverse Isotropy , (b) Horizontal Isotropy with symmetry axis along x_1, (c) Orthorhombic symmetry, $(x_1 - x_2),(x_1 - x_3)$ and $(x_2 - x_3)$ symmetry planes. Elastic parameters: $c_{11} = c_{22} = 12.519$, $c_{12} = 6.019$, $c_{13} = c_{23} = 5.538$, $c_{33} = 11.076$, $c_{44} = 2.769$, $c_{55} = 2.621$, $c_{66} = 3.076$. The orthorhombic medium is composed by mixing the media of fig (a) and (b). Layering anisotropy factors: $A_p = 1.0$, $A_{s1} = 1.083$ $A_{s2} = 1.233$. Fractures: $\Lambda_3 = 0.053$

7.4 Singularities

Singularities are those directions for which the two shear-wave velocities are equal. Figures 7.2 display stereographic projections of polarizations of the faster shear-wave mode. Figure 7.2a is for a medium with TI anisotropy. This symmetry system has a kiss singularity in the vertical direction (the center of the figure). The example in Fig. 7.2a has a line singularity in directions with dip of 37 degrees (dip, or θ, is the angle with the horizontal). Figure 7.2b is for a medium with HI anisotropy. The horizontal symmetry axis is along x_1, the fractures are thus parallel to x_2. The kiss singularity is along the symmetry axis, the line singularity is in directions that make a 60 degrees angle with the symmetry axis. Figure 7.2c is for a medium with orthorhombic symmetry. Its elastic constants are obtained from superposition of the media in figures 7.2a and 7.2b. The singularities are point singularities.

Singularities can be computed with the approximate equations. According to equation (7.15) they occur when

$$2b = a - d \tag{7.20}$$

Solving this equation for TI anisotropy gives

$$\cos^2(\theta) = 0 \tag{7.21}$$

and

$$\cos^2(\theta) = \frac{B - 3\,c_{44} - c_{66}}{B - 4\,c_{44}} \tag{7.22}$$

where

$$B = c_{11} - 2\,c_{13} + c_{33} \tag{7.23}$$

For HI anisotropy we obtain singularities in the x_1 - x_3 plane for

$$\cos^2(\theta) = \frac{c_{44} - c_{55}}{B - 4\,c_{55}} \tag{7.24}$$

and

$$\cos^2(\theta) = 1 \tag{7.25}$$

The singularities outside the x_1 - x_3 plane follow immediately from rotation of the solution given in (7.24) about the symmetry axis.

With equations (7.18), taking the background medium isotropic, equation (7.24) simplifies to

$$\cos^2(\theta) = \frac{(\lambda + 2\mu)\,\Lambda_3}{4(\lambda + 2\mu)\,\Lambda_3 - 4\mu\,\Lambda_N}, \tag{7.26}$$

For fluid-filled flat micro-cracks $Z_N = 0$. In that case (7.26) reads

$$\cos^2(\theta) = 0.25 \tag{7.27}$$

Hence, for fluid filled flat micro-cracks the singularity in the plane perpendicular to the cracks is always at 30 degrees with the vertical.

For orthorhombic symmetry the singularity of most significance to seismic exploration is the singularity in the x_1 - x_3 plane. This singularity is in most situations within the seismic data cone. Solving (7.20) for orthorhombic symmetry gives in the x_1 - x_3 plane singularities for

$$\cos^2(\theta) = \frac{B + c_{44} - 4\,c_{55} - c_{66} \pm D}{2(B - 4\,c_{55})}, \tag{7.28}$$

with B as in (7.23) and

$$D = \sqrt{B^2 + B(-2\,c_{44} - 4\,c_{55} - 2\,c_{66}) + (c_{44} - c_{66})^2 + 8\,c_{55}(c_{44} + c_{66})} \tag{7.29}$$

For various ratio's of TI and HI the near-vertical singularity, equation (7.28), moves in the x_1 - x_3 plane between the two extremes given by (7.21) and (7.24). This can be proven using equations (7.18) and (7.19).

7.5 Polarizations

It is straightforward to derive the polarizations for the HI and the TI cases. For the TI medium we have

$$\xi/\psi = 0,$$

which implies that the shear-wave polarizations are as SH and SV waves in an isotropic medium (equations 7.14).

For the HI medium we have

$$\xi/\psi = \tan(\phi) \, / \sin(\theta) \text{ if the minus sign in (7.15) is used} \qquad (7.31a)$$

and

$$\xi/\psi = \sin(\theta) \, / \tan(\phi) \text{ if the plus sign in (7.15) is used.} \qquad (7.31b)$$

The plus sign in (7.15) results in the faster shear-wave velocity in the vertical propagation direction. The polarization of the faster mode in the vertical and in all other directions that fall in between the two line singularities is therefore given by (7.31b). Remember that ϕ is the angle in the horizontal plane between plane of propagation and the fracture normal. From (7.31b) and (7.14) it follows that the polarization is parallel to the fractures. We can conclude that for anisotropy caused by fractures or thin micro-cracks the faster shear-wave polarization is parallel to these structures for propagation directions that make an angle with the vertical that is less than 30 degrees. For planes of propagation not normal to the fractures this is even true for larger angles with the vertical.

We now solve equation (7.17) for models with orthorhombic symmetry as discussed before. We model the layer-induced anisotropy by means of anisotropy factors, which are defined in chapter 4. We take the P-wave anisotropy factor to be unity as chapter 4 shows that this is a likely value. For the fractures we assume $Z_N = 0$. The shear-wave polarizations are then given by :

$$\xi = \Lambda_3 \cos(\phi) \, |\sin(\phi) \sin(\theta)| \Big[2\cos(2\theta) \, +$$

$$+ A_{s1}^2 [\, 2\cos(2\phi) + \cos(2\phi-2\theta) + \cos(2\phi+2\theta)] \Big] \qquad (7.32)$$

and

$$\psi = (H - G)/4 \pm \sqrt{((H-G)/4)^2 + \xi^2} \tag{7.33}$$

with

$$G = \left\{ 2-\Lambda_3+\Lambda_3\cos(2\phi)+A_{s1}^2(2-\Lambda_3-\Lambda_3\cos(4\phi)) \right\} +$$

$$+ \left\{ \left[-2+\Lambda_3-\Lambda_3\cos(2\phi)+A_{s1}^2(2-\Lambda_3-\Lambda_3\cos(4\phi)) \right]\cos(2\theta) \right\} \tag{7.34}$$

and

$$2H = \left\{ 7+A_{s2}^2-A_{s1}^2\Lambda_3\sin^2(2\phi)-4\Lambda_3\cos^2(\phi) \right\} +$$

$$+ \left\{ \left[1-A_{s2}^2+A_{s1}^2\Lambda_3\sin^2(2\phi)+4\Lambda_3\cos^2(\phi) \right]\cos(4\theta) \right\} \tag{7.35}$$

where

A_{s1} is the anisotropy factor for the TI S1-wave (polarized perpendicular to the propagation plane) and

A_{s2} is the anisotropy factor for the TI S2-wave (polarized in the plane of propagation).

Although this is not a simple equation for the polarizations, it is very handy to study the effects of the two types of anisotropy. The amount of layering can be varied by changing the anisotropy factors, the fracturing can be made more or less intensive by changing Λ_3.

Figure 7.3 shows the result for the model used in Fig. 7.2c. Figures 7.4 and 7.5 are examples of changing the mixture of TI and HI. For vertical rays ($\theta = 90$) the fast shear-wave polarization is always parallel to the fractures ($\Omega = 0$). This is no longer true for small deviations from the vertical if the layer-induced anisotropy is relatively large compared to the fracture-induced anisotropy. The position of the point singularity near $\phi = 45$, $\theta = 45$ (see Fig. 7.3 or Fig. 7.2c) changes when different model parameters are used. This results in large variations in the shear-wave polarizations as can be seen from the difference between curves (c) and (d) in Fig. 7.5. Figures 7.6 show the angles with the fracture strike, Ω, as a function of azimuth ϕ and dip θ.
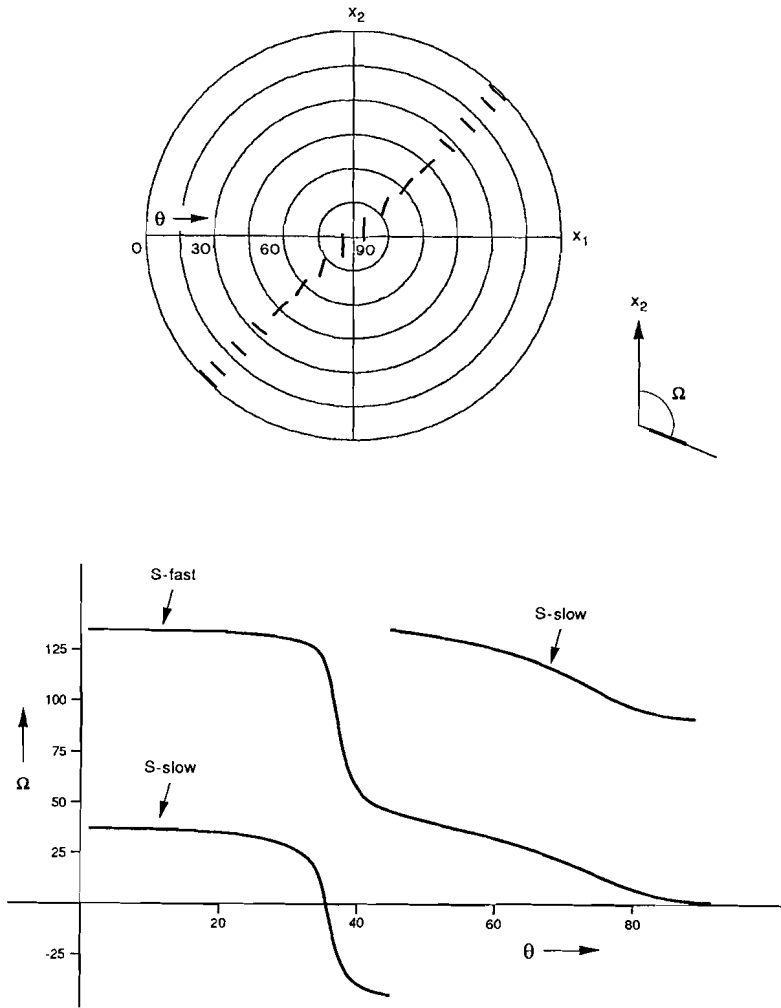
Fig. 7.3 S-wave polarizations from the approximate equations. Model parameters as in Fig. 7.2c. Plane of propagation is at 45° with the fractures, i.e. $\phi = 45°$. Upper figure: azimuth-dip display for S-fast. Lower figure: the angle between the horizontal component of the polarization vector and the fracture strike (x_2 - axis), Ω, versus θ, the dip of the slowness vector.
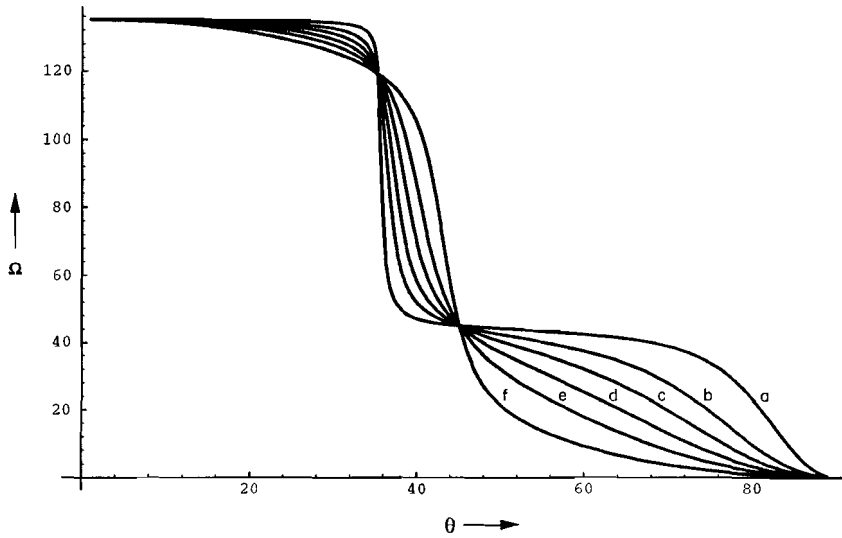
Fig. 7.4 Angle of S-fast polarization with fracture strike (from the approximate equations), $A_{s2}=1.233$, $A_{s1}=1.083$, $\phi=45°$ $\Lambda_3=0.01$ (a), $\Lambda_3=0.03$ (b), $\Lambda_3=0.05$ (c), $\Lambda_3=0.09$ (d), $\Lambda_3=0.15$ (e) and $\Lambda_3=0.30$ (f)
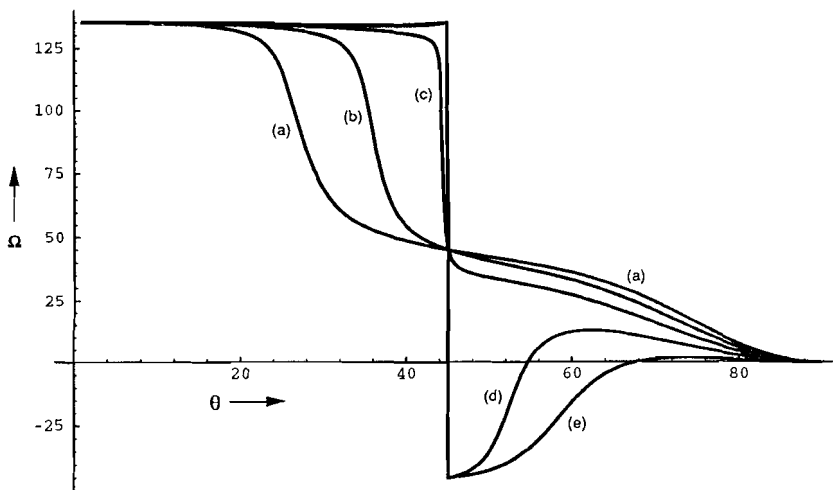
Fig. 7.5 Angle of S-fast polarization with fracture strike (from the approximate equations), $A_{s2}=1.24$, $\Lambda_3=0.053$, $\phi=45°$,
$A_{s1}=1.04$ (a), $A_{s1}=1.08$ (b), $A_{s1}=1.12$ (c), $A_{s1}=1.16$ (d) and $A_{s1}=1.20$ (e)
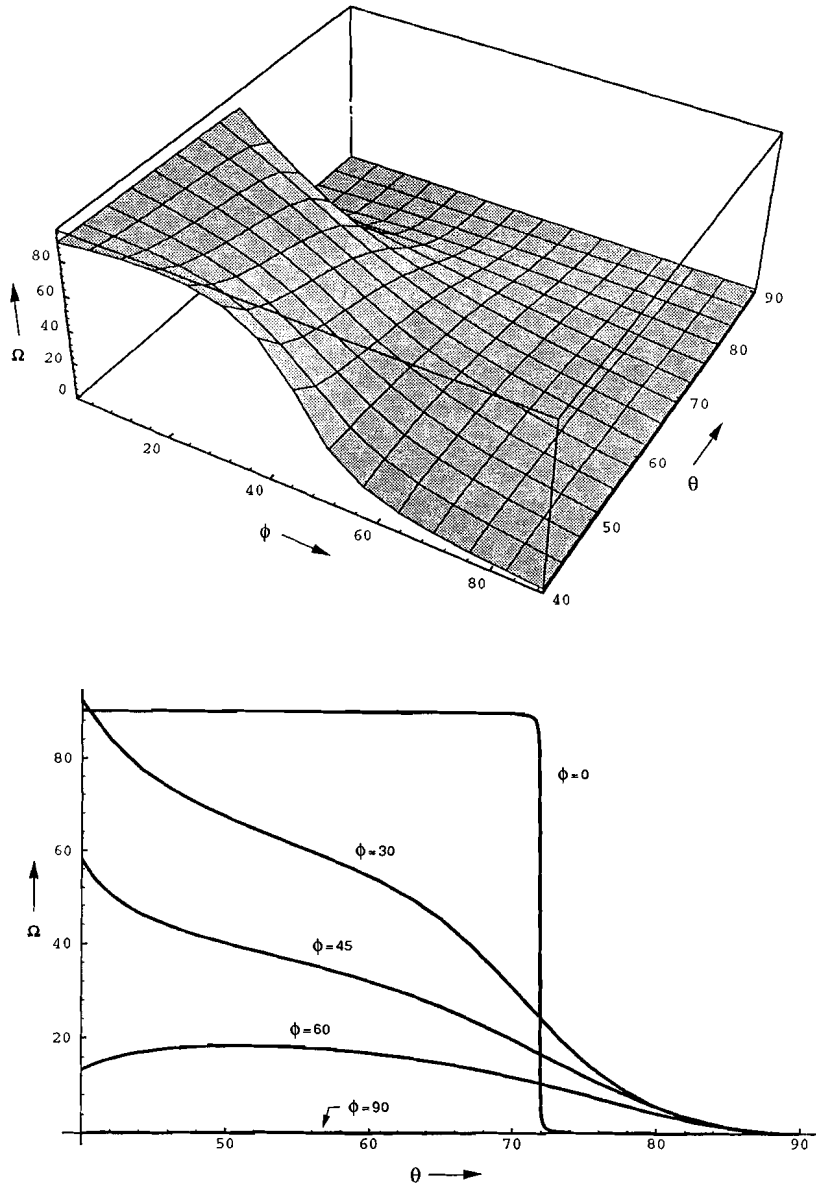
Fig. 7.6 Angle of S-fast polarization with fracture strike (from the approximate equations). Model parameters as in Fig. 7.2c, : $A_{S2}=1.233$, $A_{S1}=1.083$, $\Lambda_3=0.053$

7.6 <u>An example</u>

Figure 7.7 shows the acquisition geometry of a multi-component VSP. Shot location A1 is at (almost) zero-offset, shot locations A2, B2 and C2 have an offset of 1250 feet, shot locations A4, B4 and C4 are at 3750 feet offset.
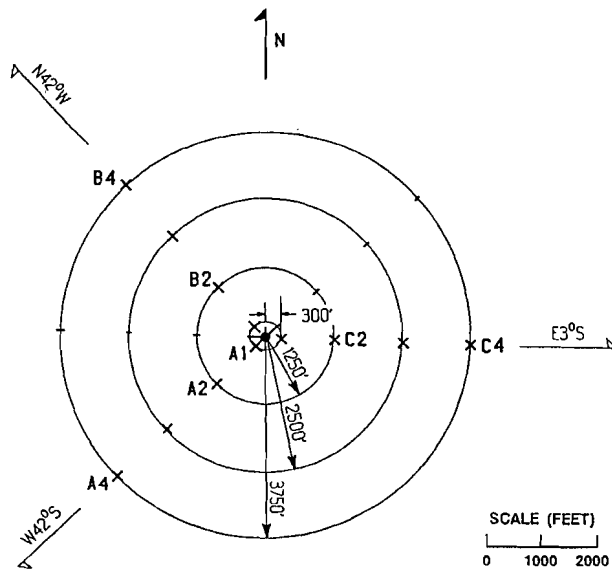
Fig. 7.7 VSP acquisition geometry

To illustrate the data quality, we display only two horizontal components (Fig. 7.8) from the in total nine-component data set. Component XX means that both source and receiver are horizontal and in-line (from shot-location to well head), component YY means horizontal source and receiver in cross-line orientation. In the shallow part (3500 ft) the shear-wave splitting is about 30 msec, at 7800 ft it is about 15 msec. The depth range between 3500 ft and 4050 ft was sampled for all shot locations. The first arrival shear wave recorded in this depth range can be used to find the variation of the shear-wave polarization with propagation direction.

Several techniques exist to derive shear-wave polarizations from multi-component data (MacBeth and Crampin 1991). For example, the particle motion

depth (ft)

Fig. 7.8 (a) Shot A4, component YY

depth (ft)
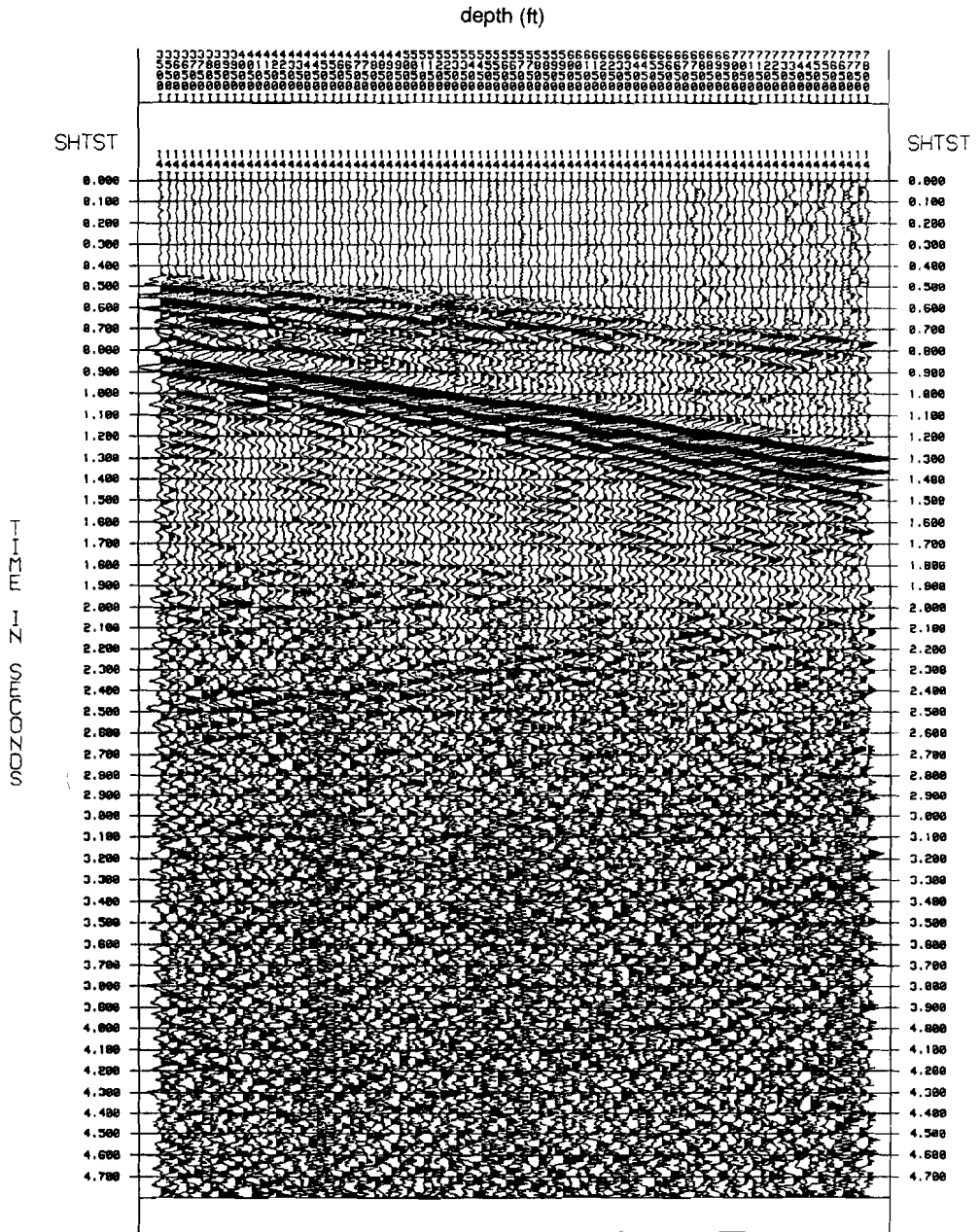
Fig. 7.8 (b) Shot A4, component XX

at the receiver is linear if the source orientation is such that only one shear-wave mode is emitted by the source. For other source orientations the recorded particle motion is non-linear as the shear-wave signal consists of the interference of the two time-split shear modes (Fig. 7.9). Analyses of the data gave the polarization of the fast shear wave as displayed in Fig. 7.10. The polarization in the zero-offset VSP is east. For the far offsets (A4, B4 and C4) the S-fast polarizations are in-line. Note that in-line is from shot location to well-head; in-line has a different azimuth with respect to north for shot locations A, B an C. For the middle offset shots, C2 has S-fast polarizations that are again in-line. For A2 and B2 the polarizations are in between those of the zero - and far offset. Considering the dips and azimuths of the ray paths involved, we conclude that this polarization behaviour is typical for an orthorhombic medium that consists of a mixture of TI and HI.

From the zero-offset polarizations we learn that the HI symmetry axis is in the east direction. To find model parameters we assume straight rays, thus no inhomogeneity between surface and the receivers. The dip θ in equations (7.32) and (7.33) is the dip of the slowness vector. If the data would have been acquired with more offsets, like a walk-away VSP, we could have used the tau-p transform to obtain the slowness vectors (chapter 6). Unfortunately this is not the case for this data set. Nevertheless, we can fit a possible model with $\Lambda_3 = 0.02$, $A_{s1} = 1.1$ and $A_{s2} = 1.2$, see Fig. 7.10. Parameter Λ_3 was actually derived from the zero-offset S-wave velocities, (c_{44} and c_{55} respectively, see (7.18)). The remaining unknown anisotropy factors were then derived by fitting the curve according to equations (7.32) - (7.35). If we translate the model parameters to elastic stiffness tensor elements we have $c_{55}/c_{44}=0.98$, $c_{66}/c_{44}=1.21$ and $(1/c_{44})[c_{11} - (c_{13}+c_{44})^2/(c_{33}-c_{44})]=1.44$.
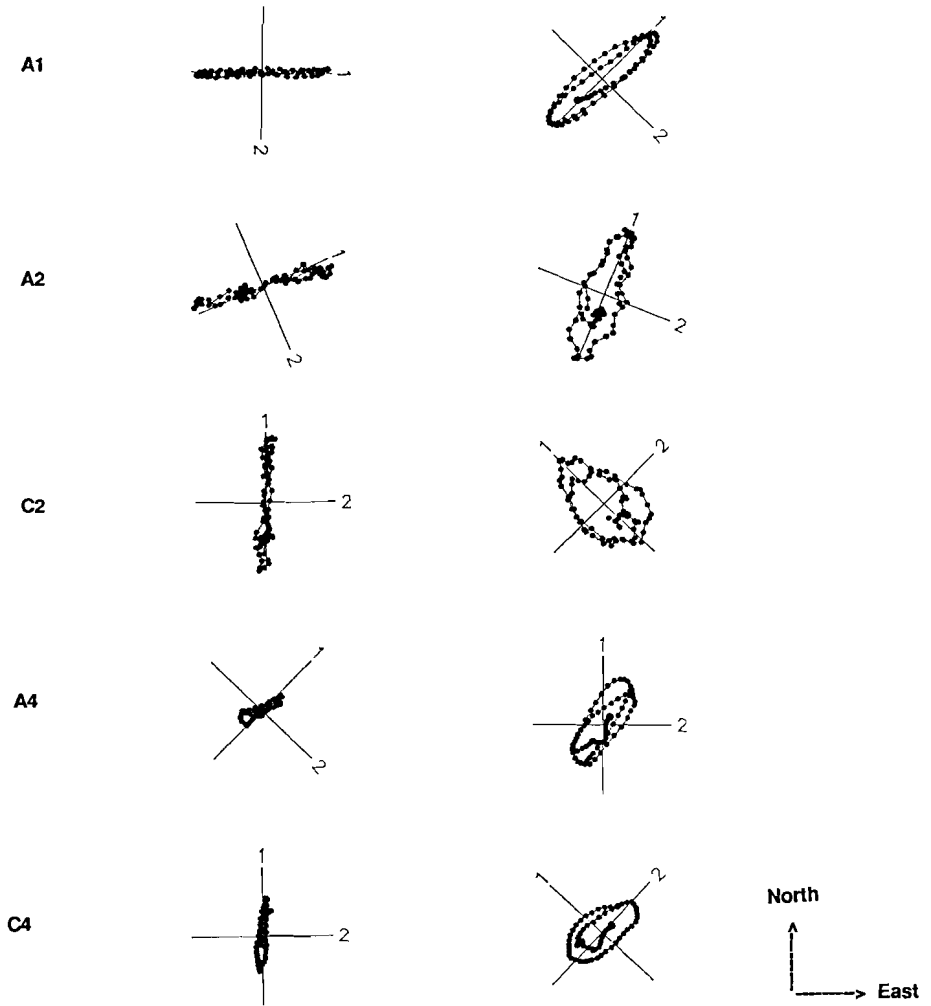
Fig. 7.9 Particle motion of the downgoing shear wave pulse, recorded with horizontal receivers. Horizontal source parallel to receiver 1. Receiver orientations are displayed with respect to the North-East coordinate system. Left column: source parallel to S-fast eigendirection. Right column: orientation not in eigendirection, interference of S1- and S2-waves.
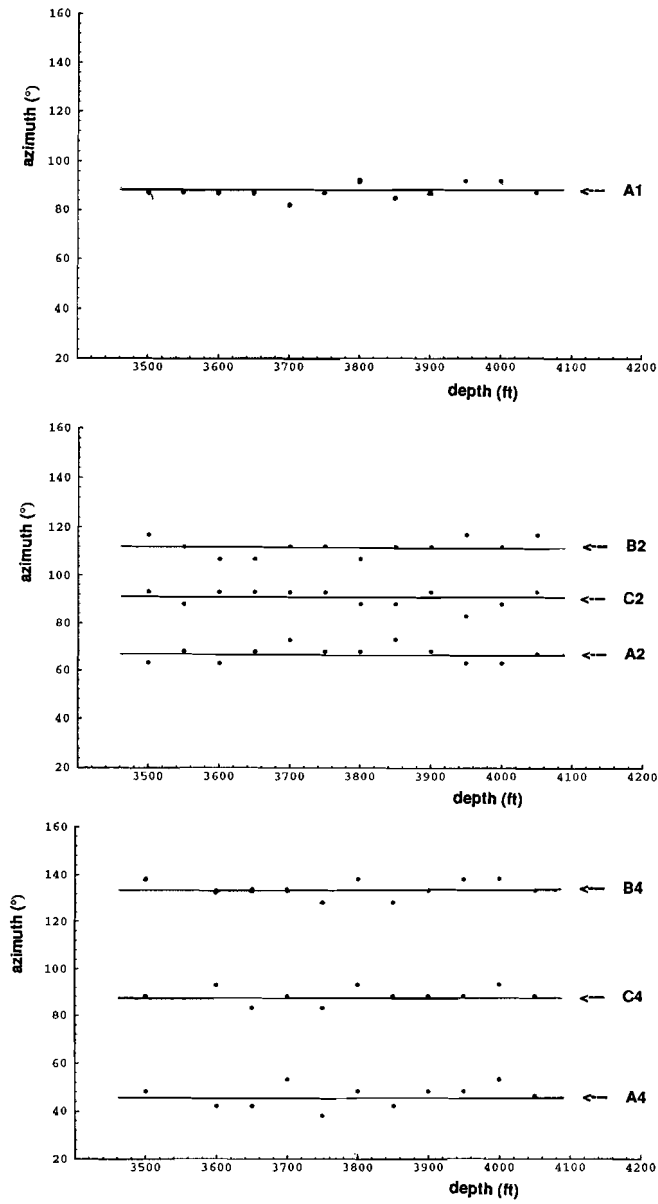
Fig. 7.10 Azimuth with respect to north (north = 0, east = 90) of the leading shear-wave polarization.
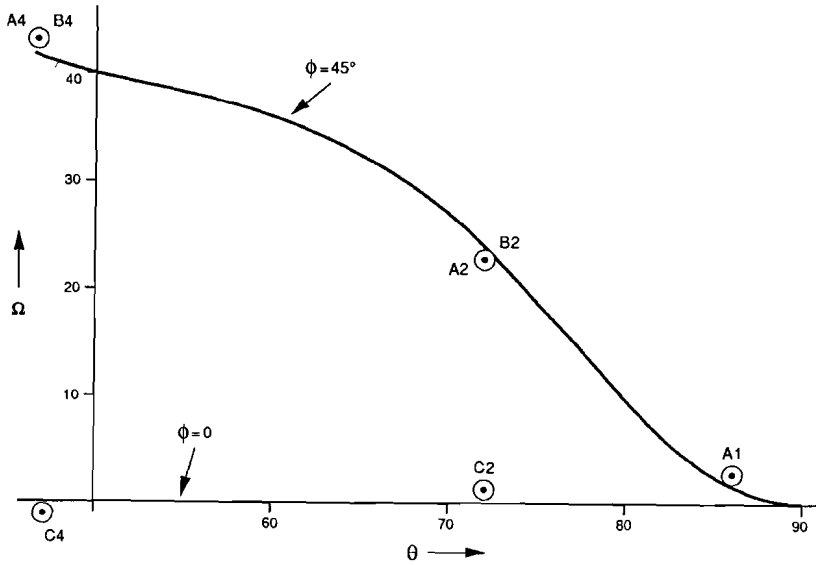
Fig. 7.11 Modelling of the observed polarizations with $\Lambda_3 = 0.02$, $A_{s1} = 1.1$ and $A_{s2} = 1.2$.

7.7 Conclusions

The approximate polarizations for an orthorhombic medium composed of layer- and fracture-induced anisotropy, depend on only five parameters. This under the assumption that the P-wave anisotropy factor, due to the layering, is unity and the assumption that the normal fracture compliance is zero. These five parameters are dip and azimuth (with respect to fracture strike) of the slowness vector, two shear-wave anisotropy factors and the tangential fracture compliance. For such an orthorhombic medium the interpretation of an observed S-fast polarization as the fracture strike may be significantly wrong. With sufficient polarization measurements one can use the expressions derived in this chapter to obtain the relative strengths of the fracture- and layer-induced anisotropy.

Appendix 7.A : <u>Tensor transform</u>

The transformation rule for a fourth order tensor is

$$c'_{ijkl} = \chi_{ip}\, \chi_{jq}\, \chi_{kr}\, \chi_{ls}\, c_{pqrs}\, , \qquad\qquad (7.A1)$$

where

$$\chi_{ip} = \cos(x_i, x_p) \qquad\qquad (7.A2)$$

For orthorhombic symmetry the elasticity tensor w.r.t. (x_1, x_2, x_3), where , $(x_1\text{-}x_2)$, $(x_1\text{-}x_3)$ and $(x_2\text{-}x_3)$ are symmetry planes, is:

$$\underline{C} = \begin{pmatrix} c_{11} & c_{12} & c_{13} & 0 & 0 & 0 \\ c_{12} & c_{22} & c_{23} & 0 & 0 & 0 \\ c_{13} & c_{23} & c_{33} & 0 & 0 & 0 \\ 0 & 0 & 0 & c_{44} & 0 & 0 \\ 0 & 0 & 0 & 0 & c_{55} & 0 \\ 0 & 0 & 0 & 0 & 0 & c_{66} \end{pmatrix} \qquad\qquad (7.A3)$$

We rotate $\underline{C}$ over angle ϕ in the $(x_1 - x_2)$ plane.

With

$$m = \cos(\phi), \qquad\qquad (7.A4)$$

and

$$n = \sin(\phi) \qquad\qquad (7.A5)$$

we have

$$c'_{11} = m^4 c_{11} + m^3 n(4c_{16}) + m^2 n^2(2c_{12}+4c_{66}) + mn^3(4c_{26}) + n^4 c_{22})$$

$$c'_{12} = m^4 c_{12} + m^3 n(-2c_{16}+2c_{26}) + m^2 n^2(c_{11}-4c_{66}+c_{22}) +$$

$$+ mn^3(2c_{16}-2c_{26}) + n^4 c_{12}$$

$$c'_{13} = m^2 c_{13} + mn(2c_{36}) + n^2 c_{23}$$

$$c'_{14} = m^3 c_{14} + m^2 n(-c_{15}+2c_{46}) + mn^2(-2c_{56}+c_{24}) - n^3 c_{25}$$

$$c'_{15} = m^3 c_{15} + m^2 n(2c_{56}+c_{14}) + mn^2(c_{25}+2c_{46}) + n^3 c_{24}$$

$$c'_{16} = m^4 c_{16} + m^3 n(-c_{11}+c_{12}+2c_{66}) +$$

$$+ m^2 n^2(-3c_{16}+3c_{26}) + mn^3(-2c_{66}-c_{12}+c_{22}) - n^4 c_{26}$$

$$c'_{22} = m^4 c_{22} + m^3 n(-4c_{26}) + m^2 n^2(2c_{12}+4c_{66}) + mn^3(-4c_{16}) + n^4 c_{11}$$

$$c'_{23} = m^2 c_{23} + mn(-2c_{36}) + n^2 c_{13}$$

$$c'_{24} = m^3 c_{24} + m^2 n(-c_{25}-2c_{46}) + mn^2(2c_{56}+c_{14}) - n^3 c_{15}$$

$$c'_{25} = m^3 c_{25} + m^2 n(c_{24}-2c_{56}) + mn^2(c_{15}-2c_{46}) + n^3 c_{14}$$

$$c'_{26} = m^4 c_{26} + m^3 n(-c_{12}-2c_{66}+c_{22}) +$$

$$+ m^2 n^2(3c_{16}-3c_{26}) + mn^3(2c_{66}+c_{12}-c_{11}) - n^4 c_{16}$$

$$c'_{33} = c_{33}$$

$$c'_{34} = mc_{34} - nc_{35}$$

$$c'_{35} = mc_{35} + nc_{34}$$

$$c'_{36} = m^2 c_{36} + mn(c_{23}-c_{13}) - n^2 c_{36}$$

$$c'_{44} = m^2 c_{44} - mn(2c_{45}) + n^2 c_{55}$$

$$c'_{45} = m^2 c_{45} + mn(c_{44}-c_{55}) - n^2 c_{45}$$

$$c'_{46} = m^3 c_{46} + m^2 n(-c_{14}-c_{56}+c_{24}) + mn^2(c_{15}-c_{46}-c_{25}) + n^3 c_{56}$$

$$c'_{55} = m^2 c_{55} + mn(2c_{45}) + n^2 c_{44}$$

$$c'_{56} = m^3 c_{56} + m^2 n(-c_{15}+c_{46}+c_{25}) + mn^2(-c_{14}-c_{56}+c_{24}) - n^3 c_{46}$$

$$c'_{66} = m^4 c_{66} + m^3 n(-2c_{16}+2c_{26}) + m^2 n^2(c_{11}- 2c_{12}-2c_{66}+c_{22}) +$$

$$+ mn^3(2c_{16}-2c_{26}) + n^4 c_{66} \qquad (7.A6)$$

Chapter 8

Summary

The Christoffel equation relates the medium parameters, contained in the elasticity tensor, to wave velocities and particle displacements. Distinct from isotropic media, where the simplicity of the elasticity tensor leads to the well-known P- and S-wave solutions, no simple analytical expressions exist in general for anisotropic media. Three wave-modes with generally different velocities have polarizations that are neither parallel nor perpendicular to the propagation direction. The direction of energy propagation does not coincide with the direction of phase propagation. The slowness surface and the normal surface illustrate how slowness and normal velocity depend on the propagation direction. The velocity of energy transport, or ray velocity, can be derived from the direction-dependence of slowness or normal velocity.

A wave incident at an interface between two anisotropic media will in general cause reflection and transmission of all three wave modes. The ray path of a reflected or transmitted wave may be unexpected if we are used to isotropic concepts only. A zero offset ray, for example, means that incident and reflected ray have the same path. In that case the slowness vectors are perpendicular to the interface, whereas the ray path can be oblique to the interface. Incident and reflected ray of the same wave mode will, in general, be a-symmetrical with respect to the interface normal.

Inflexion points in the slowness surface correspond to cusps in the wave surface. Inhomogeneity of the subsurface tends to hinder the recognition of this typical anisotropy phenomenon. To observe the characteristic shape of a wave front with cusps the receivers must be positioned close to the anisotropic layer. A-symmetrical reflection is an other reason why it may be difficult to recognize the typical arrivals belonging to a wave surface with cusps, even when the receivers are positioned inside or close to the anisotropic layer.

In this thesis we focus on anisotropy caused by fine layering. We analyse the conditions that must be satisfied so that fine layering is equivalent to anisotropy. In the long-wavelength (or quasi-static) approximation an interval of thickness H, consisting of a sequence of layers, is effectively homogeneous and anisotropic to seismic wave propagation. This approximation implies that H is much smaller than the seismic wavelength λ. Closer inspection of this approximation shows that the degree of equivalence depends on several parameters. The equivalence is exact for infinitely long wavelengths. It is also exact (for all wavelengths) for those waves which are not back-scattered at the interfaces between the layers. This is the case when reflection coefficients are zero. We use a simple model where the interval of thickness H consists of a N times repeated set of two layers. These two layers form one period, the whole interval consists of N periods. The wave field that propagates through this sequence of layers, consists of the sum of the primary wave and all the multiples. The effective medium for a given wave number depends on the interference of primary and multiples. For infinitely thin layers this results in an effectively homogeneous medium, with a pseudo-primary that is delayed compared to the primary wave.

To investigate the effects of thin layers with finite thicknesses, we position the sequence of layers between two anisotropic half-spaces. We consider an incident wave from the upper half-space. The energy that is reflected back into the upper half-space is a measure for the inhomogeneity of the model. It is thus a measure for how 'effectively anisotropic' the sequence is. For thin layers the reflected field, denoted by reflectivity R, is independent of the number of periods. It means that periodicity is not a requirement for anisotropy. The reflectivity is linearly proportional to d/λ, where λ is the seismic wavelength and d the period thickness. The role of the multiples is found in the relation between R and the plane-wave reflection coefficient r. For sub-critical angles of incidence R and r are linearly related. It means that for layers with larger impedance contrasts (larger r) the condition for the layers to be thin is more severe. Also, since r in general depends on the angle of incidence, the condition depends on the incidence angle too. For $R < 0.15$ the effective velocity differs by less than 0.5% from the anisotropic velocity. The attenuation due to the dispersion is in that case less than 0.22 dB/cycle. The condition $R < 0.15$ can be used as criterion to replace layers by an homogeneous attenuating anisotropic medium.

In a next chapter we look at velocities derived from reflection time curves

for horizontally layered transversely isotropic ground. Interval velocities obtained from stacking velocities and the Dix equation are in general not the vertical or the horizontal velocity of the anisotropic layer. The squared velocity, obtained from zero offset data, is equal to the ratio of horizontal components of ray velocity and slowness. Fitting a hyperbola to time-offset data is equivalent to fitting an ellipse to the wave surface. The horizontal axis of this ellipse corresponds with the velocity pertaining to the hyperbola. Of interest is how much this velocity, denoted by F, differs from the vertical velocity, as F is often used for time-to-depth conversion. The ratio of F to the vertical velocity is defined as the anisotropy factor. For layer-induced anisotropy F is for P-waves equal to the vertical velocity if all layers have the same Poisson ratio. For shear waves the anisotropy factor can be significantly larger than unity, for example by a factor two. For zero-offset data the anisotropy factor of the shear wave polarized perpendicular to the plane of propagation (S1-wave) is smaller than the anisotropy factor for the other shear wave (S2-wave). For larger offset data F increases with offset for P-waves. The same effect can be caused by a vertical inhomogeneity. For S2-waves F decreases with offset, which is opposite to the effect of vertical inhomogeneity. For S1-waves F is offset independent.

For an interval with a vertical velocity gradient the vertical velocity is smaller than F, the velocity derived from reflection time curves. The inhomogeneity factor is defined as the ratio of F and the vertical velocity for an isotropic layer with a vertical velocity gradient. We find that this inhomogeneity factor can have similar values as anisotropy factors typical for layer-induced anisotropy. This is illustrated with two real data examples. In a North Sea P-wave data set the velocity gradient causes a 2% mismatch between F and the vertical velocity. A shear-wave reflection experiment reveals a large shear-wave velocity gradient that results in an inhomogeneity factor between 1.07 and 1.24 (depending on selected interval thickness and offset range used). These examples illustrate that attributing mis-matches between stacking velocities and vertical velocities to anisotropy should not be done before correcting for inhomogeneity.

In the next chapter we look at the significance of the τ-p transform in relation with anisotropy. Slant stacking transforms seismic data from the time versus offset (t-x) domain to the intercept time versus ray parameter (τ-p) domain. This transform is commonly regarded as a plane wave decomposition. It means that data with a common p value can be considered as originating from a plane-wave source. This not only holds for isotropic media but also for

anisotropic media. Arrival times in the t-x domain are determined by ray velocities. In the τ-p domain they are given by normal velocities. The τ-p transform transforms the data from the wave surface (or ray-slowness surface) domain into the normal surface (or slowness surface) domain. This adds to the significance of the transform for anisotropic media, where these characteristic surfaces have different properties.

Reflection time curves for a horizontally layered subsurface are closely related to slowness surfaces. The ray parameter p is equal to the horizontal slowness component s_x in each layer. Intercept time τ is the sum over all layers of the vertical slowness component s_z multiplied by twice the layer thickness. After stripping, which means subtracting the τ values of two adjacent curves, we obtain the stretched slowness surface of the interval. The relationship between slowness surface and τ-p curve becomes more complicated if the reflectors are not horizontal. For dipping but parallel layers the curve obtained after stripping is again a stretched slowness surface. The stretching is not only in the s_z direction but also in the s_x direction. The stretch factors depend on layer thickness, layer dip and on the acquisition geometry (common-shot-point or common-mid-point). Some synthetic τ-p seismograms are generated using the reflectivity technique. These examples show that wavelet changes and the various wave modes present in the data may complicate interpretation of the data in terms of slowness surfaces.

Stress-induced anisotropy has attracted much attention in recent years. Oriented micro-cracks and fractures, the result of stresses acting on rock, are of interest to seismic exploration. Many of the waves recorded with a typical seismic acquisition geometry, have propagation directions with angles between zero and 30° with the vertical. For these directions (phase directions) the polarization of the fast shear wave is parallel to the fractures or cracks. This is no longer true if the interval is not only fractured but in addition finely layered. Approximate solutions for the Christoffel equation lead to an analytical expression for the polarizations in a medium with anisotropy caused by superposition of vertical cracks and horizontal layering. With a real-data example is illustrated how this expression can be used to explain the observed shear-wave polarizations in terms of relative contributions from the layering and the cracks.

REFERENCES

The references in this list form the basis for this thesis, although not all are explicitly mentioned in the text.

Aki, K. and Richards, P.G., 1980, Quantitative seismology, theory and methods, Vol. 1: W.H. Freeman and Co.

Al-Chalabi, M., 1973, Series approximation in velocity and traveltime computations, Geophysical Prospecting 21, 783-795.

Alford, R.M., 1987, Shear data in the presence of azimuthal anisotropy : Dilley, Texas, 56-th SEG meeting Houston Texas, Expanded Abstracts 476-479.

Ando, M., Ishikawa, Y. and Yamazaki, F., 1983, Shear wave polarization anisotropy in the upper mantle beneath Honshu, Japan, J. Geophys. Res. 88, 5850-5864.

Artyushov, E.V.,1984, On the origin of the seismic anisotropy in crystalline rocks , Geophys. J. R. astr. Soc. 76/1, 173-178.

Babuska, V. and Prosz, Z., 1984, P-wave velocity anisotropy in crystalline rocks, Geophys. J. R. astr. Soc. 76/1, 113-119.

Bachman, R.T., 1979, Acoustic anisotropy in marine sediments and sedimentary rocks, J. Geophys. Res. 84/B13, 7661-7663.

Bachman, R.T., 1983, Elastic anisotropy in marine sedimentary rocks, J. Geophys. Res. 88/B1, 539-545.

Backus, G.E., 1962, Long-wave anisotropy produced by horizontal layering, J. Geophys. Res. 67, 4427-4440.

Backus, G.E., 1965, Possible forms of seismic anisotropy of the uppermost mantle, J. Geophys. Res. 70, 3429-3439.

Bamford, D., 1977, Pn velocity anisotropy in a continental upper mantle, Geoph. J. R. astr. Soc. 49, 29-48.

Bamford, D. and Nurr, K.R., 1979, In situ seismic measurements of crack anisotropy in the carboniferous limestone of Northwest England, Geophysical Prospecting 27/2, 322-338.

Bamford, D., Crampin, S. and McGonigle, R., 1980, Estimating crack parameters from observations of P-wave velocity anisotropy, Geophysics 45/3, 345-360.

Banik, N.C., 1984, Velocity anisotropy of shales and depth estimation in the North Sea basin, Geophysics 49/9, 1411-1419.

Banik, N.C., Lerche, I. and Shuey, R.T., 1985, Stratigraphic filtering, part I: derivation of the O'Doherty-Anstey formula, Geophysics 50, 2768-2774.

Banik, N.C., Lerche, I. and Shuey, R.T., 1985, Stratigraphic filtering, part II: model spectra, Geophyisics 50, 2775-2783.

Barnett, D.M. and Lothe, J.,1985, Free surface waves in anisotropy elastic half-spaces: the surface impedance method , Proc. Royal Soc. London, Ser a, 402, 153-166.

Becker, D.F. and Perelberg, A.I., 1987, Seismic detection of subsurface fractures, Geophysics 52/5, 708-709.

Bennett, H.F., 1972, A simple seismic model for determining principal anisotropy direction, J. Geophys. Res. 77/17, 3078-3080.

Berryman, J.G.,1979, Long-wave elastic anisotropy in transversely isotropy media, Geophysics 44/5, 896-917.

Berzon, I.S., 1967, Analyses of the spectral characteristics of a thin bedded sequence, in: "Seismic wave propagation in real media", Consultants Bureau, new York, London.

Berzon, I.S. (ed.), 1969, Seismic wave propagation in real media, Consultants Bureau, New York, London.

Bisset, D., and Durrani, T.S., 1984, Migration with Radon transforms, 46-th Meeting of the EAEG, London.

Booth, D.C., and Crampin, S., 1983, The anisotropic reflectivity technique: theory, Geophys. J. R. astr. Soc. 72, 755-766.

Born, M. and Wolf, E., 1980, Principles of optics, Pergamon, Oxford.

Brodov, L.Y., Evstifeyev, V.I., Karus E.V. and Kulichikhina T.N., 1984, Some results of the experimental study of seismic anisotropy of sedimentary rocks using different types of waves, Geophys. J. R. astr. Soc. 76/1, 191-200.

Bruggeman, D.A.G., 1937, Berechnung der verschiedenen physikalischen Konstanten von heterogenen Sustanzen, Annal. der Physik 29, p. 160

Budden, K.G., 1961, Radio waves in the ionosphere, Cambridge University Press.

Bush I. and Crampin, S., 1987, Observation of EDA and PTL anisotropy in shear-wave VSPs, Expanded abstracts 57th SEG Meeting New Orleans, 476-479.

Byun, B.S., 1982, Seismic Parameters for media with elliptical velocity dependencies, Geophysics 47/12, 1621-1626.

Byun, B.S., 1989, Anisotropic velocity inversion from seismic traveltime measurements, paper read at 59-th SEG meeting Dallas, Texas.

Byun, B.S. and Young, C.Y., 1989, Effects of subsurface characteristics on surface seismic measurements: A simulation study on horizontally layered media, Geophysics 54/6, 730-736.

Campden, D.A., 1990, Analysis of multicomponent VSP data for shear-wave anisotropy, PhD dissertation, University of Edinburgh.

Carlson, R.L. and Christensen, N.I., 1979, Velocity anisotropy in semi-indurated calcareous deep-sea sediments, J. Geophys. Res. 84/B1, 205-211.

Carlson, R.L., Schaftenaar, C.H. and Moore, R.P., 1984, Causes of compressional-wave anisotropy in carbonate-bearing, deep-sea sediments, Geophysics 49/5, 525-532.

Carroll, M.M., 1979, An effective stress law for anisotropy elastic deformation, J. Geophys. Res. 84/B13, 7510-7512.

Chapman, C.H., 1981, Generalized Radon transforms and slant stacks, Geophys. J. R. astr. Soc. 66, 445-453.

Cerveny, V., 1972, Seismic rays and ray intensities in inhomogeneous anisotropic media, Geophys J. R. astr. Soc. 29, 1-13.

Cerveny, V. and Firbas, P., 1984, Numerical modeling and inversion of travel times of seismic body waves in inhomogeneous anisotropy media, Geophys. J. R. astr. Soc. 76, 41-51.

Cerveny, V., 1985, The application of ray tracing to the propagation of shear waves in complex media. In: Seismic shear waves, Part A: Theory. G.P. Dohr (ed.). In: Handbook of Geophysical Exploration, Section 1: Seismic exploration, 15A, Geophysical Press.

Cerveny, V., 1989, Ray tracing in factorized anisotropic inhomogeneous media, Geophys. J. Int., 99, 91-100.

Chesnokov, E.M., Krasnova, M.A., and Abaseyev, S.S., 1990, Shear-wave polarization research in some regions of the USSR, 4-th International Workshop on Seismic Anisotropy, Edinburgh, UK.

Chesnokov, E.M. and Zatsepin, S.V., 1991, Effect of applied stress on effective elastic anisotropy in cracked solids, Geophys. J. Int. 107, 563-569.

Combee, L., 1991, Transient diffusive electromagnetic fields in layered anisotropic media, PhD dissertation, Delft University.

Crampin, S., 1977, A review of the effects of anisotropic layering on the propagation of seismic waves, Geophysical J. R. astr. Soc. 49, p 9-27.

Crampin, S. and King, D.W., 1977, Evidence for anisotropy in the upper mantle beneath Eurasia from generalized higher mode surface waves, Geophys. J. R. astr. Soc. 49, 59-85.

Crampin, S., 1981, A review of wave motion in anisotropic and cracked elastic media, Wave Motion 3, 343-391.

Crampin, S. and Kirkwood, S.C., 1981, Velocity variations in systems of anisotropic symmetry, Journal of Geophysics 49, 35-42.

Crampin, S, and Yedlin, M., 1981, Shear wave singularities of wave propagation in anisotropic media, Journal of Geophysics 49, 43-46.

Crampin, S., 1982, Comments on 'Possible forms of anisotropy of the uppermost mantle under oceans' by George E. Backus, Journal of Geophysical Research 87, 4636-4640.

Crampin, S., 1984, An introduction to wave propagation in anisotropic media, Geophys. J. R. astr. Soc. 76/1, 17-28.

Crampin, S., Chesnokov, E.M. and Hipkin, R.G., 1984, Seismic anisotropy - the state of the art: II, Geophys. J. R. astr. Soc. , 76/1, 1-16.

Crampin, S., 1984, Effective anisotropy elastic constants for wave propagation through cracked solids, Geophys. J. R. astr. Soc. 76/1, 135-145.

Crampin, S., Booth, D.C., Krasnova, M.A. and Chesnokov, E.M., 1986, Shear-wave polarizations in the Peter the First Range indicating crack-induced anisotropy in a thrust-fault regime, Geophys. J. R. astr. Soc. 84, 401-412.

Daley, P.F. and Hron, F., 1982, Computation of synthetic seismograms for thin layered periodic structure , Can J. Earth, 19/7, 1449-1453.

Davies, E.E. and Clowes, R.M., 1986, High velocities and seismic anisotropy in Pleistocene turbidites of western Canada, Geophys. J. R. astr. Soc. 84, 381-399.

Dellinger, J.A., 1991, Anisotropic seismic wave propagation, PhD-thesis, Stanford University.

Diebold, J.B. and Stoffa, P., 1981, The traveltime equation, Tau-P mapping, and inversion of common midpoint data, Geophysics 46/3, 238-254.

Dix, C.H., 1955, Seismic velocities from surface measurements, Geophysics 20, 68-86.

Douma, J. and Helbig, K., 1987, What can the polarization of shear waves tell us?, First Break 5, 95-104.

Douma, J., 1988, The effect of aspect ratio on crack-induced anisotropy, Geophysical Prospecting 36, 614-632.

Douma, J., 1989, The representability of cracked media by periodically layered media, Geophysical Prospecting 37, 831-849.

Epinateva, A.M., Karus, E.V. and Nevskii, M.V., 1971, Nature of the anisotropy of seismic wave velocities in sedimentary strata, Dokl. Akad. Nauk. SSSR., 201/2, 331-334.

Evans, R. , 1984, Effects of the free surface on shear wavetrains, Geophys. J. R. astr. Soc. 76, 165-172.

Federov, F.I., 1968, Theory of elastic waves in crystals, Plenum Press, New York.

Felsen, L.B. and Marcuvitz, N., 1973, Radiation and scattering of waves, Prentice-Hall, Englewood Cliffs.

Forsyth, D.W., 1975, The early structural evaluation and anisotropy of the upper oceanic mantle, Geophys. J. R. astr. Soc. 43, 103-162.

Fryer, G.J. and Frazer, L.N., 1984, Seismic waves in stratified anisotropic media, Geophys. J. R. astr. Soc. 78, 691-710.

Fryer, G.J. and Frazer, L.N., 1987, Seismic waves in stratified anisotropic media, II, Elastodynamic eigensolutions for some anisotropic sytems, Geophys. J. R. astr. Soc. 91, 73-101.

Fuchs, K. and Muller, G., 1971, Computation of synthetic seismograms with the reflectivity method and comparisons with observations, Geoph. J. R. astr. Soc. 23, 417 - 433.

Gaiser, J.E., Ward, R.W. and DiSiena, J.P., 1984, Three-component vertical seismic profiles: velocity anisotropy estimates from P-wave particle motion, in: Toksoz, M.N., Stewart, R.R., Eds, Vertical Seismic Profiling, part B, Geophysical Press, 189-204.

Gajewski, D. and Psencik, I., 1987, Computation of high-frequency seismic waves in 3D laterally inhomogeneous anisotropic media, Geophys. J. R. astr. Soc. 91, 383-411.

Garmany, J., 1988, Seismograms in stratified anisotropic media I, WKBJ theory, Geophys. J. R. astr. Soc. 92, 365-377.

Geoltrain, S., 1989, Asymptotic solutions to direct and inverse scattering in anisotropic elastic media, Center for Wave Phenomena 082, Colorado School of Mines.

Gilbert, F. and Backus, G., 1966, Propagator matrices in elastic wave and vibration problems, Geophysics 31, 326-332

Goldsmith, W. and Ricketts, T.E., 1972, Wave propagation in an anisotropic half-space, Rock Mech. Mining, 9/4, 493-51.

Hake, J.H., Helbig, K. and Mesdag, C.S., 1984, Three-term Taylor series for t^2 - x^2 curves of P-and S- waves over layered transversely isotropic ground, Geophysical Prospecting 32, 828-850.

Hake, J.H., 1986, Slant stacking and its significance for anisotropy, Geophysical Prospecting 34, 595-608.

Hanyga, A., 1984, Transport equations for an anisotropic elastic medium in the presence of caustics, Gerlands Beitrag zur Geophyisic 93/4, 261-286.

Hauge, P.S., 1981, Measurements of attenuation from vertical seismic profiles, Geophysics 46/11, 1548-1558.

Helbig, K., 1956, Die Ausbreitung elastischer Wellen in anisotropen Medien, Geophysical Prospecting 4, 71-81.

Helbig, K., 1958, Elastischen Wellen in anisotropen Medien, Gerlands Beitage zur Geophysic 67, 177-211.

Helbig, K., 1966, A graphical method for the construction of rays and traveltimes in spherically layered media, part 2: anisotropic case, theoretical considerations, Bulletin of the Seismological Society of America 56, 527-559.

Helbig, K., 1981, Systematic classification of layer-induced transverse isotropy, Geophysical Prospecting, 29/4, 550-577.

Helbig, K., 1984, Anisotropy and dispersion in periodically layered media , Geophysics 49, 364-373.

Helbig, K., 1984, Transverse isotropy in exploration seismics, Geophys. J. R. astr. Soc. 76/1, 79-88.

Helbig, K., 1983, Elliptical anisotropy - its significance and meaning, Geophysics 48/7, 825-832.

Helbig, K. and Schoenberg, M., 1987, Anomalous polarization of elastic waves in transversely isotropic media, Journal of the Acoustical Soc. of America 81, 1235-1245.

Helbig, K., 1990, Rays and wavefront charts in gradient media, Geophysical Prospecting 38, 189-223.

Helbig, K., 1991, Longitudinal directions in media of arbitrary anisotropy, 61-st SEG Meeting Houston, Expanded Abstracts1542-1545.

Helbig, K., 1992, Foundations of anisotropy, Pergamon.

Hijden, J.H.M.T. van der, 1987, Propagation of transient elastic waves in stratified anisotropic media, PhD-thesis, Delft University.

Hood, J.A. and Schoenberg, M., 1989, Estimation of vertical fracturing from measured elastic moduli, Journal of Geophysical Research 94, 15611-15618.

Hsu, K., Esmersoy, C. and Schoenberg, M., 1988, Seismic velocities and anisotropy from high-resolution sonic logs, Paper presented at the 58-th Annual Meeting of the Society of Exploration Geophysicists, Anaheim.

Hudson, J.A., 1981, Wave speeds and attenuation of elastic waves in material containing cracks, Geophys. J. R. astr. Soc. 64, 133-150.

Jacobson, R.S., 1987, An investigation into fundamental relationships between attenuation, phase dispersion and frequency using seismic reflection profiles over sedimentary structures, Geophysics 52/1, 72-87.

Jech, J. and Psencik, I., 1989, First-order pertubation method for anisotropic media, Geophys. J. Int., 99, 369-376.

Jones, L.E.A. and Wang, H.F., 1981, Ultrasonic velocities in Cretacious shales from the Williston Basin, Geophysics 46, 288-297.

Keith, M.C. and Crampin, S., 1977, Seismic body waves in anisotropic media: reflection and refraction at a plane interface, Geophys. J. R. astr. Soc. 49, 181-208.

Kennett, B.L.N., 1981, Slowness techniques in seismic interpretation, J. Geoph. Res. 86, 11575-11584.

Kim, D.C., Katahara, K.W., Manghnani, M.H. and Schlanger, S.O., 1983, Velocity and attenuation anisotropy in deep-sea carbonate sediments, J. Geophys. Res. 88/B3, 2337-2343.

Koefoed, O. and De Voogd, N., 1980, The linear properties of thin layers, with an application to synthetic seismograms over coal seams, Geophysics 45, 1254-1268.

Kosaryev, G.L., Makeyeva, L.K., Savaryenskiy, E.F. and Chesnokov, E.M.,1979, Effect of anisotropy beneath seismic stations on body waves , Earth Physics 15/2, 102-110.

Koshubin, S.I., Pavlenkva, N.I. and Yegorkin, A.V., 1984, Crustal heterogeneity and velocity anisotropy from seismic studies in the USSR, Geophys. J. R. astr. Soc. 76/1, 221-226.

Krey, T., 1951, An approximate correction method for refraction in reflection seismic prospecting, Geophysics 16, 468-485.

Krey, T. and Helbig, K., 1956, A theorem concerning anisotropy of stratified media and its significance for reflection seismics, Geophysical Prospecting 4, 294-302.

Kulikov, V.M. and Sibiryakov, B.P., 1973, Elastic waves in two-dimensional finely laminated media exiced by directed force source, Geol. Geofiz. 5, 79-87.

Leary, P.C. and Henyey, T.L., 1985, Anisotropy and factures zones about a geothermal well from P-wave velocity profiles, Geophysics 50/1, 25-36.

Leary, P.C., Li, Y.G. and Aki, K., 1987, Observation and modeling of fault-zone fracture seismic anisotropy: P, SV and SH travel times, Geophys. J. R. astr. Soc. 91, 461-484.

Levin, F.K., 1978, The reflection, refraction, and diffraction of waves in media with an elliptical velocity dependence, Geophysics 43/3, 528-537.

Levin, F.K., 1979, Seismic velocities in transversely isotropic media, Geophysics 44, 918-936.

Levin, F.K., 1980, Seismic velocities in transversely isotropic media II, Geophysics 45, 3-17.

Levin, F.K., 1984, Anisotropy due to bedding - a computer study, Geophysical Prospecting 32/2, 187-197.

Levine, J.R. and Davis, A., 1984, Optical anisotropy of coals as an indicator of tectonic deformation, Broad Top coal field Pennsylvania, Geol. Soc. Amer. Bull. 95, 100-108

Levshin, A. and Ratnikova, L., 1984, Apparent anisotropy in inhomogeneous media, Geophys. J. R. astr. Soc. 76/1, 65-69.

Lyakhovitskiy, F.M., 1984, Transverse isotropy of thinly layered media, Geophys. J. R. astr. Soc. 76, 71-77

Lynn, H.B., 1991, Field measurements of azimuthal anisotropy: First 60 meters, San Francisco Bay area, L.A., and estimation of the horizontal stresses' ratio from Vs1/Vs2, Geophysics 56/6, 822-832.

MacBeth, C., 1991, Inverting shear-wave polarizations for anisotropy using three-component offset VSPs: synthetic seismograms, Geophysical Journal Int. 107, 571 - 583.

MacBeth, C., and Crampin, S., 1991, Comparison of signal processing techniques for estimating the effects of anisotropy, Geophysical Prospecting 39, 357-385.

Mair, J.A. and Lyons, J.A., 1981, Crustal structure and velocity anisotropy beneath the Beaufort Sea, Can J. Earth, 18/4, 724-741.

McMechan, G.A. and Yedlin, M.J., 1980, Analyses of dispersive waves by wave-field transformation, Stanford Exploration Project SEP-25, 101-113.

McNiven, H.D. and Mengi, Y., 1978, Propagation and decay of waves in porous media, J. Acoust. Soc. Am. 64/4, 1125-1131.

Meadows, M. and Coen, S., 1986, Exact inversion of plane-layered isotropic and anisotropic elastic media by the state-space approach, Geophysics 51/11, 2031-2050.

Melia, P.J. and Carlson, R.I., 1984, An experimental test of P-wave anisotropy in stratified media, Geophysics 49/4, 374-378.

Milholland, P., Manghnani, M.H., Schlanger, S.O. and Sutton, G.H., 1980, Geoacoustic modeling of deep-sea carbonate sediments, J. Acoust. Soc. Am. 68/5, 1351-1360.

Morelli, A., Dziewonski, A.M. and Woodhouse, J.H., 1986, Anisotropy of the inner core inferred from PKIKP travel times, Geophys. Res. Lett. 13, 1545-1548.

Musgrave, M.J.P., 1970, Crystal acoustics, Holden Day, San Francisco.

Naville, C. and Crampin, S., 1987, Detection of anisotropy using shear wave splitting in VSP surveys : requirements and applications, Geophysics 52/3, 416-417.

Negi, J.G., 1968, Effect of anisotropy on Love wave propagation, Bull. Seismol. Soc. Amer., 58/1, 259-266.

Nestvold, E.O., 1992, 3-D seismic: is the promise fulfilled?, The Leading Edge 11, 12-19.

Nikitin, L.V. and Chesnokov, E.M., 1984, Wave propagation in elastic media with stress-induced anisotropy, Geophys. J.R. astr. Soc. 76, 129-133.

Nur, A. and Simmons, G., 1969, Stress-induced velocity anisotropy in rock: an experimental study, J. Geophys. Res. 74, 6667-6674.

Nur, A., 1971, Effects of stress on velocity anisotropy in rocks with cracks, J. Geoph. Res. 76, 2022-2034.

Nye, J.F., 1957, Physical properties of crystals, Oxford University Press, London.

O'Doherty, R.F. and Anestey, N.A., 1971, Reflections on amplitudes, Geophysical Prospecting, 19, 430-458.

Postma, G.W., 1955, Wave propagation in a stratified medium, Geophysics 20, 780-806.

Puzyrev, N.N., Obolentseva, I.R., Trigubov, A.V. and Gorshkalev, S.B., 1984, On the anisotropy of sedimentary rocks from shear-wave analysis, Geophys. J. R. astr. Soc. 76/1, 243-252.

Radovich, B.J. and Levin, F.K., 1982, Instantaneous velocities and reflection times for transversely isotropic solids, Geophysics 47, 316-322.

Rai, C.S. and Hanson, K.E., 1987, Shear wave birefringence : a laboratory study, Geophysics 52/3, 424.

Raitt, R.W., 1969, Anisotropy of the upper mantle, Amer. Geophys. Union, 13, 250-256.

Resnick, J.R., Lerche, I. and Shuey, R.T., 1986, Reflection, transmission and the generalized primary wave, Geophys. J. R. astr. Soc. 87, 349-377.

Resnick, J.R., 1990, Stratigraphic filtering, Pageoph. 132, 49-65.

Riznichenko, Y.V., 1949, Seismic quasi-anisotropy, Bull. Acad. Sci. USSR, Geographical and Geophysical Series 13, 518-544.

Rytov, S.M., 1956, Acoustical properties of a thinly laminated medium, Soviet Physical Acoustics 2, 67-80.

Roberts, G. and Crampin, S., 1986, Shear-wave polarizations in a hot dry rock geothermal reservoir: anisotropy effects of fractures, Int. J. Rock Mech. Min. Sci. and Geomech. Abstr. 23, 291-302.

Rundle, J.B., Schuler, K.W., 1981, A composite model for the anisotropy elastic moduli of lean oil shale, Geophysics 46/2, 163-171.

Sayers, C.M., 1987, Orientation of olivine in dunite from elastic velocity measurements, Geophysical Research Letters 14/10, 1050-1052.

Schaftenaar, C. and Carlson, R.L., 1984, Calcite fabric and acoustic anisotropy in deep-sea carbonates, J. Geophys. Res. 89, 503-510.

Schans, C.A. van der and Ziolkowsky, A.M., 1983, Angular-dependent signature deconvolution, 53-rd Ann. Int. Meeting of the SEG, Las Vegas, Nevada.

Schoenberg, M., 1980, Elastic wave behaviour across linear slip interfaces, J. Acoust. Soc. Am. 68, 1516-1521.

Schoenberg, M., 1983, Reflection of elastic waves from periodically stratified media with interfacial slip, Geophysical Prospecting, 31, 265-292.

Schoenberg, M. and Douma, J., 1988, Elastic wave propagation in media with parallel fractures and aligned cracks, Geophysical Prospecting 36, 571-590.

Schoenberg, M. and Muir, F., 1989, A calculus for finely layered anisotropic media, Geophysics 54/5, 581- 589.

Schoenberger, M and Levin, F.K., 1974, Apparent attenuation due to intrabed multiples, Geophysics 39/3, 278-291.

Schoenberger, M. and Levin, F.K., 1978, Apparent attenuation due to intrabed multiples, II, Geophysics 43/4, 730-737.

Schoenberger, M. and Levin, F.K., 1979, The effect of subsurface sampling on one-dimensional synthetic seismograms, Geophysics 44/11, 1813-1829.

Schultz, P.S. and Claerbout, J.F., 1978, Velocity estimation and downward continuation by wavefront synthesis, Geophysics 43, 691 - 714.

Schultz, P.S., 1982, A method for direct estimation of interval velocities, Geophysics 47, 1657 - 1671.

Serrif, A.J., 1987, Polar anisotropy: observations and significance, Presented at the 57-th SEG meeting, New Orleans.

Shearer, P.M. and Orcutt, J.A., 1986, Compressional and shear wave anisotropy in the oceanic lithosphere: the Ngendei seismic refraction experiment, Geophys. J. R. astr. Soc. 87, 967-1003.

Shearer, P.M. and Chapman, C.H., 1989, Ray tracing in azimuthally anisotropic media-I. Results for models of aligned cracks in the upper crust, Geophys. J. R. astr. Soc. 96, 51-64.

Shearer, P.M. and Chapman, C.H., 1989, Ray tracing in azimuthally anisotropic media-II. Quasi-shear wave coupling, Geophys. J. R. astr. Soc. 96, 65-83.

Sriram, K.P., Fulton, T.W., Nooteboom, J.J. and Seriff, A.J., 1983, Velocity anisotropy of seismic waves, paper read the 53-rd SEG meeting Las Vegas, expanded abstracts 596-598.

Sriram, K.P., 1987, Observations of weak azimuthal anisotropy at Cotulla, Texas, Presented at the 57-th SEG meeting, New Orleans.

Stephan, R.A., 1981,Seismic anisotropy observed in upper oceanic crust, Geophysical Research Letters, 8/8, 865-868.

Stoffa, P.M., Buhl, P., Diebold, J.B. and Wenzel, F., 1981, Direct mapping of seismic data to the domain of intercept time and ray parameter; a plane wave decomposition, Geophysics 46, 255-267.

Stoep van der, D.M., 1966, Velocity anisotropy measurements in wells, Geophysics 31, 900-916.

Tatham, R., Keeney, J.W. and Noponen, I., 1982, Application of the tau-p transform (slant stack) in processing seismic reflection data, 52-nd SEG meeting, Dallas, Texas.

Thomsen, L., 1986, Weak elastic anisotropy, Geophysics 51/10, 1954-1966.

Thomsen, L., 1988, Reflection seismology in azimuthally anisotropic media, Geophysics 53/3, 304-313.

Treitel, S., Gatowski, P.R. and Wagner, D.E., 1982, Plane-wave decomposition of seismograms, Geophysics 47, 1375-1401.

Uhrig, L.F. and van Melle, F.A., 1955, Velocity anisotropy in stratified media, Geophysics 20, 774-779.

Veltmeyer, H. and Voogd de, N., 1982, High resolution mining seismics: Quantitative interpretation of reflections from thin layers, Special Report, EEC project 118-80-MPP-NL.

Vlaar, N.J., 1968, Ray theory for an anisotropic inhomogeneous elastic medium, Bulletin of the Seismological Soc. of Am. 58, 2053-2072.

Vlaar, N.J., 1969, Rays and traveltimes in a spherical anisotropic earth, Bulletin of the Seismological Soc. of Am. 59, 1051-1060.

Wetzel, A., 1986, Anisotropy and modes of deposition of pelitic Mississippi fan deposits ,The Deep Sea Drilling Project, 96, 811-818.

White, J.E., 1982, Computed waveforms in transversely isotropy media, Geophysics 47/5, 771-783.

White, J.E., Monash, C. and Martineau-Nicoletis, L., 1983, Measured anisotropy in Pierre shale, Geophysical Prospecting 31/5, 709-725.

Wild, P, and Crampin, S., 1991, The range of effects of azimuthal isotropy and EDA anisotropy in sedimentary basins, Geophysical Journal Int. 107, 513-529.

Willis, H.A., Rethford, G.L. and Bielanski, E.,1987, Azimuthal anisotropy : occurrence and effect on shear wave data quality, Geophysics 52/3, 425.

Winterstein, D.F., 1986, Anisostropic effects in P-wave and SH-wave stacking velocities contain information on lithology, Geophysics 51/3, 661-672.

Winterstein, D.F., 1987, Vector attenuation: Some implications for plane waves in anelastic layered media (Short Note), Geophysics 52/6, 810-814.

Winterstein, D.F., 1990, Velocity anisotropy terminology for geophysicists, Geophysics 55/8, 1070-1088.

Winterstein, D.F. and Meadows, M.A., 1991, Changes in shear-wave polarization azimuth with depth in Cymric and Railroad Gap oil fields, Geophysics 56/9, 1331-1348.

Woeber, A.F. and Penhollow, J.O., 1975, Depth prediction from velocity profiles on the Texas Gulf Coast, Geophysics 40/3, 388-398.

Wright, J., 1987, The effects of transverse isotropy on reflection amplitude versus offset, Geophysics 52/4, 564-567.

Yedlin, M.J., 1980, The wave front in a homogeneous anisotropy medium, Bull. Seismol Soc. Amer, 70/6, 2097-2101.

Ziolkowski, A.M. and Fokkema, J.T., 1986, The progressive attenuation of high frequency energy in seismic reflection data, Geophysical Prospecting 34, 981-1001.

Zykov, Y.D., Lyakhovitskiy, F.M. and Chervinskaya, O.P., 1984, Experimental investigation of transverse isotropy in ice/clay thin-layered periodic models, Geophys. J. R. astr. Soc. 76/1, 269-272.

Samenvatting

(summary in Dutch)

De Christoffel vergelijking relateert de medium parameters, gegeven door de elasticiteitstensor, aan golfsnelheid en deeltjesuitwijking. Anders dan in isotrope media, waar de eenvoud van de elasticiteitstensor resulteert in de bekende uitdrukkingen voor P- en S-golven, bestaan er in anisotrope media in het algemeen geen eenvoudige analytische uitdrukkingen. Drie golftypes, met in het algemeen verschillende snelheden, hebben uitwijkingen in richtingen die noch parallel noch evenwijdig aan de voortplantingsrichting zijn. De voortplantingsrichting van de energie valt niet samen met de voortplantingsrichting van de fase. Het traagheids-oppervlak en het "normal"-oppervlak illustreren de voortplantingsrichting-afhankelijkheid van traagheid en van "normal"-snelheid. De snelheid waarmee energie zich voortplant, de straalsnelheid, kan worden afgeleid uit de richtingsafhankelijkheid van traagheid of normal-snelheid.

Een golf die invalt op het grensvlak tussen twee anisotrope media veroorzaakt in het algemeen reflectie en transmissie van al de drie golftypes. Het stralenpad van een gereflecteerde of doorgelaten golf kan onverwacht zijn als men alleen gewend is aan isotrope situaties. De 'zero-offset' straal, bijvoorbeeld, betekent dat invallende en gereflecteerde straal hetzelfde pad hebben. De traagheidsvectoren staan in dat geval loodrecht op het grensvlak terwijl de straal scheef kan staan ten opzichte van het grensvlak. Invallende en gereflecteerde stralen van hetzelfde golftype zijn in het algemeen niet symmetrisch ten opzichte van de grensvlaknormaal.

Inflectiepunten in het traagheids-oppervlak komen overeen met 'cusps' in het golf-oppervlak. Inhomogeniteit van de ondergrond leidt er toe dat dit typische anisotropie fenomeen vaak moeilijk te herkennen is. Om de karakteristieke vorm van een golf-oppervlak met cusps waar te nemen moeten de seismische ontvangers dicht bij de anisotrope laag gepositioneerd zijn. Asymmetrische reflectie is een andere oorzaak voor het moeilijk herkenbaar zijn van de typische

signalen die horen bij een golf-oppervlak met cusps, zelfs wanneer de ontvangers
in of dichtbij de anisotrope laag geplaatst zijn.

In dit proefschrift wordt de nadruk gelegd op anisotropie veroorzaakt door
fijne gelaagdheid. Gekeken wordt naar de voorwaarden waaronder fijne
gelaagheid equivalent is met anisotropie. Met de lange golflengte (of quasi-
statische) benadering komt een interval met dikte H, bestaande uit een serie
laagjes, voor seismische golfvoortplanting overeen met een homogeen en
anisotroop medium. Deze benadering houdt in dat H veel kleiner is dan de
seismische golflengte λ. Nader onderzoek van deze benadering laat zien dat de
mate van overeenkomst van vele factoren afhangt. De overeenkomst is exact
wanneer de golflengtes oneindig groot zijn. Het is ook exact (en voor alle
golflengtes) voor die golven die niet reflecteren aan de grensvlakken tussen de
laagjes. Dit houdt in dat de reflectiecoëfficiënten dan nul zijn. Een eenvoudig
model wordt gebruikt waarbij het interval met dikte H bestaat uit twee laagjes
die N keer herhaald worden. De twee laagjes vormen een periode en het hele
interval bestaat dus uit N periodes. Het golfveld dat zich door deze serie laagjes
voortplant bestaat uit de primaire golf en al de meervoudig gereflecteerde golven
(multiples). Het effectieve medium hangt af van de interferentie van de primaire
golf en de multiples. Voor oneindig dunne laagjes resulteert dit in een effectief
homogeen medium, met een pseudo-primaire golf die vertraagd is ten opzichte
van de primaire golf.

Om het effect van dunne laagjes met een eindige dikte te onderzoeken,
plaatsen we het interval tussen twee anisotrope half-ruimtes. We beschouwen
een golf invallend vanuit de bovenste half-ruimte. De hoeveelheid energie die
teruggekaatst wordt in deze half-ruimte is een maat voor de effective anisotropie
van het interval. Voor dunne laagjes is het teruggekaatste golfveld, aangegeven
door reflectiviteit R, onafhankelijk van het aantal periodes. Dit betekent dat
periodiciteit geen noodzakelijke voorwaarde is om tot anisotropie te leiden. De
reflectiviteit is recht evenredig met d/λ, waarbij λ de seismische golflengte is en d
de dikte van een periode. De betekenis van de multiples komt tot uiting in de
relatie tussen R en de vlakke-golf reflectiecoëfficiënt r. Voor sub-kritische hoeken
van inval zijn R en r rechtevenredig. Het betekent dat voor laagjes met een
groter impedantiecontrast de voorwaarde dat de laagjes dun moeten zijn sterker
is. Bovendien, omdat r in het algemeen afhangt van de hoek van inval, is de
conditie dus ook hoekafhankelijk. Wanneer R kleiner is dan 0.15 verschilt de
effectieve snelheid minder dan 0.5% van de anisotrope snelheid. In dat geval is

de demping ten gevolge van dispersie minder dan 0.22 dB per golfperiode. De
voorwaarde R kleiner dan 0.15 kan worden gebruikt als criterium om lagen te
vervangen door een homogeen dempend anisotroop medium.

Vervolgens wordt gekeken naar snelheden zoals die afgeleid worden uit
looptijd-curves voor een horizontaal gelaagde transversaal isotrope ondergrond.
Intervalsnelheden afgeleid uit "stacking" snelheden met behulp van de Dix-
formule, verschillen in het algemeen van de verticale of de horizontale snelheid
in de anisotrope laag. Het kwadraat van de snelheid verkregen uit zero-offset
data, is gelijk aan de verhouding tussen de horizontale componenten van
straalsnelheid en traagheid. De benadering van de looptijd-curve door een
hyperbool komt overeen met een elliptische benadering van het golf-oppervlak.
De horizontale as van deze ellips komt overeen met de snelheid zoals die uit de
hyperbool volgt. Van belang is hoeveel deze snelheid, aangegeven met F,
verschilt van de verticale snelheid omdat F vaak gebruikt wordt voor tijd-diepte
conversie. De anisotropiefactor is gedefinieerd als de verhouding tussen F en de
verticale snelheid. Voor anisotropie ten gevolge van gelaagdheid is F voor P-
golven gelijk aan de verticale snelheid wanneer alle laagjes dezelfde Poisson-
verhouding hebben. Voor shear-golven kan de anisotropiefactor aanzienlijk
groter zijn dan 1, bijvoorbeeld 2. De anisotropiefactor afgeleid uit zero-offset data
is kleiner voor shear-golven met een deeltjes uitwijking loodrecht op het
voortplantingsvlak (de S1-golf) dan voor de andere shear-golf (de S2- golf). Voor
data met grotere offsets neemt voor P-golven F toe met offset. Dit zelfde gebeurt
ook door verticale inhomogeniteit. Voor S2-golven neemt F af met offset, hetgeen
dus tegengesteld is aan het effect van verticale inhomogeniteit. Voor S1-golven is
F onafhankelijk van offset.

Voor een interval met een verticale snelheidsgradiënt geldt dat de verticale
snelheid kleiner is dan F, de snelheid afgeleid uit reflectietijd-curves. Snelheid F
hangt af van het offsetbereik dat gebruikt is bij het bepalen van de hyperbool. De
inhomogeniteitsfactor is gedefinieerd als de verhouding tussen F en de verticale
snelheid voor een isotrope laag met een verticale snelheidsgradiënt. Het blijkt
dat deze factor gelijke waardes kan bereiken als de waardes die kenmerkend zijn
voor anisotropie factoren voor anisotropie ten gevolge van gelaagdheid. Dit wordt
geïllustreerd met twee voorbeelden. Seismische data uit de Noordzee met P-
golven laten zien dat de verticale snelheidsgradiënt een verschil van 2%
veroorzaakt tussen F en de verticale snelheid. Een experiment met shear-golven
toont een grote snelheidsgradiënt die resulteert in een inhomogeniteitsfactor

tussen 1.07 en 1.24 (afhankelijk van intervaldikte en geselecteerde offset). Deze voorbeelden laten zien dat het toekennen van verschillen tussen stacking-snelheden en verticale snelheden aan anisotropie niet gedaan moet worden voordat gecorrigeerd is voor het effect van inhomogeniteit.

In een volgend hoofdstuk wordt gekeken naar het belang van de tau-p transformatie voor anisotropie. Deze transformatie, ook slant stacking genoemd, verplaatst de seismische data van het tijd-offset (t-x) domein naar het domein van intercepttijd (tau) en straalparameter (p). Deze transformatie wordt beschouwd als een decompositie van de data in vlakke golven. Dit betekent dat data met dezelfde p-waarde gezien kunnen worden als afkomstig van een vlakke-golf bron. Dit geldt niet alleen voor isotrope media maar ook voor anisotrope media. Aankomsttijden in het t-x domein worden bepaald door de straalsnelheid. In het tau-p domein worden ze bepaald door de normal-snelheid. De tau-p transformatie verplaatst de data van het golf-oppervlak (of straal-traagheids-oppervlak) domein naar het normal-oppervlak (of traagheids-oppervlak) domein. Hierdoor neemt de betekenis van de transformatie toe voor anisotrope media, waar deze karakteristieke oppervlaktes verschillende eigenschappen hebben.

Reflectietijd-curves voor een horizontaal gelaagde ondergrond zijn nauw verwant aan traagheids-oppervlaktes. De straalparameter p is gelijk aan de horizontale component van de traagheidsvector s_x in elke laag. De intercepttijd tau is de som van de verticale componenten van de traagheids-vectoren s_z in al de lagen, vemenigvuldigd per laag met twee keer de laagdikte. Strippen, waarbij het verschil in tau-waarde van twee curves wordt genomen, resulteert in het opgerekte traagheids-oppervlak van het betreffende interval. De relatie tussen traagheids-oppervlak en tau-p curve wordt ingewikkelder wanneer de lagen niet horizontaal zijn. Voor hellende evenwijdige lagen is het resultaat na strippen weer een uitgerekt traagheids-oppervlak. Het uitrekken is nu niet alleen in de s_z-richting maar ook in de s_x-richting. De mate van uitrekken hangt af van laagdikte, helling en de acquisitiegeometrie (common-shot-point of common-mid-point). Synthetische seismogrammen zijn gemaakt met de reflectiviteitsmethode. Deze voorbeelden laten zien dat veranderingen in golf-vormen en de vele verschillende golftypes het moeilijk kunnen maken om de data op de juiste wijze te interpreteren in traagheids-oppervlaktes.

Anisotropie ten gevolge van spanningen staat de laatste jaren in de belangstelling. Georiënteerde scheurtjes en breukjes, het resultaat van

spanningen werkzaam op gesteente, zijn van belang voor de seismische exploratie. Veel van de waargenomen golven in een typische seismische acquisitiegeometrie planten zich voort in richtingen variërend tussen nul en 30 graden met de verticale richting. De deeltjesuitwijking van de snelste shear-golf is voor deze voortplantingsrichtingen evenwijdig aan de scheurtjes en breukjes. Dit is niet meer het geval wanneer een interval niet alleen scheurtjes bevat maar bovendien fijn gelaagd is. Een benaderde oplossing voor de Christoffel-vergelijking resulteert in een analytische uitdrukking voor de deeltjesuitwijkingen in een medium dat anisotroop is door zowel scheurtjes als door gelaagdheid. Een data-voorbeeld wordt gebruikt om te laten zien hoe met behulp van deze uitdrukking de gemeten shear-golf-uitwijkingen kunnen worden geïnterpreteerd in termen van de relatieve bijdragen van gelaagdheid en scheurtjes.

Acknowledgements

Curriculum vitae

De schrijver van dit proefschrift werd op 2 oktober 1956 te Emmen geboren. Hij behaalde in 1975 het diploma Atheneum aan het Katholiek Drents College te Emmen. In datzelfde jaar begon hij zijn studie aan de Rijksuniversiteit te Utrecht. Het kandidaatsexamen Geologie (G4) werd in 1978 afgelegd, gevolgd door het doctoraalexamen Geofysica van de vaste aarde in 1981 met als hoofdrichting exploratie geofysica en als bijvak structurele geologie. Van 1982 tot en met 1984 was hij, in dienst van de Nederlandse organisatie voor Wetenschappelijk Onderzoek (NWO), werkzaam bij de afdeling Exploratie Geofysica van het Instituut voor Aardwetenschappen van de Rijksuniversiteit te Utrecht. Vanaf 1985 is hij werkzaam als research geofysicus bij het Koninklijke/Shell Exploratie en Produktie Laboratorium te Rijswijk.